Alma Mater Studiorum · Università di Bologna

Scuola di Scienze
Dipartimento di Fisica e Astronomia
Corso di Laurea Magistrale in Fisica

DISORDER AND LOCALIZATION IN 1D LONG-RANGE FERMIONIC CHAINS

Relatore:
Prof. Elisa Ercolessi

Correlatore:
Dott. Piero Naldesi

Presentata da:
Leonardo Benini

Anno Accademico 2015/2016

ABSTRACT

The microscopic mechanism leading a quantum system towards its thermodynamical equilibrium state, i.e. the *thermalization* process, has been at the center of a debate since the very early days of quantum statistical mechanics. During the 90's, thanks to the works of J.M. Deutsch and M. Srednicki, this topic was founded on more solid theoretical grounds with the development of what is now known as the *Eigenstate Thermalization Hypothesis* (ETH), which appears to explain thermalization in a large class of closed quantum systems. Recently, experimental advances in atomic, optical, nuclear and condensed matter physics has generated a wide range of new possibilities for the study of highly tunable many-body systems in an isolated environment. This gave birth to a renaissance of theoretical interest towards systems which fail to thermalize, violating the ETH. The focus of this thesis is on a well-known phenomenon which protects a system against thermalization and emerges in disordered environments, named *Anderson localization*. In the first chapter we give a pedagogical introduction to the ETH, combining elements from quantum chaos and Random Matrix Theory. The second chapter deals with localization theory and its recent extension to interacting systems, i.e. *Many-Body localization*, reviewing the main features of these phenomena and the basic hallmarks which allows one to distinguish between ergodic and localized phases. In the third and fourth chapter we present and analyze the model on which we performed numerical investigations in order to detect localization signatures. Such a model is a generalization of the 1D Kitaev chain for fermions with long-pairing, on which we induced the disorder and numerically studied its spectral and entanglement properties. Our results highlight some new aspects of localization in free-fermionic chains, with respect to the interplay between the disorder and the long-range pairing, opening new perspectives for future works.

SOMMARIO

Il processo di *termalizzazione* è l'insieme di fenomeni microscopici che porta un sistema fisico verso quello che chiamiamo stato di equilibrio termodinamico. Nel corso degli anni '90 il lavoro di J.M. Deutsch e M. Srednicki ha posto solide fondamenta teoriche per la comprensione della termalizzazione in sistemi quantistici, con la formulazione della cosiddetta *Eigenstate Thermalization Hypothesis* (ETH), fornendo un'elegante descrizione di questo meccanismo. Recentemente, progressi sperimentali nei campi della fisica atomica e dello stato solido hanno dato vita a nuove possibilità nello studio di sistemi quantistici a molti corpi isolati, con una grande precisione nel controllo dei parametri macroscopici. Questi avanzamenti in campo sperimentale hanno dato vita, nell'ultimo decennio, a un rinnovato interesse teorico nei confronti di sistemi che, non rispettando l'ETH, evitano la termalizzazione. Questo lavoro si concentra su un fenomeno caratterizzante di sistemi quantistici disordinati chiamato *Localizzazione di Anderson*. Nel primo capitolo viene fornita una introduzione al concetto di termalizzazione quantistica e alla derivazione dell'ETH, combinando elementi di teoria quantistica del chaos e Random Matrix Theory. Il secondo capitolo tratta la teoria della localizzazione e la sua recente estensione a sistemi interagenti, chiamata *Many-Body localization*: vengono spiegate le principali caratteristiche e implicazioni di questi fenomeni, introducendo i principali indicatori utilizzati per distinguere fasi localizzate da fasi ergodiche. Infine, nel terzo e nel quarto capitolo viene presentato e analizzato il modello di Kitaev unidimensionale disordinato con decadimento a lungo raggio del termine di pairing, oggetto del nostro studio. I risultati numerici presentati consistono principalmente in un'analisi spettrale delle autofunzioni dell'Hamiltoniana del nostro modello e in un'indagine sulle proprietà di entanglement, dimostrando l'esistenza di una fase localizzata.

CONTENTS

INTRODUCTION

During the twenties of the past century, when quantum theory was developed by some of the most brilliant physicists ever lived, classical statistical mechanics was a well-established field of research. Indeed, it was in 1902 that Gibbs saw his landmark book "Elementary principles in statistical mechanics" published [1], setting what is widely recognized as the birth of modern statistical mechanics. [2] As the mathematical background of the new quantum mechanics was settled, John Von Neumann spent significant efforts in order to generalize the fundamental concept of *ergodicity* and to prove the tendency of a quantum state to evolve towards the state of maximum entropy, the so called *H-theorem*. [3]. Really soon, a new field of research, which can now be considered one of the pillars of modern physics, emerged: quantum statistical mechanics. [4] However, some fundamental questions, strictly related to the studies of Von Neumann, remained open till nowadays. For example, let us first consider an isolated *classical* system subject to some macroscopic constraints, such as conservation of volume, number of particles and total energy. Statistical mechanics allows the derivation of its equilibrium properties starting from a fictitious ensemble of systems evolving under the same Hamiltonian and constrained by the same imposed restrictions. Then, we assign a probability to each member of the ensemble, and the macroscopic behaviour of the system is described by some thermodynamic quantities that we are able to calculate through averages over the ensemble. [1] For an isolated system, the ensemble is tipically chosen to be the microcanonical one, in which to every microscopic configuration (every *microstate*) is given an equal a-priori probability, i.e. the states of the system are uniformly distributed over the accessible hypersurface in phase space, accordingly to the microcanonical distribution. [5] The correctness of the procedure used in statistical mechanics, however, is not so obvious: in actual experiments, generally there is no ensemble of systems (but only one) and the relation between the method just depicted and the measurable outcome is often doubtful.

To address this issue, the main line of thought offered in most textbooks is the invocation of the *ergodic hypothesis*: during its time evolution, an ergodic system dynamically explores every region of phase space (accordingly with the external constraints) and, in the long-time limit, the time spent in each state is proportional to its volume. Thanks to ergodicity, we can equal time averages to ensemble averages, which are easier to calculate. Ergodicity has been formally proved only for few systems, such as the Sinai billiard[6], the Bunimovich stadium[7], and systems with more than two hard spheres on a torus[8].

Within this framework, a crucial problem concerns the nature of *thermalization*, i.e. the process of relaxation of a system towards an equilibrium state in which we can exploit the ergodic hypothesis. We should stress that the ergodic hypothesis does not hold for every class of interacting systems, especially in low dimensions. In 1D, actually, there are many notable examples of systems which fail to thermalize, even in the weak sense. A famous example is the Fermi-Pasta-Ulam numerical experiment in a chain of anharmonic oscillators, for which the most recent results show no thermalization (or extremely slow)[9]. Relaxation towards the equilibrium state can also be extremely slow in turbulent systems[10] and in glassy systems[11].

Remarkably, the understanding of quantum thermalization has been recently grounded on quite solid foundations, thanks to the formulation of the *Eigenstate Thermalization Hypothesis* (ETH)[12–14]. In a nutshell, the ETH implies that thermalization may occur in isolated quantum systems only if they can act as their own bath. In this case, the hypothesis states that the long-time behaviour of any physical observable in an eigenstate $|\psi\rangle$ of the system is equal to its microcanonical average if $|\psi\rangle$ is the only eigenstate in the microcanonical window. Thus, it is possible to describe the thermodynamics of closed systems with the so called "Single Eigenstate Ensembles", i.e. ensembles constructed with only one Hamiltonian eigenstate. However, not all closed quantum systems do act as reservoirs that thermalize their subsystems, and the ETH do not apply to almost two important classes of systems: integrable systems, which possess an infinite set of extensive conserved quantities, and localized systems, which are strictly connected to the role of disorder in quantum physics.

In the context of condensed matter physics, disorder is often an unavoidable factor, and it is the cause of a rich phenomenology, which implications were first made concrete by Anderson[15] in his seminal work of 1958. His idea of the suppression of transport in a quantum lattice, due to the randomness of onsite potentials, paved the way for a quantum theory of dynamics in a disordered environment, and goes far beyond this, with deep implications on the basic assumptions regarding the theory of thermalization and equilibration in isolated quantum systems. Whether the interplay of disorder and interactions between the constituents in quantum systems keeps the absence of diffusion and the other typical properties of Anderson localized systems alive was the fundamental doubt that motivated the search for the so-called Many-Body Localized phase in the past ten years, first addressed in[16,17] with a systematic perturbative approach.

This recent renaissance of the localization subject has to be framed in the more general renewed interest in the physics of closed systems, i.e. isolated systems without any coupling with an external reservoir, which is mainly due to three concomitant factors:

- *An experimental revolution* has been fueled by huge advances in experimental techniques, which has made it possible to manipulate quantum systems with many degrees of freedom. A whole new range of methods, including *ultra-cold atoms* arranged in *optical lattices*[18–20] or some sort of similar confinements, or *ion trapping*[21,22], permits the set up, control and study in laboratory of strongly-interacting quantum systems[23–25]. Such improvements expanded enormously our possibilities to explore and understand some features of quantum systems, like *equilibration* and *thermalization*. In particular, thanks to setups with optical lattices, it has been made possible to realize condensed-matter-like interacting systems with fine grained control over the model parameters, leading to a massive interest in questions concerning out of equilibrium dynamics of such systems, motivated by the need to understand experimentally realisable physical situations and not only theoretical curiosities.
- The second great development lies in the availability of new extremely powerful machines: *supercomputers*. Simulations of the dynamical behaviour of large quantum systems for relatively long times became possible, thanks to a big increase in computing power as well as new numerical methods such as Density Matrix Renormalization Group[26] or tensor network methods[27]. Other advances have been new improvements of exact diagonalization methods[14,28,29], quantum

Monte Carlo techniques[30], dynamical mean field theory[31] and density functional theory[32]. Moreover, a lot of numerical works were produced in recent years on questions about equilibration and thermalization in closed quantum systems and on dynamics of quantum phase transition, with particular focus on so-called quantum *quenches*, i.e. abrupt changes of the Hamiltonian that lead the system out of equilibrium.

- Finally, the third driving force is the development of new *mathematical and theoretical methods*, motivated in part by research in quantum information theory. These techniques brought to new approaches to the central key questions, inspiring works on *tipicality* and *random states*[33,34] , other than contributing with notions developed in quantum information propagation research, such as *Lieb-Robinson bounds*[35–37] and *entanglement in many-body systems*[38–40].

As we already said, the most intriguing feature of localized system is that their long-time properties are not captured by the conventional ensembles of quantum statistical mechanics. This leads to striking memory effects, since these systems can locally remember for long times information about initial conditions, which are normally erased by the thermalization process. Thus, interest towards localized systems goes far beyond their connection with open questions on the foundations of statistical mechanics, embracing new possibilities in terms of quantum information storing.

In this thesis we explore localization properties of a fermionic one dimensional model known as the Kitaev chain[41]. In its original formulation, the Kitaev model described a superconductive wire which supports unpaired Majorana modes at the edges of the chain, implying the existence of a topological superconducting phase[42]. Recent observations[43–46] of Majorana zero modes in spin-orbit coupled semiconductors gave a new push to research interest in topological features of many-body systems, opening new perspectives in the field of topological quantum computation[42,47]. We consider a disordered version of a recently proposed generalization of the Kitaev chain with long-range pairing[48], decaying with distance l as a power-law $\sim 1/l^{\alpha}$. Such long-range model has been recently proposed as a candidate for helical Shiba chains, made of magnetic impurities on an s-wave superconductor[49]. The novelty of this work resides in the study of the relation between the long-range pairing and the disordered environment, a subject which has not received a lot of attention so far, except for few works on interacting spin

models[50–54].

The manuscript is organized as follows: in the first chapter we will review the concepts which underlie the modern understanding of the thermalization mechanism in quantum systems, starting from the notion of quantum chaos in the framework of Random Matrix Theory. We will explain which properties characterize a quantum ergodic system, showing the derivation of the Eigenstate Thermalization Hypothesis. In the second chapter we will introduce the main ideas that led to the formulation of localization theory, briefly reviewing Anderson's original results and implications. Then we will turn to the recently developed theory of Many-Body Localization (MBL), describing its basic hallmarks and setting the basis for the comprehension of our investigations. Chapter 3 revolves around the description of both short-range and long-range Kitaev models, with focus on critical behaviour of correlation functions and entanglement properties. Finally, in chapter 5 we will show our original results, based on numerical investigations of the disordered Kitaev chain with long-range pairing. We will mutuate some ideas from MBL theory, analyzing spectral features and spectral statistics in order to identify signatures of a localized phase. Moreover, the final part of the chapter contains some entanglement results, concerning in particular the scaling of the bipartite entanglement entropy with the size of a subsystem of the chain.

1

FROM CHAOS TO QUANTUM THERMALIZATION

The derivation of the ETH and its implications for statistical mechanics are the subject of this first chapter. As we will see, ETH combines basic ideas from quantum chaos and Random Matrix Theory in a clear mathematical sense that is somehow unparalleled in classical physics. This fact is impressive in itself, since the relation between the microscopic dynamics and macroscopic behaviour is more subtle in the quantum world than in classical mechanics. In fact, the notion of phase space is absent in the quantum picture because of the uncertainty principle, which denies the possibility of measuring the position and the momentum of a particle simultaneously. Furthermore, the linearity of Schrödinger equation implies that the key ingredient leading to chaos in classical systems, i.e. nonlinear equations of motion, can not be exploited in the quantum framework.

1.1 CHAOTIC SYSTEMS AND RANDOM MATRIX THEORY

1.1.1 CLASSICAL CHAOTIC SYSTEMS

Although there is not a universal recognized definition of *chaos*, a classical system is considered chaotic if it shows strong sensitivity of phase-space trajectories to small perturbations. While chaotic dynamics in this sense is quite common in classical physics, there is an important class of systems which do not show this type of behaviour: *integrable systems*. A classical system described by an Hamiltonian $H(\boldsymbol{p}, \boldsymbol{q})$, with canonical coordinates and momenta $\boldsymbol{q} = (q_1, \cdots, q_N), \boldsymbol{p} = (p_1, \cdots, p_N)$, is said to be integrable if

it has a set of N independent conserved quantities $\{I_i\}$ in involution:

$$\{I_i, H\} = 0, \quad \{I_i, I_j\} = 0, \tag{1.1}$$

where

$$\{f, g\} = \sum_{i=1}^{N} \frac{\partial f}{\partial q_i}\frac{\partial g}{\partial p_i} - \frac{\partial f}{\partial p_i}\frac{\partial g}{\partial q_i} \tag{1.2}$$

is the Poisson bracket. Exploiting Liouville's integrability theorem, we can define a canonical transformation to action-angle variables $(p, q) \to (I, \theta)$ such that $H(p, q) = H(I)$ [55]. Thus, the solutions of the equations of motion become trivial: $I_i(t) = I_i(0) =$ constant, and $\theta_i(t) = \Omega_i(t) + \theta_i(0)$. Such a motion is obviously not chaotic. Figure 1.1 provides a feeling about trajectories of a particle in a cavity subject to chaotic dynamics: if one follows two initially close trajectories one finds that after some bounce against the walls, they become completely uncorrelated.

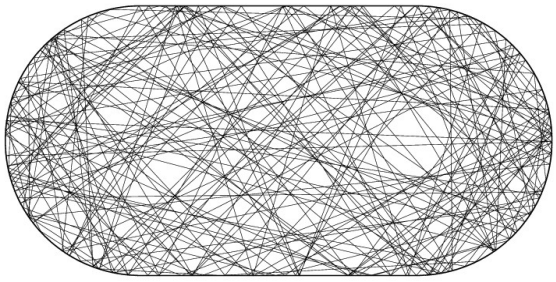

Figure 1.1: Example of a chaotic trajectory of a particle in a cavity: Bunimovich stadium [7].

A necessary, and often sufficient, condition for chaotic dynamics to occur is that the number of independent conserved quantities in involution is smaller than the number of total degrees of freedom. The motion of a single particle in one dimension is obviously integrable, since the conservation of energy provides a unique (up to a sign) relation between its coordinate and momentum. In two dimensions chaos becomes possible, since the constraint imposed by the energy is not sufficient anymore. In order to make the motion regular, we have to add another conservation law, e.g. conservation of total angular momentum. In many-particle systems, we consider a system chaotic if there is not an extensive set of integrals of motion.

We can ask what happens to an integrable systems if subject to a small perturbation that, in some sense, breaks its integrability. An important argument related to this question is the KAM theorem [56], which implies that for a large set of initial conditions the motion of a system under small perturbations remains perpetually quasiperiodic.

1.1.2 RANDOM MATRIX THEORY

In this section we will briefly discuss some notions about quantum chaos that will be needed for the derivation of the ETH. For more complete reviews on quantum chaos and Random Matrix Theory (RMT) see references [57,58].

As mentioned in the introduction of this chapter, the classical notion of chaos does not directly fit quantum systems. The main reason lies in the linearity of the Schrödinger equation, that does not allow an exponential divergence of trajectories of the wave functions even after long times. Actually, the overlap between different states, evolved with the same Hamiltonian, remains constant. Also, one does not have a proper definition of what a trajectory is, since coordinates and momenta cannot be determined simultaneously due to the uncertainty principle. Thus, what is chaos in quantum systems?

This question was largely ignored until the 70s when, after a seminal work by Gutzwiller [59], it began to attract massive interest, which led to the foundation of a research field broadly known as quantum chaos. Still nowadays, many questions remain unsolved, including a precise definition of quantum chaos.

The grounds of quantum chaos theory were provided by some fundamental works by Wigner [60,61], Dyson [62] and others, who developed a theory for explaining the random spectra of some atomic nuclei, now known as Random Matrix Theory (RMT). RMT is a powerful theory and, as we will explain later, underlies our understanding of thermalization in quantum systems. Speaking about complex quantum systems such as atomic nuclei, Wigner, in his original works, formulated the idea that it is hopeless to try to calculate all the exact eigenstates and eigenenergies, and it is more suitable to focus on statistical properties. The second main idea is that, restricting to a certain energy shell in which the density of states is constant, the Hamiltonian looks like a random matrix. From the statistical study of this kind of random matrices one can get useful informations about the properties of energy levels and eigenstates.

We can get a deeper understanding of these concepts using simple 2×2 Hamiltonians, whose elements are random numbers taken from a gaussian distribution:

$$H = \begin{pmatrix} \epsilon_1 & \frac{V}{\sqrt{2}} \\ \frac{V^*}{\sqrt{2}} & \epsilon_2 \end{pmatrix}, \tag{1.3}$$

where the introduction of the $\sqrt{2}$ leaves the Hamiltonian in an invariant form under basis

rotations. We can diagonalize (1.3) and obtain the spectrum

$$E = \frac{\epsilon_1 + \epsilon_2}{2} \pm \frac{\sqrt{(\epsilon_1 - \epsilon_2)^2 + 2|V|^2}}{2}. \tag{1.4}$$

In the presence of time-reversal symmetry [1] we can write the Hamiltonian as a real matrix ($V = V^*$). From the eigenvalues (1.4), we can calculate the energy-level statistics, i.e. the distribution of the spacings between adjacent levels $P(E_1 - E_2 = \omega) = P(\omega)$:

$$\begin{aligned} P(\omega) &= \frac{1}{(2\pi)^{3/2}\sigma^3} \int d\epsilon_1 \int d\epsilon_2 \int dV \delta(\sqrt{(\epsilon_1 - \epsilon_2)^2 + 2V^2} - \omega) \exp\left(-\frac{\epsilon_1^2 + \epsilon_2^2 + V^2}{2\sigma^2}\right) \\ &= \frac{1}{2\pi\sigma^2} \int\int d\xi dV \delta(\sqrt{2\xi^2 + 2V^2} - \omega) \exp\left(-\frac{\xi^2 + V^2}{2\sigma^2}\right), \end{aligned} \tag{1.5}$$

where we set $\epsilon_2 = \epsilon_1 + \sqrt{2}\xi$ and we evaluated the Gaussian integral over ϵ_1. Swithcing to cylindrical coordinates, $V = r\cos(x), \xi = r\sin(x)$, we are left with

$$P(\omega) = \frac{\omega}{2\sigma^2} \exp\left(-\frac{\omega^2}{4\sigma^2}\right). \tag{1.6}$$

If the system does not present invariance under time reversal, we can treat independently $\Re(V)$ and $\Im(V)$, and using spherical coordinates in a similar calculation leads to

$$P(\omega) = \frac{\omega^2}{2\sqrt{\pi}(\sigma^2)^{3/2}} \exp\left(-\frac{\omega^2}{4\sigma^2}\right). \tag{1.7}$$

We can note some remarkable features of these two distributions:

a) $P(\omega) \to 0$ as $\omega \to 0$. This basically means that there is level repulsion.

b) At large energy separations, $P(\omega)$ decays as a Gaussian.

We can write (1.6) and (1.7) as a single expression:

$$P(\omega) = A_\beta \omega^\beta \exp(-B_\beta \omega^2), \tag{1.8}$$

with $\beta = 1$ for systems with time-reversal symmetry and $\beta = 2$ otherwise and the coefficients A, B are found by normalizing $P(\omega)$ and fixing the mean value of the spacing. This calculation can be easily generalized to larger matrices, and it is possible to define an ensemble of random matrices drawn from a Gaussian distribution [63]:

$$P(H) \propto \exp\left(-\frac{\beta}{2a^2} \operatorname{Tr}\{H^2\}\right) = \exp\left(\frac{\beta}{2a^2} \sum_{ij} H_{ij} H_{ji}\right), \tag{1.9}$$

[1] For example, consider systems without an external magnetic fields.

where a indicates the overall energy scale. For systems with time-reversal symmetry ($\beta = 1$) all the entries in H are real, satisfying $H_{ij} = H_{ji}$, and we get the so-called Gaussian Orthogonal Ensemble (GOE). For $\beta = 2$ we have $H_{ij} = H^*_{ji}$, that is the Gaussian Unitary Ensemble (GUE). It can be noted that the $\sqrt{2}$ factor in (1.3) ensures the possibility of describing the Hamiltonian by the distribution (1.9).

Although we do not provide a detailed derivation of the level statistics, we point out some crucial properties of this result: first, the choice of the ensemble in (1.9) is natural, since the ensemble must be invariant under any orthogonal (GOE) or unitary (GUE) transformation. So, the distribution can only depend on the invariant $\mathrm{Tr}\{H^2\}$, which is a sum of many independent contributions and should satisify the central limit theorem. Second, the exact level spacing distributions (known as Wigner-Dyson distributions) do not have a precise analytical form, but they are both qualitatively and quantitatively close to (1.8), named the Wigner Surmise.

Since its formulation, Wigner's idea was intended to explain statistical properties of "complex" systems, but the range of validity of this theory was unclear until 1984, when Bohigas, Giannoni and Schmidt found that the level statistics of a system composed by a single particle in an infinite potential well with the shape of a Sinai billiard at high energies (i.e. in the semi-classical limit) was described by a Wigner-Dyson distribution[64]. Thus, they conjectured that RMT is able to describe quantum systems which have a classical chaotic counterpart. This conjecture, known as BGS conjecture, has been confirmed in many different setups, and very few counterexamples has been shown to violate it. The Wigner-Dyson level statistics is therefore considered a defining property of quantum chaotic systems.

Another important statement we can make exploiting RMT is about the eigenvectors of random matrices. In particular, the joint probability distributions of eigenvectors components is given by[65]

$$P_{GOE}(\psi_1, \psi_2, \cdots, \psi_N) \propto \delta\left(\sum_j \psi_j^2 - 1\right), \quad P_{GUE}(\psi_1, \psi_2, \cdots, \psi_N) \propto \delta\left(\sum_j |\psi_j|^2 - 1\right), \tag{1.10}$$

where ψ_j are the components of eigenvectors in some fixed basis. This expression follows from the orthogonal (unitary) invariance of the random matrix ensemble, since the distribution can depend only on the norm $\sqrt{(\sum_j \psi_j^2)}(\sqrt{(\sum_j |\psi_j|^2)})$ of the eigenvectors, and the normalization imposes the proportionality to the δ-functions. The essence of

(1.10) lies in the following statement: the eigenvectors of random matrices are random unit vectors, which can be real (GOE) or complex (GUE). One may wonder how can two eigenvectors be truly random, i.e. independent, if the orthogonality between them is required. However, in a large-dimensional space two uncorrelated random vectors are, in any case, nearly orthogonal, and thus these correlations due to the orthogonality can be neglected.

1.1.3 MATRIX ELEMENTS OF OPERATORS

We derive now the structure of matrix elements of hermitian operators such as

$$\hat{O} = \sum_i O_i \left|i\right\rangle \left\langle i\right| . \tag{1.11}$$

For any random Hamiltonian with eigenvectors $\left|m\right\rangle, \left|n\right\rangle$, the matrix elements of $\hat{O}$ are given by

$$O_{mn} = \langle m|\hat{O}|n\rangle = \sum_i O_i \left\langle m|i\right\rangle \left\langle i|n\right\rangle = \sum_i O_i (\psi_i^m)^* \psi_i^n, \tag{1.12}$$

where $\psi_i^m = \langle i|m\rangle$ and similarly for ψ_i^n. Recalling (1.10), we know that $\left|m\right\rangle, \left|n\right\rangle$ are essentially random orthogonal unit vectors. For a Hilbert space of dimension D we have

$$\left\langle (\psi_i^m)^* \psi_j^n \right\rangle = \frac{1}{D} \delta_{mn} \delta_{ij}, \tag{1.13}$$

which implies that the expectation values of diagonal and off-diagonal matrix elements of $\hat{O}$ are very different:

$$\left\langle \hat{O} \right\rangle_{mm} = \frac{1}{D} \sum_i O_i \equiv \langle \hat{O} \rangle , \qquad \left\langle \hat{O} \right\rangle_{mn} = 0, \text{ for } m \neq n. \tag{1.14}$$

Furthermore, we can note that the fluctuations of the diagonal and off-diagonal matrix elements are suppressed as the size of the Hilbert space increases:

$$\begin{aligned} \langle \hat{O}^2 \rangle_{mm} - \langle \hat{O} \rangle_{mm}^2 &= \sum_{ij} O_i O_j \left\langle (\psi_i^m)^* \psi_i^m (\psi_j^m)^* \psi_j^m \right\rangle - \sum_{ij} O_i O_j \left\langle (\psi_i^m)^* \psi_i^m \right\rangle \left\langle (\psi_j^m)^* \psi_j^m \right\rangle \\ &= \sum_i O_i^2 (\langle |\psi_i^m|^4 \rangle - \langle |\psi_i^m|^2 \rangle) = \frac{3-\beta}{D^2} \sum_i O_i^2 \equiv \frac{3-\beta}{D} \langle \hat{O}^2 \rangle , \end{aligned} \tag{1.15}$$

where we used the relations

$$\langle (\psi_i^m)^4 \rangle = 3[\langle (\psi_i^m)^2 \rangle]^2 \text{ for GOE} , \qquad \langle |\psi_i^m|^4 \rangle = 2[\langle |\psi_i^m|^2 \rangle]^2 \text{ for GUE} , \tag{1.16}$$

which are consequences of the components of the random vector ψ_i^m. For the off-diagonal terms, we have

$$\langle \hat{O}^2 \rangle_{mn} - \langle \hat{O} \rangle_{mn}^2 = \sum_i O_i^2 \, \langle |\psi_i^m|^2 |\psi_i^n|^2 \rangle = \frac{1}{D} \langle O^2 \rangle \, . \tag{1.17}$$

We can combine these expressions to get the matrix elements of any operator:

$$O_{mn} = \langle \hat{O} \rangle \, \delta_{mn} + \sqrt{\frac{\langle \hat{O}^2 \rangle}{D}} R_{mn}, \tag{1.18}$$

where R_{mn} is a random variable (real for the GOE and complex for the GUE) which has zero mean value and unit variance.

1.1.4 LEVEL STATISTICS OF QUANTUM INTEGRABLE SYSTEMS

As we discussed earlier, a classical indicator of integrability or chaoticity is the behaviour of trajectories in phase space at long times. In quantum systems, we can use as such an indicator the energy level statistics described in sect. 1.1.2, and chaotic quantum systems follow the Wigner-Dyson distribution. What happens in quantum integrable systems? This question was first raised by Berry and Tabor [66]. A simple example of a non-ergodic system with many degrees of freedom is an array of harmonic oscillators which oscillate with incommensurate frequencies, e.g. the normal modes in a harmonic chain. These oscillators can be diagonalized independently, and we can write the energy levels as

$$E = \sum_i n_i f_i, \tag{1.19}$$

where n_i are the occupation number and f_i the oscillation frequencies. At high energies, when n_i becomes very large and adjacent energy levels can be obtained from very different sets of $\{n_i\}$, we can consider E as effectively randomly distributed and uncorrelated from each other. If we take the particular energy shell $[E, E + \delta E]$, the level statistics can be described by Poisson statistics, which gives the probability of finding n energy levels in that particular interval, that is

$$P_n = \frac{\lambda^n}{n!} \exp(-\lambda), \tag{1.20}$$

where λ is the average number of levels in the given shell. The main difference between Poisson and Wigner-Dyson statistics is that in the former there is no level repulsion,

i.e. the possibility of degenerate energy levels appears. The distribution of energy levels spacing $P(\omega)$ in integrable systems is

$$P_0(\omega) = \exp(-\omega), \tag{1.21}$$

in which we set the mean separation to one. The idea that, in quantum systems whose classical counterpart is integrable (and in integrable quantum systems without a classical counterpart), the energy eigenvalues behaviour can be described by Poisson statistics, is known as the Berry-Tabor conjecture[66]. For systems in which the BT conjecture does not hold, deviations from Poisson distribution are usually due to additional symmetries in the Hamiltonian that lead to extra degeneracies.
What we have discussed so far about level statistics is commonly used in the study of many-particle systems. The emergence of Wigner-Dyson or Poisson distribution of energy levels separation serves as on of the main indicators of quantum chaos or integrability in a quantum system. In other words, it often indicates whether a system is ergodic or not. Although its success, the applicability of RMT, as of any other theory, has limits: it requires energy levels far from the spectrum edges, i.e. no ground states, low-lying excited states and highest energy excited states, and the density of states as a function of energy must be accounted for.

1.1.5 BERRY'S CONJECTURE

We now discuss one of the most remarkable connections between the structure of eigenstates of chaotic systems in the semi-classical limit and classical chaos: the Berry's conjecture[67]. In order to explain this significant result, we have to introduce the Wigner function $W(\boldsymbol{x}, \boldsymbol{p})$, defined as the Weyl transform of the density matrix $\hat{\rho}$[68,69]. The Weyl transform (or Weyl symbol) is the key ingredient in the phase space description of quantum systems, and gives a one to one map between quantum operators and the ordinary functions defined in the phase space. The Weyl symbol $A_W(\boldsymbol{x}, \boldsymbol{p})$ of an operator $\hat{A}(\hat{\boldsymbol{x}}, \hat{\boldsymbol{p}})$ is formally defined by

$$A_W(\boldsymbol{x}, \boldsymbol{p}) = \int d\boldsymbol{\xi} \left\langle \boldsymbol{x} - \frac{\boldsymbol{\xi}}{2} \middle| \hat{A}(\hat{\boldsymbol{x}}, \hat{\boldsymbol{p}} \middle| \boldsymbol{x} + \frac{\boldsymbol{\xi}}{2} \right\rangle \exp\left(i \frac{\boldsymbol{p}\boldsymbol{\xi}}{\hbar} \right), \tag{1.22}$$

where we use the vector notations to highlight that we are dealing with general d-dimensional multi-particle phase space of the dimension 2D, where the factor two reflects

that for each degree of freedom we are dealing with pairs of conjugate variables. For a pure state, i.e. $\rho = |\psi\rangle\langle\psi|$, the Wigner function $W(\boldsymbol{x}, \boldsymbol{p})$ is

$$W(\boldsymbol{x}, \boldsymbol{p}) = \frac{1}{(2\pi\hbar)^{3N}} \int d^{3N}\boldsymbol{\xi} \psi^* \left(\boldsymbol{x} + \frac{\boldsymbol{\xi}}{2}\right) \psi \left(\boldsymbol{x} - \frac{\boldsymbol{\xi}}{2}\right) \exp\left(-i\frac{\boldsymbol{p}\boldsymbol{\xi}}{\hbar}\right), \tag{1.23}$$

for a system of N particles spanning a $6N$-dimensional phase space. If we consider a mixed state, we must operate the substitution

$$\psi^* \left(\boldsymbol{x} + \frac{\boldsymbol{\xi}}{2}\right) \psi \left(\boldsymbol{x} - \frac{\boldsymbol{\xi}}{2}\right) \to \left\langle \boldsymbol{x} - \frac{\boldsymbol{\xi}}{2} \middle| \hat{\rho} \middle| \boldsymbol{x} + \frac{\boldsymbol{\xi}}{2} \right\rangle = \rho \left(\boldsymbol{x} - \frac{\boldsymbol{\xi}}{2}, \boldsymbol{x} + \frac{\boldsymbol{\xi}}{2}\right). \tag{1.24}$$

We can equivalently define the Wigner function by integrating over momentum

$$W(\boldsymbol{x}, \boldsymbol{p}) = \frac{1}{(2\pi\hbar)^{3N}} \int d^{3N}\eta \phi^* \left(\boldsymbol{p} + \frac{\eta}{2}\phi\right) \phi \left(\boldsymbol{p} - \frac{\eta}{2}\phi\right) \exp\left(i\frac{\boldsymbol{x}\eta}{\hbar}\right), \tag{1.25}$$

where $\phi(\boldsymbol{p})$ is the Fourier transfom of $\psi(\boldsymbol{x})$. It can be seen from both the representations that

$$\int d^{3N}p W(\boldsymbol{x}, \boldsymbol{P}) = |\psi(\boldsymbol{x})|^2, \quad \int d^{3N}x W(\boldsymbol{x}, \boldsymbol{P}) = |\phi(\boldsymbol{p})|^2. \tag{1.26}$$

The Wigner function allows us to compute the expectation value on any observable $\hat{A}$ as[68,69]

$$\langle \hat{A} \rangle = \int d^{3N}x d^{3N}p \; A_W(\boldsymbol{x}, \boldsymbol{p}) W(\boldsymbol{x}, \boldsymbol{p}), \tag{1.27}$$

with $A_W(\boldsymbol{x}, \boldsymbol{p})$ is the Weyl sybol of $\hat{A}$ given by (1.22). The intuitive conjecture formulated by Berry suggests that, in the semiclassical limit of a quantum system which has a chaotic classical counterpart, the Wigner function of energy eigenstates (over a small phase space) reduces to the microcanonical distribution. In mathematical terms it states that, once defined

$$\overline{W(\boldsymbol{X}, \boldsymbol{P})} = \int_{\Delta\Omega_1} \frac{dx_1 dp_1}{2\pi\hbar} \cdots \int_{\Delta\Omega_N} \frac{dx_N dp_N}{2\pi\hbar} W(\boldsymbol{x}, \boldsymbol{p}), \tag{1.28}$$

where $\Delta\Omega_j$ is a small phase-space volume centered in (X_j, P_j), chosen in order to have $\Delta\Omega_j \to 0$ as $\hbar \to 0$ and at the same time $\hbar/\Delta\Omega_j \to 0$, then

$$\overline{W(\boldsymbol{X}, \boldsymbol{P})} = \frac{1}{\int d^{3N}X d^{3N}P \delta[E - H(\boldsymbol{X}, \boldsymbol{P})]} \delta[E - H(\boldsymbol{X}, \boldsymbol{P})]. \tag{1.29}$$

Essentially, Berry considered $\psi(\boldsymbol{x})$ as a Gaussian random variable whose spectrum at $\boldsymbol{x}$ is simply the local average of the Wigner function $\overline{W(\boldsymbol{x}, \boldsymbol{p})}$.

DILUTE GAS OF HARD SPHERES

Srednicki[13], following Berry's conjecture, studied the behaviour of a dilute gas of hard spheres, arguing that the energy eigenstate expectation value of any observable in the semiclassical limit is the same as a microcanonical average. Given an energy eigenvalue E_n, the corresponding eigenstate can be written as

$$\psi_n(\boldsymbol{x}) = N_n \int d^{3N}p \; A_n(\boldsymbol{p})\delta(\boldsymbol{p}^2 - 2mE_n) \exp\left(i\frac{\boldsymbol{p}\boldsymbol{x}}{\hbar}\right), \tag{1.30}$$

where N_n is a normalization factor determined by

$$\int d^{3N}x \; \psi_n^2(\boldsymbol{x}) = 1, \tag{1.31}$$

and $A_n^*(\boldsymbol{p}) = A_n(-\boldsymbol{p})$. The energy eigestates with energy E_n are given by a superposition of plane-waves with momentum $\boldsymbol{p}$ such that $E_n = \boldsymbol{p}^2/2m$. For this system, Berry's conjecture is equivalent to assuming that $A(\boldsymbol{p})$ can be treated as a Gaussian random variable with a two-point correlation function given by

$$\langle A_m(\boldsymbol{p})A_n(\boldsymbol{p'})\rangle_{EE} = \delta_{mn}\frac{\delta^{3N}(\boldsymbol{p}+\boldsymbol{p'})}{\delta(|\boldsymbol{p}|^2 - |\boldsymbol{p'}|^2)}, \tag{1.32}$$

where the subscript EE stands for *Eigenstate Ensemble*, which is a fictitious ensemble which describe the properties of a typical eigenfunction. Individual eigenfunctions behave as if they were selected at random from the eigenstate ensemble.

Starting from these assumptions, Srednicki described how to compute observables of interest in the Hamiltonian eigenstates. For example, he was able to calculate the momentum distribution function of particles within the eigenstate ensemble as

$$\langle \phi_{nn}(\boldsymbol{p}_1\rangle_{EE} = \int d^3p_2 \cdots d^3p_n \;\; \langle \phi_n^*(\boldsymbol{p})\phi_n(\boldsymbol{p})\rangle_{EE} = N_n^2 L^{3N} \int d^3p_2 \cdots d^3p_n \delta(\boldsymbol{p^2} - 2mE_n), \tag{1.33}$$

where $\phi_n(\boldsymbol{p})$ is the $3N$-dimensional Fourier transform of $\psi_n(\boldsymbol{x})$ and we used[13]

$$\langle \phi_m^*(\boldsymbol{p})\phi_n(\boldsymbol{p'})\rangle_{EE} = \delta_m n N_n^2 (2\pi\hbar)^{3N}\delta(\boldsymbol{p}^2 - 2mE_n)\delta_V^{3N}(\boldsymbol{p}-\boldsymbol{p'}), \tag{1.34}$$

where

$$\delta_V^{3N}(\boldsymbol{p}) = (2\pi\hbar)^{-3N}\int_V d^{3N}x \;\; \exp\left(i\frac{\boldsymbol{p}\boldsymbol{x}}{\hbar}\right), \tag{1.35}$$

and $V = L^3$ is the volume of the system.

Since

$$I_N(A) \equiv \int d^N p \; \delta(\boldsymbol{p}^2 - A) = \frac{(\pi A)^{N/2}}{\Gamma(N/2A)}, \tag{1.36}$$

one obtains

$$\langle \phi_{nn}(\boldsymbol{p}_1) \rangle_{EE} = \frac{I_{3N-3}(2mE_n - \boldsymbol{p}_1^2)}{I_{3N}(2mE_n)} = \frac{\Gamma(3N/2)}{\Gamma[3(N-1)/2]} \left(\frac{1}{2\pi m E_n}\right)^{\frac{3}{2}} \left(1 - \frac{\boldsymbol{p}_1^2}{2mE_n}\right)^{\frac{3N-5}{2}}. \tag{1.37}$$

Exploiting the classical equipartition of energy, i.e. $E_n = 3Nk_bT_n/2$, we can define a microcanonical temperature T_n, and taking the limit $N \to \infty$ we get

$$\langle \phi_{nn}(\boldsymbol{p}_1) \rangle_{EE} = \left(\frac{1}{2\pi m k_B T_n}\right)^{\frac{3}{2}} \exp\left(\frac{\boldsymbol{p}_1^2}{2mk_bT - n}\right), \tag{1.38}$$

where we used the Gamma function property

$$\lim_{N\to\infty} \frac{\Gamma(N+B)}{\Gamma(N)N^B} = 1, \quad \text{if } B \in \mathbb{R}. \tag{1.39}$$

We can immediately notice that the result obtained is exactly the Maxwell-Boltzmann momenta distribution in a thermal gas. Furthermore, it can be shown that if one considers a symmetric (antisymmetric) $\psi_n(\boldsymbol{x})$ one obtains the canonical Bose-Einstein (Fermi-Dirac) distribution[13]. The ideas described so far underlie the focus of the next section, i.e. the eigenstate thermalization hypothesis.

1.2 CHAOS AND THERMALIZATION IN QUANTUM SYSTEMS

Since its introduction by Wigner, random matrix statistics has been applied to a wide variety of systems, extending far beyond the framework of its original motivation. Examples of quantum systems which are known to show Wigner-Dyson statistics are:

- Heavy nuclei[70]
- Sinai billiards[64]
- Highly excited energy levels of the hydrogen atom in a strong magnetic field[71]
- Spin-1/2 systems and spinless fermions in one-dimensional lattices[72,73].

In this section, we briefly discuss the latter example of lattice models and we then turn to the definition of thermalization in quantum systems and the eigenstate thermalization hypothesis.

1.2.1 LATTICE MODELS

As we mentioned in 1.1.4, the Berry-Tabor conjecture and RMT theory results also apply to interacting many-body systems that do not have a classical counterpart. Here, we

show some results from [72], in which a prototyipical lattice model of spinless fermions with nearest and next-nearest-neighbor hoppings and interactions is considered:

$$\begin{aligned}\hat{H} = \sum_{j=1}^{L} \Big[& - J(f_j^\dagger f_{j+1} + h.c.) + V\Big(n_j - \frac{1}{2}\Big)\Big(n_{j+1} - \frac{1}{2}\Big) \\ & - J'(f_j^\dagger f_{j+2} + h.c.) + V'\Big(n_j - \frac{1}{2}\Big)\Big(n_{j+2} - \frac{1}{2}\Big)\Big],\end{aligned} \tag{1.40}$$

where f_j and $f_j^\dagger$ are fermionic annihilation and creation operators at site j, n_j is the occupation number at site j and L is the total number of lattice sites.

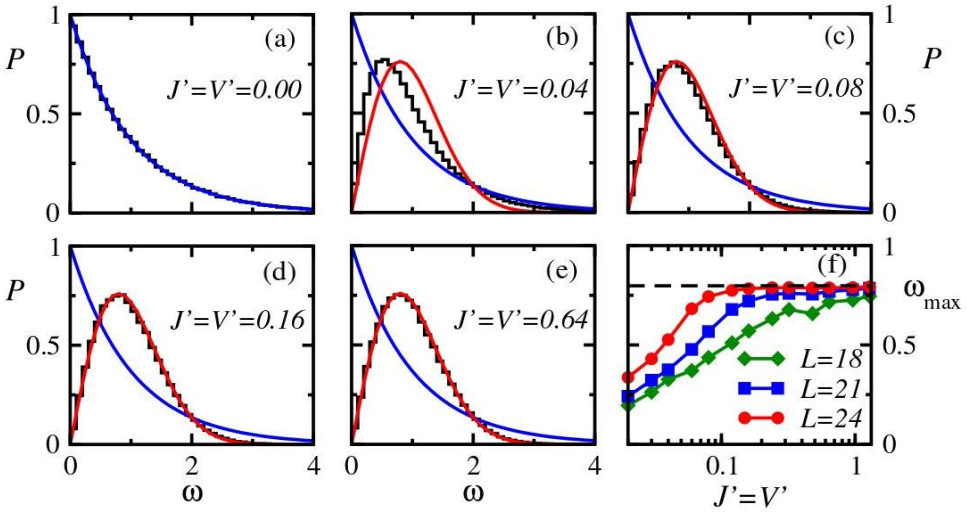

Figure 1.2: (a)-(e) Black line: level spacing distribution of spinless fermions in a one-dimensional chain, described by (1.40), for $L = 24$, $N = L/3$, $J = V = 1$ and $J' = V'$ vs the normalized spacing ω. The blue and red lines are the reference Poisson and GOE distributions, respectively. (f) Position of the maximum value of $P(\omega)$, denoted as ω_{max}, vs $J' = V'$. The dashed horizontal line is the GOE prediction. Plots from [72] .

In this example, we approach a dense energy spectrum, and quantum chaos, by increasing the system size L. The Hamiltonian (1.40) becomes integrable if $J' = V' = 0$, and can be mapped into the well-known XXZ spin-1/2 model [74].

In figure 1.2(a)-1.2(g) we report the level spacing distribution $P(\omega)$ of a system described by (1.40). We can clearly see how the increasing of the integrability, i.e. the increasing of $J' = V'$, starting from 0, produces a transition from a distribution almost indistinguishable from the Poisson one to the Wigner-Dyson distribution[2]. During this transition from integrability to ergodicity, there is a crossover distribution which does not resemble either Poisson or Wigner-Dyson distribution. However, it can be noticed from panel (h) how the system size growth causes a saturation of the level spacing statistics towards the value suggested from RMT calculations. This result suggest that, for this type of lattice models, quantum chaos in thermodynamic limit can be generated by an infinitesimal perturbation that breaks integrability. Recent numerical works have tried to quantify how the strength of the integrability breaking terms should scale with respect to the system size in order for the GOE predictions to hold in one-dimension [75,76]. The results of these studies indicate that the strength needs to scale $\propto L^{-3}$, but the origin of this exact scaling is still unclear. Moreover, in systems which are of particular interest for the present work, i.e. disordered many-body localized systems, the transition from Poisson to Wigner-Dyson statistics has been argued to occur at a finite value of the interaction strength [77], leading to a finite value of the integrability breaking perturbation even in the thermodynamic limit.

1.2.2 QUANTUM CHAOS AND ENTROPY

As we already discussed, chaos in classical systems is usually associated with the exponential divergence in time of nearby trajectories in phase-space. This language, since there is not a well-defined analogue of a trajectory in quantum mechanics, does not translate to quantum chaotic systems. Thus, the challenge is to find a common framework in which this discrepancy between quantum and classical chaos vanishes. In fact, one can treat quantum and classical systems on the same footing by studying the *delocalization* of the system either in phase space or in energy space, and with appropriate entropy measures to characterize this delocalization it is possible to analyze various quantum to classical crossovers. Let us consider a system prepared in some initial state, allowed to evolve according to a time-dependent Hamiltonian $\hat{H}$. If the initial state is a stationary state of some different Hamiltonian $\hat{H}_0 \neq \hat{H}$, this procedure is usually called a

[2]GOE in this case, since (1.40) is time-reversal invariant.

quench. For example, consider a system of spins (classical or quantum) in which one suddenly changes the strength of an external magnetic field or the coupling between the spins. From a classical point of view, the manifestation of chaos is represented by the delocalization in the available phase space after the quench. This delocalization can be quantified by the entropy, defined in phase space as

$$S = -\int\int \frac{d\boldsymbol{x}d\boldsymbol{p}}{(2\pi\hbar)^D}\rho(\boldsymbol{x},\boldsymbol{p})\ln[\rho(\boldsymbol{x},\boldsymbol{p})], \tag{1.41}$$

in which $\rho(\boldsymbol{x},\boldsymbol{p})$ is the classical probability distribution and D is the dimension of the phase-space. In an isolated system, as a consequence of the incompressibility of classical trajectories, which implies that volumes in phase-space do not change in time, the entropy (1.41) is a conserved quantity[4]. The lack of entropy increase was at the center of controversy for long time, since Boltzmann introduced his H-theorem. To avoid this problem, one can restrict the entropy measure to a portion of the total particles, using the reduced probability distribution of N_A particles obtained by averaging over the positions and momenta of the other particles,

$$\rho_A(\boldsymbol{x}_1,\cdots,\boldsymbol{x}_{N_A},\boldsymbol{p}_1,\cdots,\boldsymbol{p}_{N_A},t) = \int\int \prod_{i=N+1}^{N} d\boldsymbol{x}_i d\boldsymbol{p}_i\ \rho(\boldsymbol{x},\boldsymbol{p},t), \tag{1.42}$$

with $\boldsymbol{x} = (\boldsymbol{x}_1,\cdots,\boldsymbol{x}_N)$ and $\boldsymbol{p} = (\boldsymbol{p}_1,\cdots,\boldsymbol{p}_N)$. The entropy computed on this reduced probability distribution is not restricted by Liouville's theorem and after a quench it is expected to grow in time to the maximum value prescribed by the Gibbs distribution.
In quantum systems, we use the formalism of the density matrices instead of probability distribution. Given a density matrix $\hat{\rho}$, an analogue of the classical entropy (1.41) is given by the von Neumann Entropy:

$$S = -\operatorname{Tr}\{\hat{\rho}\log\hat{\rho}\}. \tag{1.43}$$

Even in the quantum case, the entropy is conserved for isolated systems, as a consequence of unitary evolution. Extending the analogy with the classical framework, we can work with reduced density matrices, defined using a partial trace,

$$\hat{\rho}_A = \operatorname{Tr}_B\{\hat{\rho}\} = \sum_{n_A,n'_A} |n_A\rangle\langle n'_A| \sum_{n_B}\langle n_A,n_B|\hat{\rho}|n'_A,n'_B\rangle\,, \tag{1.44}$$

where $|n_A\rangle$ and $|n_B\rangle$ are complete basis sets for two subsystems A and B. We can now define the von Neumann entropy of $\hat{\rho}_A$ as

$$S^A = -\operatorname{Tr}_A\{\hat{\rho}_A\log\hat{\rho}_A\}. \tag{1.45}$$

The von Neumann entropy, often called entanglement entropy, has been intensively studied in many different contexts, such as quenching and thermalization in interacting systems[78–80] or disordered systems showing many-body localization, and has been used as a fundamental indicator of peculiar transitions from ergodic to non-ergodic phases.

We can reveal delocalization of classical systems in phase-space also studying the entropy of the time-averaged probability distribution over a time interval $[0, \tau]$

$$\rho_\tau(\boldsymbol{x}, \boldsymbol{p}, t) = \frac{1}{\tau} \int_0^\tau \rho(\boldsymbol{x}, \boldsymbol{p}). \tag{1.46}$$

Since the negative logarithm is a convex function, we can notice that such an entropy can only increase as a function of τ. The difference between ergodic and non ergodic systems is straightforward: ergodic ones are expected to increase their entropy to its maximal allowed value, i.e. the microcanonical expected value, because the system on average visits all the accessible points in phase space with equal probability. On the other hand, non-ergodic systems are expected to stay more localized in phase-space even after long times, so that the entropy never reaches its microcanonical value. Once again in analogy with the classical picture, a second possibility to reveal quantum delocalization using entropy, is to study the entropy of the time-averaged density matrix. The off-diagonal matrix elements of the density matrix in the Hamiltonian basis oscillate according to[81]

$$\rho_{\alpha\beta}(t) = \rho_{\alpha\beta}(t_0)\, \mathrm{e}^{-i(E_\alpha - E_\beta)(t-t_0)}\,. \tag{1.47}$$

It is therefore clear that in quantum language time-averaging operations are equivalent to projecting the initial density matrix onto the diagonal subspace of the Hamiltonian, and this lead to the so-called *diagonal ensemble* density matrix[14]

$$\hat{\rho}_D \equiv \bar{\hat{\rho}} \equiv \lim_{\tau\to\infty} \frac{1}{\tau} \int_0^\tau \hat{\rho}(t) dt = \sum_\alpha \rho_{\alpha\alpha} \left|\alpha\right\rangle \left\langle\alpha\right|. \tag{1.48}$$

Thus, studying delocalization of classical probability distribution in phase space corresponds to the study of the spreading of the initial density matrix in the eigenstates basis of the Hamiltonian. For quantum chaotic system the prediction is that the diagonal density matrix will generically be delocalized. Conversely, for integrable systems, the diagonal density matrix can be more or less localized depending on the inital state.

1.2.3 QUANTUM THERMALIZATION

As we mentioned in the introduction to this chapter, von Neumann was one of the first to address the issue of ergodicity and thermalization in quantum mechanical systems[3]. One of the crucial intuitions underlying his work was to focus on macroscopic observables, as opposed to focusing on the wave function or the density matrix of the total system. His quantum ergodic theorem, which was a very important first step in the study of quantum thermalization, states that for a finite family of commuting macroscopic observables, every wave function, starting from an initial microcanonical energy shell, evolves so that for most times in the long run, the probability distribution of these observables obtained from the unitarily time-evolved wave function is close to their microcanonical distribution[82]. Considering all the ideas presented so far, it is obvious that this theorem, although fundamental, lacks something: for example, it does not distinguish between the behaviour of integrable and non-integrable systems. We will see how von Neumann's theorem is linked to the RMT and how it contains the seed for the eigenstate thermalization hypothesis, the nucleus of this section.

Suppose that a closed system is prepared in a nonstationary state, which has a well-defined mean energy. We said that an observable thermalizes if, evolving under its own Hamiltonian dynamics, it expectation value relaxes towards the microcanonical prediction and remains close to it for almost every later time. Let us prepare a setup in which an isolated system described by a time-independent Hamiltonian $\hat{H}$ is prepared in a pure state $|\psi(0)\rangle$[3]. Denote the the eigenstates of this system by $|E_\alpha\rangle$, corresponding to the eigenvalues E_α, given by $\hat{H}\,|E_\alpha\rangle = E_\alpha\,|E_\alpha\rangle$. The initial state and its well-defined mean energy can be written as

$$|\psi(0)\rangle = \sum_\alpha c_\alpha\,|E_\alpha\rangle\,, \qquad \langle E\rangle = \langle\psi(0)|\hat{H}|\psi(0)\rangle \sum_\alpha |c_\alpha|^2 E_\alpha, \tag{1.49}$$

with $c_\alpha = \langle E_\alpha|\psi(0)\rangle$, and the time-evolving state is

$$|\psi(t)\rangle = \sum_\alpha c_\alpha\,\mathrm{e}^{-iE_\alpha t}\,|E_\alpha\rangle\,. \tag{1.50}$$

Let us look now at the time evolution of some observable $\hat{A}$, which can be written in the

[3]This discussion can be straightforwardly generalized to the case of a mixed state.

basis of the Hamiltonian eigenstates,

$$\begin{aligned} A(t) \equiv \langle\psi(t)|\hat{A}|\psi(t)\rangle &= \sum_{\alpha,\beta} c_\alpha^* c_\beta \, \mathrm{e}^{i(E_\alpha - E_\beta)t} \, A_{\alpha\beta} \\ &= \sum_\alpha |c_\alpha|^2 A_{\alpha\alpha} + \sum_{\alpha\neq\beta} c_\alpha^* c_\beta \, \mathrm{e}^{i(E_\alpha - E_\beta)t} \, A_{\alpha\beta}, \end{aligned} \tag{1.51}$$

where $A_{\alpha\beta} = \langle E_\alpha|\hat{A}|E_\beta\rangle$.

The conditions required for an observable to thermalize, i.e. agreement of the average expectation value with the microcanonical prediction, and small fluctuations of this value at most later times, present some difficulties in reconciling with (1.51). In fact, some of the natural questions emerging are: (a) Since in the long-time average we are left with the sum of the diagonal elements of $\hat{A}$ weighted by $|c_\alpha|^2$, which are conserved in time, how is it possible for $\overline{A}$ to agree with the microcanonical prediction? (b) In many-body systems, the eigenvalues are exponentially close to each other, and to make sure that the second sum in (1.51) effectively sum to 0 one may wait for an exponentially long time, which, even for relatively small systems, could exceed the age of our universe. This is of course in open contrast with our daily experience and measurements, that prove that even large systems thermalize over time scales much shorter than the age of the universe. The answer to these questions were provided during the 1990s by Srednicki's groundbreaking works, in which he constructed a generalization of the RMT prediction about observables in quantum systems (see eq. (1.18)), known as the ETH.

1.2.4 THE EIGENSTATE THERMALIZATION HYPOTHESIS

We can state the ETH as an ansatz for the matrix elements of observables in the hamiltonian eigenstates basis[83]:

$$A_{\alpha\beta} = A(\overline{E})\delta_{\alpha\beta} + \mathrm{e}^{-S(\overline{E}/2)} \, f_A(\overline{E}, \omega) R_{\alpha\beta}, \tag{1.52}$$

where $\overline{E} = (E_\alpha + E_\beta)/2$, $\omega = E_\alpha - E_\beta$, and $S(E)$ is the thermodynamic entropy at energy E. $A(\overline{E})$ is identical to the expectation value of the microcanonical ensemble at energy $\overline{E}$ and $R_{\alpha\beta}$ is a random (real or complex) number with zero mean value and unit variance. ETH has been numerically verified for few-body observables, i.e. n-body observables with $n \ll N$, in many lattice models. This kind of observables form the class of physically measurable quantities, which can be studied experimentally in macroscopic

systems. The ansatz (1.52) is similar to the RMT result (1.18), but it presents some differences: first, the diagonal elements of $A(\overline{A})$ are not the same in all eigenstates, but they are smooth functions of the eigenenergies. Second, for the off-diagonal elements, there is a function $f_A(\overline{E}, \omega)$ that depends on the mean energy and the energy mismatch between the states involved. One recovers the original RMT prediction focusing on a very narrow energy shell, where $f_A(\overline{E}, \omega)$ is constant. In a single-particle system with diffusive dynamics, this scale is given by the Thouless energy [84]:

$$E_T = \frac{\hbar L^2}{D}, \tag{1.53}$$

where D is the diffusion constant. Thus, if one focus on an energy window with $\omega < E_T$ the ETH ansatz is identical to RMT result.

Now, let us focus on the implications of the ETH ansatz to the thermalization mechanism. Starting from (1.51), we can define the time-average of $A(t)$ as

$$\overline{A} \equiv \lim_{\tau\to\infty} \frac{1}{\tau} \int_0^\tau dt\, \langle\psi(t)|\hat{A}|\psi(t)\rangle = \sum_\alpha |c_\alpha|^2 A_{\alpha\alpha}, \tag{1.54}$$

and we note that the off-diagonal terms in (1.51) dephase on taking the time average (in the thermodynamical limit), such that $\overline{A}$ is determined only by the diagonal contribution. On the other hand, the time averaged observable should agree with the microcanonical average

$$A_{mc} = \frac{1}{\mathcal{N}} \sum_{\alpha=1}^{\mathcal{N}} A_{\alpha\alpha}, \tag{1.55}$$

where the sum runs over all accessible states in the microcanonical window $[\overline{E}-\Delta, \overline{E}+\Delta]$. We then see that, independently from the actual values of c_α, so long as the quantum uncertainty

$$\Delta \equiv \sqrt{\langle\psi(0)|\hat{H}^2|\psi(0)\rangle - \langle\psi(0)|\hat{H}|\psi(0)\rangle^2} \tag{1.56}$$

is sufficiently small, $\overline{A}$ will agree with the statistical mechanics prediction thanks to the ETH ansatz. In fact, using (1.52), one can rewrite (1.51) and (1.55) as

$$\overline{A} \simeq A(\langle E\rangle) \simeq A_{mc}. \tag{1.57}$$

Furthermore, we can expand the smooth function $A(E)$ around the mean energy $\langle E\rangle$, obtaining

$$A_{\alpha\alpha} \approx A(\langle E\rangle) + (E_\alpha - \langle E\rangle)\frac{dA}{dE}\bigg|_{\langle E\rangle} + \frac{1}{2}(E_\alpha - \langle E\rangle)^2 \frac{d^2A}{dE^2}\bigg|_{\langle E\rangle}, \tag{1.58}$$

and inserting this expansion in (1.54), we get

$$\overline{A} \approx A(\langle E\rangle) + \frac{1}{2}(\delta E)^2 A''(\langle E\rangle) \approx A_{mc} + \frac{1}{2}[(\delta E)^2 - (\delta E_{mc})^2]A''(\langle E\rangle), \tag{1.59}$$

where δE_{mc} are the energy fluctuations in the microcanonical ensemble, which are subextensive. If the energy fluctuations δE in the time-evolving system are subextensive too, the second term is just a small subextensive correction to the A_{mc}, which we can neglect for large system sizes. Thus, using ETH, one can show that $\overline{A} \simeq A_{mc}$ without any assumption about the distribution of c_α, except that it is narrow.
Moreover, using the ETH ansatz, we can compute the long-time average of the temporal fluctuations of the expectation value of $\hat{A}$,

$$\begin{aligned}
\sigma_A^2 &\equiv \lim_{\tau\to\infty} \frac{1}{\tau}\int_0^\tau dt\ [A(t)]^2 - (\overline{A})^2 \\
&= \lim_{\tau\to\infty} \frac{1}{\tau}\int_0^\tau dt \sum_{\alpha,\beta,\gamma,\delta} A_{\alpha\beta}A_{\gamma\delta}c_\alpha^* c_\beta c_\gamma^* c_\delta\, \mathrm{e}^{i(E_\alpha - E_\beta + E_\gamma - E_\delta)t} - (\overline{A})^2 \\
&= \sum_{\alpha,\beta\neq\alpha} |c_\alpha|^2|c_\beta|^2|A_{\alpha\beta}|^2 \leq \max|A_{\alpha\beta}|^2 \sum_{\alpha,\beta} |c_\alpha|^2|c_\beta|^2 = \max|A_{\alpha\beta}|^2 \propto \mathrm{e}^{-S(\overline{E})}\,.
\end{aligned} \tag{1.60}$$

Thus, the time fluctuations of the expectation value of $\hat{A}$ are exponentially small as the system size is increased. Eq. (1.60) tells us that at almost any point in time an observable $\hat{A}$ relaxes towards the value prescribed by its diagonal ensemble, meaning that ETH implies ergodicity without needing time-averaging operations.

Summarizing what we have discussed in this chapter, we saw how the language by which we describe classical thermalization changes when studying quantum systems. Every crucial aspect that characterizes the thermalization mechanism, i.e. chaos and ergodicity, can be found in the nature of the Hamiltonian eigenstates. Relaxation of the observables towards their equilibrium values follows from dephasing, as emphasized by the second term of eq. (1.54). The information about thermalization are hidden in the system from the very beginning, and what reveals them is simply the time evolution. Now, turning to the next chapter, we would like to stress again that the ETH is a hypothesis and need not hold for all kinds of quantum systems. Besides integrable systems, we will see very soon that another important class of systems, which have gained a massive interest in the past decade and represent the focus of this thesis, completely fail to thermalize: localized systems.

2

ERGODICITY BREAKING AND LOCALIZATION

The ambitious aim of P. W. Anderson's most famous paper was to "lay the foundation for a quantum mechanical theory of transport"[15]. His study was motivated by some unexplained experimental observations made by Fletcher and Feher at Bell Laboratories, in which they measured anomalously long relaxation times for electron spins in semiconductor samples doped with a large injection of impurities[85,86]. In his work, Anderson showed that the eigenfunctions of non-interacting electrons in the presence of disorder are exponentially localized around a certain site or position. This spatial localization denies the possibility of heat or electrical conduction, leading to macroscopic consequences in the behaviour of disordered materials. This significant result stands at the intersection between two fundamental streams of research in condensed matter physics, i.e. the study of transport and conductance in solids and the role of disorder and impurities, which are almost always present.

2.1 SINGLE-PARTICLE LOCALIZATION

We briefly discuss now Anderson's calculation more precisely. Anderson simplified Feher's problem, restricting to a tight-binding model with free electrons hopping on a lattice with disordered onsite potentials

$$HatH = \sum_i \epsilon_i c_i^\dagger c_i + \sum_{i \neq j} [V_{ij} c_i^\dagger c_i + h.c.], \tag{2.1}$$

where $c_i^\dagger$, c_i are the usual fermionic creation and annihilation operators on site i, V_{ij} are the shot-ranged translationally invariant hopping terms and ϵ_i are onsite energies, taken as random variables within a uniform distribution of width $[-W, W]$. It is important to note that when this Hamiltonian is expressed in terms of spin operators through the Jordan-Wigner transformation, it amounts to neglecting the $S_i^z S_j^z$ term in the Hamiltonian. We can specialize to the case $V_{ij} = V$, i.e. we consider only nearest-neighbor hopping between sites, and we are able to analyze the so-called *locator limit* in which $V \ll W$, where we can proceed with a perturbative calculation, in which the unperturbed states are eigenstates of $HatH_0 = \sum_i \epsilon_i c_i^\dagger c_i$, while the hopping term is the perturbation. In this particular limit, the eigenstates essentially lie on single sites, $|i\rangle = c_i^\dagger |0\rangle$, and the hopping is highly detuned from the typical nearest-neighbor potential mismatch $(\epsilon_{i+1} - \epsilon_i) \sim W \gg V$. This weak hopping is not able to hybridize nearby sites, and two sites at distance r typically become "mixed" at rth order of perturbation theory with a strength $V(\frac{V}{W})^r \sim V\,\mathrm{e}^{-\frac{r}{\xi}}$, leading to eigenstates with an exponentially localized asymptotic form

$$|\psi(r)|^2 \sim \mathrm{e}^{-\frac{r-R}{\xi}}, \tag{2.2}$$

where R is the localization centre of $\psi(r)$ and ξ is known as the *localization length*, and it depends on the disorder strength and on the energy[77]. This lack of thermalization can be easily understood by considering a system initialized in a precise spatially non-uniform distribution density of particles in the localized states over a large length scale: this non-uniform distribution will survive for all times, due to localization. Anderson pointed out[15] that this heuristic perturbative approach can break down in some samples at high perturbation order n due to "resonances" wherein two sites separated by a distance n could have almost degenerate potentials, i.e. $|\epsilon_i - \epsilon_{i+n}| \lesssim V\,\mathrm{e}^{-\frac{r}{\xi}}$, leading to a vanishing energy denominator and a large tunneling. These resonances could affect the convergence of the perturbation theory, and it is therefore necessary to estimate these resonances probability and prove that they are extremely rare. This can be addressed by renormalizing the bare energy levels of the resonating sites self consistently, mitigating the divergence. Thus, by taking into account terms at all orders of the perturbation theory, for weak enough hopping and infinite system size, the initial state has an infinite life time with probability one.

Anderson's model marked the beginning of a long and flourish research stream on quantum properties of delocalization-localization transitions [1], a research stream still very active to this date. It was shown that in one and two dimensions *all* electronic wavefunctions at all energies are exponentially localized for any finite disorder strength, implying a vanishing conductivity $\sigma(T) = 0$ for every T. In 1967, Mott[88] introduced the idea that in three (or higher) dimension the localized and extended states are separated by a sharp *mobility edge* in energy. Thus, for $d \geq 3$, the conductivity is strictly zero only at $T = 0$, while obeys an exponential law:

$$\sigma(T) \sim \mathrm{e}^{\frac{-E_c}{T}} \tag{2.3}$$

for finite temperatures, where E_c is the difference between the mobility edge and the Fermi level.

2.1.1 SCALING THEORY FOR ANDERSON LOCALIZATION TRANSITION

A scaling theory of single-particle localization transition was developed by Abrahams, Anderson, Licciardello and Ramakrishnan[89], and it crucially depends on the idea of Thouless energy[84] (1.53), mentioned in 1.2.4. The Thouless energy is basically a measure of the shift between eigenenergies of a finite-size system after changing the boundary conditions from periodic to anti-periodic. From an intuitive point of view, a twist in boundary conditions should not affect appreciably the eigenenergy of a state exponentially localized in the bulk. Hence, the shift in energy is only exponetially small in system size L,

$$E_{loc} \sim \mathrm{e}^{-\frac{L}{\xi}} . \tag{2.4}$$

On the other hand, in the delocalized part of the spectrum, boundary conditions deeply influence the extended states and their corresponding energy. The shift is comparable to the inverse of the diffusion time across the finite-size sample $t_{diff} = L^2/D$, with D the diffusion constant. Thus, in the diffusive phase the Thouless energy obeys

$$E_{diff} = \frac{Hbar}{t_{diff}} = \frac{HbarD}{L^2}. \tag{2.5}$$

In[84,90] Edwards and Thouless proposed the ratio of the energy shift to the energy spacing δW as a useful indicator of the localization transition. The average level-spacing

[1] Delocalization-localization transitions are a subset of more general metal-insulator transitions, e.g. transitions from a Mott insulator to a metal[87].

for single-particle states in a finite-size system scales as a power-law in the middle of the band and is given by

$$\delta W = \left(\frac{dE}{dn} L^{-d} \right), \tag{2.6}$$

where d is the dimension of the space and $\frac{dE}{dn}$ is the inverse of the density of states per unit volume. The fundamental requirement for a scaling theory is that the eigenstates of a system of linear dimension aL has to be expressible as a mixture of states of a^d subsystems of linear dimension L. At the boundary between adjacent subsystems the energy levels mix and are broadened due to tunnelling matrix elements. The essential insight from Thouless' work was that the physical observable which behaves *universally* is the conductance G, defined in units of $e^2/Hbar$, called the *Thouless number*[89]:

$$g = \frac{GHbar}{e^2}. \tag{2.7}$$

Combining a^d blocks of linear dimension L to form a larger block of size aL, we can express this dimensionless conductance as a one-parameter scaling function which satisfies the following equation,

$$\frac{d \ln g(L)}{d \ln L} = \beta(g(L)). \tag{2.8}$$

For weak enough disorder (large conductance g), the system obeys traditional macroscopic transport theory, providing a finite value for the conductivity and we have[91]

$$G(L) = \sigma L^{d-2}. \tag{2.9}$$

Thus, for $g \to \infty$ we get $\beta \to d-2$. For strong disorder (small g), we have the following behaviour at long distances:

$$g = g_0 \, \mathrm{e}^{-\alpha L}, \tag{2.10}$$

and $\beta \to \ln(g/g_0)$.

If the beta function is continuous and does not possess singularities, its behaviour is shown in figure 2.1.

This phenomenological theory was put on solid basis after Wegner found a field-theoretical description of localization[92] in terms of a non-linear σ model, which was followed in consecutive works by a microscopic description that completed the field theory of the phenomenon[93,94]. For a recent review of these results, which go beyond the aim of this thesis, we refer to[95].

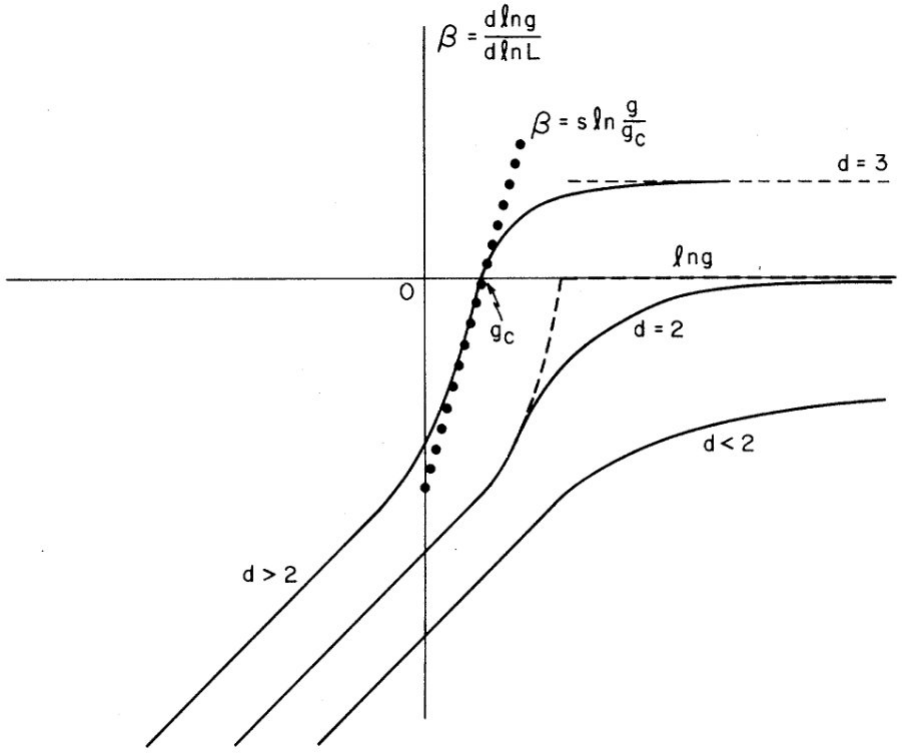

Figure 2.1: Plot of $\beta(g)$ for $d > 2$, $d = 2$, $d < 2$ vs $\ln g$. For $d > 2$ there is a critical value g_c above which the conductance flows to infinity, implying a metallic behaviour. For $d \leq 2$ for any initial value g_0 the conductance renormalizes to 0 and the system is localized. Figure taken from [89].

It turned out that the physical observables whose scaling is of primary importance at the transition are the localization length ξ for the delocalized phase ($E < E_c$) and the DC conductivity σ in the localized phase ($E > E_c$), described by two critical exponents,

$$\xi \propto (E_c - E)^{-\nu}, \qquad \sigma = (E - E_c)^s. \tag{2.11}$$

Wegner [96] first derived a relationship between the two exponents,

$$s = \nu(d - 2). \tag{2.12}$$

On a more technical level, without going into too much detail, we can see how the transition affects the behaviour of the diffusion propagator

$$\Pi(r_1, r_2; \omega) = \langle G^R_{E+\omega/2}(r_1, r_2) G^A_{E-\omega/2}(r_2, r_1) \rangle \,, \tag{2.13}$$

where $G^R_{E+\omega/2}(r_1, r_2)$ and $G^A_{E-\omega/2}(r_2, r_1)$ are the retarded and advanced Green functions, given by

$$G^{R,A}_E(r, r') = \langle r|(E - HatH \pm i\eta|r'\rangle\,, \qquad \eta \to 0. \tag{2.14}$$

In the extended regime, Π has the well-known Goldstone form

$$\Pi = 2\pi \frac{\rho(E)}{Dq^2 - i\omega}, \tag{2.15}$$

where ρ is the density of states and D is the diffusion coefficient given by the Einstein relation $\sigma = e^2\rho D$. On the other hand, in the localized phase the diffusion propagator does not show the Goldstone form (2.15) anymore and becomes massive

$$\Pi(r_1, r_2; \omega) = -2\pi \frac{\rho}{i\omega} F\left(\frac{|r_1 - r_2|}{\xi}\right), \qquad F\left(\frac{|r_1 - r_2|}{\xi} \sim \mathrm{e}^{\frac{r}{\xi}}\right), \tag{2.16}$$

with a behaviour determined by the exponential decay of the F function on the scale of the localization length.

2.2 MANY-BODY LOCALIZATION

After a short introduction to the topic of localization in free-systems, we turn now to the many-body Anderson problem with interactions. It is interesting to note that, although Anderson's original work was effectively motivated by experimental results for a system of interacting spins in a doped semiconductor, the phenomenon of Anderson localization in the presence of weak, short-ranged interactions has been a long-standing problem for decades. The first effort in this sense was produced by Anderson himself[97], followed by many other attempts at a full solution[17,98]. However, the issue remained deeply unsolved till the work of Basko, Aleiner and Altshuler in 2006[16], which we will describe in the next section.

Let us consider a non-interacting system in one or two dimensions. If all the eigenstates are localized and we consider only elastic scattering between localized states, the conductivity is obviously strictly vanishing for all finite temperatures. Conversely, Mott[99] showed that the presence of a heat bath allows electrons hopping between localized states through the exchange of phonons with the external reservoir, leading to a *variable range-hopping conductivity*

$$\sigma(T) = \sigma_0\, \mathrm{e}^{-(T_0/T)^{1/d+1}}, \tag{2.17}$$

which remains finite even for very low T. The question motivating the research for the existence of a many-body localized phase surges when one asks whether the interactions in a many-particle *isolated* system can play the role of a sort of "internal bath" and lead to finite conductivity by an analogous mechanism.

2.2.1 LOCALIZATION TRANSITION IN WEAKLY INTERACTING SYSTEMS

In 2006 Basko, Aleiner and Altshuler (BAA) presented a work which contained the first evidence in favor of MBL. They used a rigorous perturbative treatment of the many-body interactions to all orders, utlimately showing that the localization persists upto a finite energy density, extensive in the system size L. Their results predicted both the existence of a many-body mobility edge separating the extended and the localized phases and a finite critical temperature T_c below which the system shows a strictly zero conductivity,

$$\sigma(T) = 0 \text{ for } T < T_c. \tag{2.18}$$

BAA assumed weak short-range electron-electron interactions of the type

$$V(\vec{r}_1 - \vec{r}_2) = \frac{\lambda}{\rho}\delta(\vec{r}_1 - \vec{r}_2), \tag{2.19}$$

where $\lambda \ll 1$ is the dimensionless interaction constant and ρ is again the single-particle density of states per unit volume. Considering an Anderson insulator, in which all the single-particle (SP) eigenstates are localized, the Hamiltonian takes the form

$$HatH = \sum_{\alpha} \epsilon_\alpha c_\alpha^\dagger c_\alpha + \sum_{\alpha\beta\gamma\delta} V_{\alpha\beta\gamma\delta} c_\alpha^\dagger c_\beta^\dagger c_\gamma c_\delta, \tag{2.20}$$

where $c_\alpha^\dagger$ (c_α) creates (annihilates) a localized SP state with energy ϵ_α around position $\vec{r}_\alpha$, with localization length ξ. It is worth noting that the localization appears now in Fock space, where the unperturbed eigenstates are labeled by the occupation numbers $n_\alpha \in \{0, 1\}$ (since we are dealing with fermions) of SP orbitals $|n\rangle = |n_{\alpha_1} n_{\alpha_2} \cdots n_{\alpha_N}\rangle$, with $N = L^d$ sites.

The main energy scale of the problem at this stage is the *local spectral gap* δ_ξ, defined as the typical energy spacing between SP states whose spatial separation is below ξ,

$$\delta_\xi = \frac{1}{\rho\xi^d} \sim \mathcal{O}(1). \tag{2.21}$$

Consider the matrix elements $V_{\alpha\beta\gamma\delta}$: since the interaction potential V is short-range, they decrease exponentially when the spatial separation between states exceeds the characteristic length scale, i.e. the localization length ξ. An additional constraint is provided by the spectral gap, which implies a quick suppression of the matrix elements when the energy difference, say $\epsilon_\gamma - \epsilon_\delta$ increases over δ_ξ. This occurs because the localized wave functions oscillate randomly, and the bigger the energy difference, the weaker are these random oscillations correlated[100]. Thus, if the restrictions

$$|\vec{r}_\alpha - \vec{r}_\beta| \lesssim \xi,\ |\vec{r}_\alpha - \vec{r}_\gamma| \lesssim \xi,\ |\vec{r}_\beta - \vec{r}_\gamma| \lesssim \xi,\ \text{etc..} \tag{2.22}$$

$$|\epsilon_\alpha - \epsilon_\delta|, |\epsilon_\beta - \epsilon_\gamma| \lesssim \delta_\xi \ \text{ or } \ |\epsilon_\alpha - \epsilon_\gamma|, |\epsilon_\beta - \epsilon_\delta| \lesssim \delta_\xi \tag{2.23}$$

are fulfilled, then we can set $V_{\alpha\beta\gamma\delta} \sim \lambda\delta_\xi$. Conventionally, an elementary inelastic process is a decay of one single-particle excitation (an electron occupying a state $|\alpha\rangle$) into three single-particle excitations (a hole in $|\beta\rangle$ and two electrons in $|\gamma\rangle$ and $|\delta\rangle$). We can describe such a decay also saying that the Hamiltonian couples the single-particle excitation with the three particle excitation by the matrix element $V_{\alpha\beta\gamma\delta}$[16]. Further applications of the interacting Hamiltonian produce five-particle, seven-particle excitations, etc.,

$$\epsilon_\alpha \to \epsilon_\gamma + \epsilon_\delta - \epsilon_\beta \to \epsilon_1 + \epsilon_2 + \epsilon_3 - \epsilon_4 - \epsilon_5 \to \cdots . \tag{2.24}$$

If on each stage the coupling is strong enough, i.e. the matrix element is of the same order or larger than the corresponding energy mismatch, the exact many-body eigenstates become localized in Fock space[16]. On the contrary, if three-particle states contribute only a weak perturbative admixture to the one-particle state, the contribution from five-particle states is even weaker and so on, the initial electron will never decay completely, and one can say that it is localized in the Fock space. Thus, the full many-body problem across all particle number sectors looks like the Anderson problem on an N -dimensional hypercubic lattice where each "site" is a basis state in Fock space and $V_{\alpha\beta\gamma\delta}$ generates "hops" in Fock space. Following BAA intuition, we can attempt an identification of the many-body Hamiltonian (2.20) with the original Anderson tight-binding Hamiltonian (2.1), through the following correspondences:

- $V \to \lambda\delta_\xi$: typical value of the coupling matrix element,
- $W \to \delta_\xi$: typical energy mismatch in each consecutive virtual transition,
- the coordination number $2d \to T/\delta_\xi$: number of electrons within a localization volume available for collision with the probe electron α.

We can now use the Anderson estimate[15] for the localization-delocalization transition,

$$\frac{Vd}{W}\ln\frac{W}{V} \to \frac{\lambda T}{\delta_\xi}\ln\frac{1}{\lambda} \sim 1, \tag{2.25}$$

predicting a finite temperature transition for the many-body problem. Of course, the original calculation is much more nuanced. In fact, Anderson's prediction of the transition depends on the lattice details and structure and the analogy between real and Fock space, albeit fascinating, is not exact. Anyway, BAA's remarkable calculation led to a strictly zero conductivity below a finite temperature T_c (fig. 2.2), even in the many-body setting, and this constitutes the first notable result in this context.

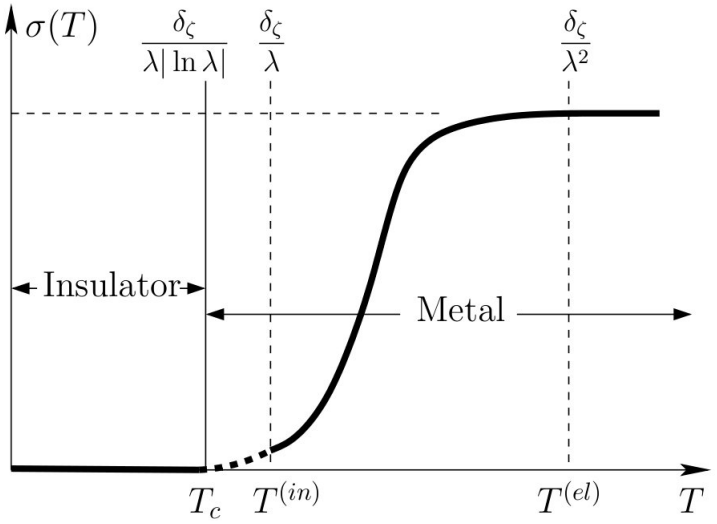

Figure 2.2: Schematic temperature dependence of the dc conductivity $\sigma(T)$. Below the many-body transition point ($T < T_c$) no relaxation occurs and $\sigma(T) = 0$. At higher temperatures, the system becomes ergodic and delocalized, and has a finite conductivity in a developed metallic phase. Figure from[16].

2.2.2 SPIN MODEL

BAA's work was able to give a solid theoretical footing to the theory of MBL. Nonetheless, the combination of disorder and interactions represents a challenging problem with few available theoretical tools. Progresses on this topic would not have been possible without the massive use of numerical techniques and simulations, which in the last five years has led to great strides in our understanding of this phenomenon, uncovering several properties of the MBL phase which we will discuss later. A model which is now

canonical in MBL studies was introduced by Pal and Huse[101], who studied via an exact diagonalization technique an Heisenberg spin-1/2 chain with random z-field components,

$$HatH = \sum_i [J(S_i^x S_{i+1}^x + S_i^y S_{i+1}^y) + J_z S_i^z S_{i+1}^z + h_i S_i^z], \tag{2.26}$$

where $S_i^\alpha = \sigma_i^\alpha$, $\alpha = x, y, z$ and σ_i^α are Pauli spin matrices on site i. The random h_i are inpendently drawn from a distribution uniform in $[-h, h]$. Without loss of generality, we can set $J = J_z = 1$. Through a Jordan-Wigner map[102], this spin model becomes the Anderson model (2.1) with an additional nearest-neighbor density-density interaction of strength $J_z = 1$[101].

If $J = 0$, the many-body eigenstates of this model are simple product states of S_i^z of the form $|n\rangle = |\uparrow\downarrow\uparrow\uparrow\cdots\downarrow\rangle$. There is a set of 2^L basis states which are simultaneous eigenstates of all the $\{S_i^z\}$ that form the corners of an hypercube of dimension L, with nearest neighbors on the hypercube differing by a single spin flip[103]. As discussed previously, if the disorder is strong enough, or the perturbation $J \ll h$, the sites are unable to hybridize and the system looks many-body localized on all sites of the hypercube. Furthermore, it has been shown that for large enough disorder, the system presents MBL even at *infinite* temperature[101,104]. Accordingly to[29,101], this model presents a localization transition at a critical value of disorder $h_c \approx 3.5$ (fig. 2.3), even though a more recent work[105] provided evidence that the true critical point may be at a larger value of h. It worth remarking that the nature of this transition is purely quantum-mechanical even if it occurs at finite temperature, across which the eigenstates of the system changes in a peculiar way. It is also a *dynamical* transition and not a thermodynamical one, since there are no singularities in macroscopic thermodynamical observables.

2.3 DIAGNOSTICS FOR THE MBL PHASE

Since the MBL phase is a particularly rich phase, there are many diagnostics that can be used to distinguish it from the ergodic extended phase. In this section we will see which properties of MBL systems can be used as defining probes of this phase, with particular focus on the following topics:

1. Adjacent energy levels spacing statistics, which we discussed in the first chapter both for ergodic systems and non-ergodic ones.

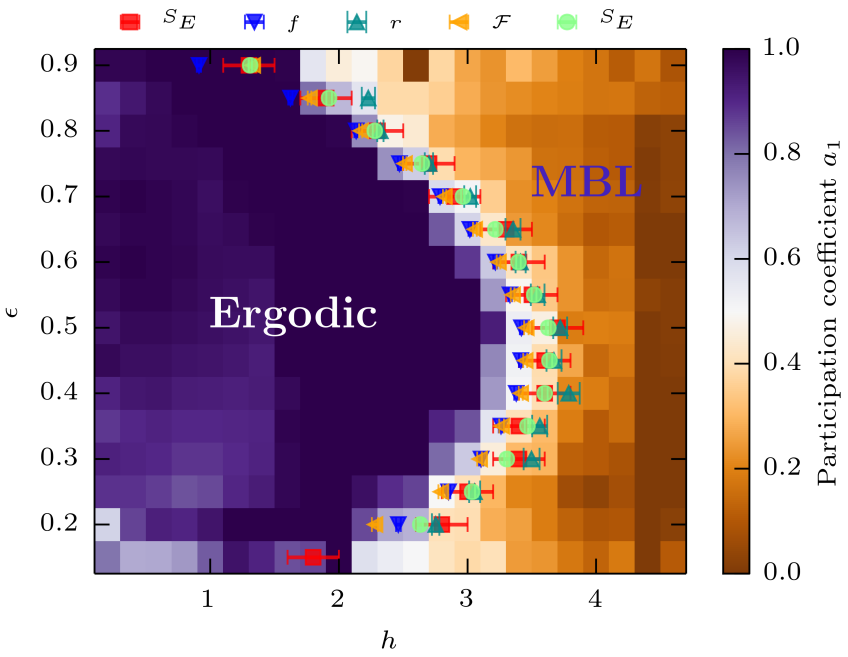

Figure 2.3: Phase diagram of the disordered Heisenberg model (2.26) as a function of energy density ϵ and disorder strength h [29]. The diagram shows the many-body localized and ergodic phases separated by a many-body mobility edge. For $h \gtrsim 3.5$ all eigenstates are localized.

2. Existence of *local integrals of motion* (LIOMs), which prevent thermalization in the sense described by the ETH.
3. Area-law for the entanglement in high excited states.
4. Logarithmic growth of entanglement in time.
5. Suppression of transport.

2.3.1 ABSENCE OF LEVEL REPULSION

As we saw in the first chapter, the level spacing distribution is a good indicator of the ergodicity or non-ergodicity of a system dynamics. In particular, we recall that for ergodic and chaotic systems RMT predicts a Wigner-Dyson distribution described by (1.8), while integrable systems, which represent an example of non-ergodic behaviour, show a Poisson distribution (1.21). Starting from earlier works [106,107], the energy levels statistics of disordered samples has been extensively exploited in order to detect the MBL phase [104,108]. The average value $\langle r \rangle$ of the dimensionless ratio $r_n = \min(\delta_n, \delta_{n+1})/\max(\delta_n, \delta_{n+1})$, where $\delta_n = E_{n+1} - E_n$, has been used as a numerical probe of the absence of level repulsion in

the MBL phase. This was signaled by the fact that in the MBL phase $\langle r \rangle$ approaches the theoretical value of 0.39 associated with the Poisson distribution, as the system size increases. In some sense, the absence of level repulsion is interpreted as a symptom of "integrability"[66], and thus of non-ergodicity, as opposed to the level repulsion exhibited by quantum chaotic systems[64]. In the single-particle case, the connection between the absence of level repulsion and localization is rather intuitive: the exponential decay of the eigenfunctions (2.2) implies that disjoint, distant regions of space are essentially uncorrelated and create almost independent eigenvalues, described by a Poisson process. This statement has been rigorously proven in Anderson localized systems by Minami[109], who bounded the probability of occurrence of two eigenvalues (of the finite volume Hamiltonian) in a small energy window. On the contrary, extended states imply that distant regions have mutual influence, and thus create some repulsion between energy levels[110].

In the MBL phase, the localization in Fock space implies that eigenstates that are close in energy are typically localized far apart in Fock space and do not interact. Consider, for example, the model (2.26) with $J = 0$: $HatH = \sum_{i=1}^{L} h_i S_i^z$. The average many-body level spacing is exponentially small in L, because while the many-body bandwidth is extensive and scales with L, the Hilbert space for this spin-system scales as 2^L. A certain eigenstate $|n\rangle = |\uparrow\downarrow\uparrow\uparrow \cdots \downarrow\rangle$ has energy $E_n = \sum_i s_i h_i$, where s_i is the σ_i^z quantum number on site i. With a single spin flip (or few) one obtains a new eigenstate that is close to $|n\rangle$ on the hypercube but with a difference in energy $\mathcal{O}(1) \sim h$ (h is the disorder strength). To get an exponentially small energy spacing, one has to flip extensively many $\sim \mathcal{O}(L)$ spins.
Figure 2.4 shows the results obtained from a numerical study of a disordered chain of interacting electrons, whose Hamiltonian is[104]

$$H = \sum_i [\epsilon_i n_i + V \left(n_i - \frac{1}{2}\right) \left(n_{i+1} - \frac{1}{2}\right) + c_i^\dagger c_{i+1} + c_i^\dagger c_{i+2} + h.c.], \tag{2.27}$$

where also the hopping between second-nearest-neighbors is present. The on-site potentials ϵ_i are independent Gaussian random numbers with mean zero and variance W^2. The plot in the left image in 2.4 reports various distributions of the energy levels spacing, for different values of randomness W. The red line is the distribution obtained in the localized phase with $W = 11$, and the data mostly overlap the solid line, which is a Poisson distribution. The green data represent the GOE distribution in the diffusive phase,

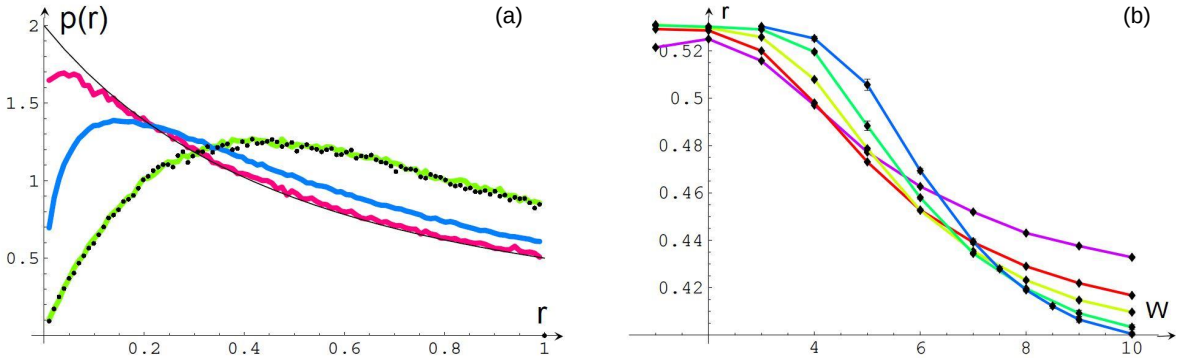

Figure 2.4: (a) disorder averaged probability distribution $p(r)$ for a system described by (2.27). The solid line is the Poisson distribution, while the black dots are GOE distributed eigenvalues. The colored lines are the results obtained for the interacting fermionic model at different disorder strenghts: the green line is obtained for $W = 3$ (extended regime), the blue line for $W = 7$ (intermediate regime) and the red line for strong disorder $W = 11$ (localized regime). (b) size L and disorder W dependence of $\langle r \rangle$. The curves correspond to different system sizes, $L = 8$ (pink), $L = 10$ (red), $L = 12$ (yellow), $L = 14$ (green), $L = 16$ (blue). Plots taken from [104]

at $W = 3$. The blue line is the result from the study of intermediate behaviour across the transition ($W = 7$). Moreover, in the right panel of 2.4 we can appreciate the evident transition from chaotic behaviour to localization, as the mean value $\langle r \rangle$ goes from the typical GOE value of ~ 0.52 to the predicted Poisson value of 0.39. As expected, larger samples have more Poisson-like statistics than smaller ones for strong disorder, $W > 8$, in an apparently localized regime. On the other hand, for weak disorder, $W < 4$, the level statistics converge toward GOE with increasing L, since this is the diffusive phase.

2.3.2 PHENOMENOLOGY OF MBL SYSTEMS

We already discussed how integrability breaks ergodicity and how conserved quantities highly constrain the dynamics of such systems, preventing thermalization in the form depicted by the ETH (although these systems can be described by what is known as a generalized Gibbs ensemble [111,112], and they seem to show their own mechanism of thermalization). In 1.2.4, following [13], we formulated the ETH as the conjecture that the diagonal matrix elements of (few-body) observables $HatA$ on the individual eigenstates are smooth functions of the eigenstate energy, being approximately constant in each

energy shell and equal to their microcanonical value. Recalling the ansatz (1.52),

$$A_{\alpha\beta} = A(\overline{E})\delta_{\alpha\beta} + \mathrm{e}^{-S(\overline{E}/2)}\, f_A(\overline{E}, \omega) R_{\alpha\beta},$$

the ETH guarantees that any initial condition reaches a stationary state that is locally thermal at $t \to \infty$, up to corrections that are exponentially small in the system size. The framework that underlies this hypothesis is that eigenstates of thermalizing quantum systems are locally *indistinguishable*. This goes against the Fock space localization picture, in which the MBL eigenstates in the same energy window are distinguishable, since the expectation values of local observables are far from their equilibrium values, strongly fluctuating between states really close in energy. Thus, it is possible to distinguish them. Furthermore, as we will discuss soon, the ETH is also incompatible with the peculiar area-law scaling of the entanglement entropy of highly excited localized eigenstates, since it requires that the entanglement equals to the thermal equilibrium entropy of the subsystem, that scales with the number of its degrees of freedom, i.e. shows a volume law.

A crucial difference between localization and integrability is that the latter only exists in highly fine-tuned models and is not robust under small perturbations. MBL, instead, is expected to exist for generically interacting Hamiltonians with strong enough disorder, and is very robust under small changes in the Hamiltonian. Nevertheless, it is a common expectation that the failure of ergodicity in closed, interacting systems is related to some sort of integrability. In fact, the behavior of MBL systems points toward the existence of an extensive number of conservation laws that strongly constrain the quantum dynamics, preventing transport and thermalization.

In[113,114] was argued that in fully MBL systems, in which all eigenstates are localized, the Hamiltonian is a non-linear functional of a complete set of conserved operators I_α, called *local integrals of motion*(LIOMs), or *l-bits*, of the form

$$HatH_{LIOMs} = h_0 + \sum_\alpha h_\alpha I_\alpha + \sum_{\alpha\beta} h_{\alpha,\beta} I_\alpha I_\beta + \sum_{\alpha,\beta,\gamma} h_{\alpha\beta\gamma} I_\alpha I_\beta I_\gamma + \cdots . \tag{2.28}$$

The integrals I_α are expected to be mutually independent and commuting with each other, and they form a complete set, meaning that every eigenstate of the Hamiltonian can be labeled in a unique way with the eigenvalues of the I_α.[2] Looking at (2.28),

[2]In the non-interacting fermionic case, the Hamiltonian is a *linear* functional of the conserved operators, which are simply the occupation numbers n_α, $HatH = \sum_\alpha E_\alpha n_\alpha$.

the expansion seems a bit generic, since for example to determine $HatH_{LIOMs}$ properly one needs to find a number of coefficients that scales with the dimension of the Hilbert space[115]. Nonetheless, localization manifests itself in the "quasilocality" of the I_α: in the same way as in (2.2), the operator norm is expected to show an exponential decay away from a certain region of typical size ξ_{op} centered in a given point R_α. The I_α can be expanded in a basis of local operators $\mathcal{O}_\mathcal{I}$,

$$I_\alpha = \sum_{\alpha \in \mathcal{I}} c_\mathcal{I}^{(\alpha)} \mathcal{O}_\mathcal{I}. \tag{2.29}$$

Let $S(\mathcal{I})$ denote the *support* of $\mathcal{O}_I$, i.e. the set o points/sites on which the operators act non-trivially. Quasilocality means that

$$|c_\mathcal{I}^{(\alpha)}| \lesssim \exp\left(-\frac{d[R_\alpha, S(\mathcal{I})]}{\xi_{op}}\right), \tag{2.30}$$

where $d[R_\alpha, S(\mathcal{I})]$ is the distance between R_α and the furthest degree of freedom in the set $S(\mathcal{I})$. This relation gives an insight on the typical decay of coefficients, with respect to the realization of randomness.
For example, in a spin system like the one described by (2.26), a suitable basis is given by the tensor product of local spin operators $\sigma_{i_1}^{\alpha_1} \otimes \sigma_{i_2}^{\alpha_2} \otimes \cdots \otimes \sigma_{i_n}^{\alpha_n}$ with $\alpha = \{x, y, z\}$. In spin language, the I_α are often called *pesudospin*s or *l-bits* (local bits) τ_i^z, constructed via a unitary rotation of the real operators, or *p-bits* (physical bits)[114],

$$\tau_i^\alpha = U \sigma_i^\alpha U^\dagger, \tag{2.31}$$

where U is the rotation that diagonalizes the Hamiltonian and relates the basis states to the MB eigenstates which are product states of $\{\tau_i^z\}$.

The existence of a set of local integrals of motion leads to novel features of the MBL phase, which distinguish it from ergodic or integrable systems. Following[116], we can consider an MBL system with Hamiltonian (2.26) subject to an instantaneous quantum quench, focusing on the behaviour of local observables. The aim is to prove that in the MBL phase the system reaches a highly nonthermal stationary state at long times, where the local observables assume an expectation value that depends on the initial conditions, and thus they retain memory of initial state. MBL systems exhibit peculiar temporal fluctuations of local observables around their long-time values, in according

to a power-law decay with an exponent determined by the localization length and the properties of the initial state. This power-law relaxation law is a characteristic property of MBL systems, which distinguishes them both from Anderson insulators (in which no relaxation is expected) and from ergodic systems (in which the decay is expected to be exponential).

Figure 2.5: Graphic illustration of the dynamics of pseudospins τ_i^z. These are a set of spins whose z component is conserved, but which precess around the z axis at a rate determined by the effective interactions with all other pseudospins. Figure from [77].

In terms of pseudospins $\{\tau\}$, (2.26) takes the form (2.28), which in spin notation is

$$HatH = \sum_i h_i \tau_i^z + \sum_{i,j} J_{ij} \tau_i^z \tau_j^z + \sum_{i,j,k} J_{ijk} \tau_i^z \tau_j^z \tau_k^z + \cdots , \tag{2.32}$$

where we remark the absence of any hopping terms, as it only depends on τ_i^z. The h_i describe the random field acting on the effective spin in site i. The spin-spin interaction came from the actual interactions in the original Hamiltonian, and thus they are absent in the free case. These interacting terms are expected to show an exponential decay with distance r_{ij} with respect to ξ_1,

$$J_{ij} \propto J_0 \, \mathrm{e}^{-\frac{r_{ij}}{\xi_1}}, \qquad J_{ijk} \propto J_0 \, \mathrm{e}^{-\frac{\max(r_{ij}, r_{jk}, r_{ik})}{\xi_1}}, \qquad \cdots . \tag{2.33}$$

Despite the simple form of this diagonal Hamiltonian, the MBL phase presents unusual and non-trivial dynamics when the system is prepared in a superposition of different eigenstates. In fact, each pseudospin is affected by an effective magnetic field in the z direction that depends on the state of all the other pseudospins, in a quite complicated manner. Hence, if we initially prepare the system in a state where every τ_i^z is in a superposition of ± 1, during the time evolution different spins will get entangled. This entanglement is due to the dephasing of the off-diagonal elements of the reduced density matrix in the τ basis [113,114,117].

The magnetic field experienced by the k-th effective spin can be expressed as

$$H_k(\tau') = h_k + H_k^1(\{\tau'\}) + H_k^2(\{\tau'\}) + \cdots , \tag{2.34}$$

where τ' is the set of the configurations of all the pseudospins except k. H_k^l is the magnetic field arising from interactions between spins within a distance $|j-k| \leq l$ from k. We can explicitly write the first two terms as

$$H_k^1 = J_{k,k+1}\tau_{k+1}^z + J_{k,k-1}\tau_{k-1}^z + J_{k,k-1,k+1}\tau_{k-1}^z\tau_{k+1}^z, \tag{2.35}$$

and

$$\begin{aligned} H_k^2 = {} & J_{k,k+2}\tau_{k+2}^z + J_{k,k-2}\tau_{k-2}^z \\ & + {\sum_{|\sigma|\leq 2}}' {\sum_{2\geq\sigma'>\sigma}}' J_{k,k+\sigma,k+\sigma'}\tau_{k+\sigma}^z\tau_{k+\sigma'}^z \\ & + {\sum_{|\sigma|\leq 2}}' {\sum_{2\geq\sigma'>\sigma}}' {\sum_{2\geq\sigma''>\sigma'}}' J_{k,k+\sigma,k+\sigma',k+\sigma''}\tau_{k+\sigma}^z\tau_{k+\sigma'}^z\tau_{k+\sigma''}^z \\ & + J_{k-2,k-1,k,k+1,k+2}\tau_{k-2}^z\tau_{k-1}^z\tau_{k+1}^z\tau_{k+2}^z, \end{aligned} \tag{2.36}$$

where we denote with the prime the sums that exclude zero ($\sigma \neq 0$). Generally, it is believed that the effective fields decay exponentially according to

$$H_k^l \sim J_0\, \mathrm{e}^{-\frac{l}{\xi}}, \tag{2.37}$$

with $\xi \neq \xi_1$ generally. Now we assume our system to be initially prepared in a product state (or in a weakly entangled state) and we proceed with a global quantum quench, evolving the system for $t > 0$ with the Hamiltonian (2.32). We choose a simple initial state in which effective spins are prepared in a product state, rather than physical ones, because even if such a state is hard to prepare this example captures almost all the dynamical features in the MBL phase and it is analytically treatable. We initialize the system in a superposition of different states, given by

$$|\psi(0)\rangle = \otimes_{i=1}^N [A_{i,+}\,|+\rangle_i + A_{i,-}\,|-\rangle_i], \tag{2.38}$$

where $|+\rangle_i$ ($|-\rangle_i$) are the eigenstates corresponding to $\tau_i^z = \pm 1$ and $A_{i,+}$, $A_{i,-}$ are complex numbers satisfying $|A_{i,+}|^2 + |A_{i,-}|^2 = 1$. At time t, the wave function is

$$|\psi(t)\rangle = \sum_\tau \left(\prod_{i=1}^N A_i\tau_i\right) \mathrm{e}^{-iE_\tau t}\,|\tau\rangle\,, \tag{2.39}$$

where $|\tau\rangle$ is an eigenstate of (2.32) for a certain configuration of pseudospins, e.g. $|\tau\rangle = |\uparrow\uparrow\cdots\downarrow\uparrow\rangle$, and E_τ is its corresponding energy. We consider single-spin observables on spin j, described by operators $\tau_k^\alpha(t)$, $\alpha \in \{x, y, z\}$, and we can explicitly write the elements of the reduced density matrix for spin k: the diagonal elements are time-independent, since the τ_j^z are integrals of motion,

$$\rho_{++}(t) = |A_{k,+}|^2, \quad \rho_{--}(t) = |A_{k,-}|^2, \tag{2.40}$$

while the off-diagonal elements are

$$\rho_{+-}(t) = \rho_{-+}^*(t) = A_{k,+}A_{k,-}^* \sum_{\tau'} P_{\tau'}\, \mathrm{e}^{i(E_{+,\tau'} - E_{-,\tau'})t}, \tag{2.41}$$

where τ' represents all the configurations of $N-1$ spins excluding the k-th. $E_{+(-),\tau'}$ is the energy of the state with $\tau_k^z = +(-)$, and the other spins are in τ'. The probability of finding such a state is conserved in time and it is denoted by $P_{\tau'}$, given for the state (2.38) by

$$P_{\tau'} = \prod_{i \neq k} |A_{i\tau_i}|^2. \tag{2.42}$$

Using (2.32) we can recast the off-diagonal elements as

$$\rho_{+-}(t) = A_{k,+}A_{k,-}^* \sum_{\tau'} P_{\tau'}\, \mathrm{e}^{2iH_k(\tau')t}, \tag{2.43}$$

where we used the effective magnetic field[3] experienced by the spin k defined in (2.34). In the MBL phase, different configurations of the surrounding spins lead to different magnetic fields experienced by k and to the dephasing and suppression of the off-diagonal elements ρ_{+-}. Using the hierarchical structure which follows from (2.34), if the localization length is short enough, every successive term in the sum in (2.34) is typically much smaller than the previous one, $|H_k^l| \gg |H_k^{l+1}|$. This leads to[116]

$$\frac{1}{H_k^l} \lesssim t \lesssim \frac{1}{H_k^{l+1}}, \tag{2.45}$$

[3]In the non-interacting case, the effective field experienced in a certain site is not affected by the state of the spins in all other sites. Therefore, we can write $H_k(\tau') = h_k$ and thus

$$\rho_{+-}(t) = \mathrm{e}^{2ih_k t}. \tag{2.44}$$

This results in a process of precession of the spin k without any dephasing, leading to an oscillatory behaviour of single-spin observables. Thus, no equilibrium state is reached, which is the dynamical probe of Anderson localization.

which means that at time t the magnetic field does not depend on the state of the spins for which $|i-k| > l$, but all other configurations differing in one ore more spins for which $j - k \leq l$ show a phase difference much greater than 2π. In other words, the k-th spin gets entangled with the spins within a distance l, i.e. $k-l, \cdots, k-1, k+1, \cdots, k+l$. Let us assume that the probabilities $P_{\tau'}$ are equal, for example when $|A_{i\tau_i}| = \frac{1}{\sqrt{2}}$. Thus, we can estimate $\rho_{+-}(t)$ as

$$|\rho_{+-}(t)| \sim \frac{|A_{k,\uparrow} A^*_{k,\downarrow}|}{\sqrt{N(t)}}, \tag{2.46}$$

where $N(t)$ is the number of configurations of spins for which $|i-k| \leq l$. At time t, the off-diagonal element of the reduced density matrix consists of $N(t) = 2^{2l}$ terms with random phases. Combining (2.37) and (2.45) we obtain the relation $l \sim \xi \ln(J_0 t)$, which we insert in (2.46) obtaining

$$|\rho_{+-}(t)| \sim \frac{|A_{k,\uparrow} A^*_{k,\downarrow}|}{(J_0 t)^{\xi \ln 2}}. \tag{2.47}$$

Hence, the off-diagonal element of the reduced density matrix decays as a power law, depending on ξ and on the details of the initial state, in particular on the probabilities of all spin configurations. The same kind of power-law decay also holds for a generic initial state[116]. These results allow us to understand the dynamics of the single-spin observables: τ^z_k remains fixed, while τ^x_i, τ^y_i show a power-law decay in time to zero,

$$\langle \tau^z_k(t) \rangle = \langle \tau^z_k(0) \rangle \,, \qquad |\, \langle \tau^{x,y}_k(t) \rangle \,| \propto \frac{1}{t^{\xi \ln 2}}, \tag{2.48}$$

for a simple initial state as (2.38) and for $t \gg 1/J_0$, i.e. for long times. In[116], this particular behaviour is proven to hold for generic observables, not only single-spin ones.

The LIOMs formalism provides a useful phenomenological description of the properties of the MBL phase and highlights its typical dephasing dynamics. We conclude this discussion summarizing what we said:

- MBL systems can be described by a set of emergent *local* integrals of motion, which strongly restrict the quantum dynamics.
- Temporal fluctuations of local observables decay according to a power-law, with an exponent that depends on the properties of the initial state.
- The dephasing dynamics is extremely slow, due to the exponentially weak interactions between τ^z_i spins.

- There is no dissipation, since there are no spin-flips in (2.32).

The persistent memory of initial conditions in MBL phase combined with exponentially slow dephasing (which can be also reversed with echo-spin procedures[118,119]) has raised the fascinating idea of using localized systems as novel platforms for a new generation of quantum computing devices.

2.3.3 ENTANGLEMENT IN LOCALIZED SYSTEMS

The notion of entanglement belongs to the ensemble of ideas from quantum information that have been ported to the study of modern condensed matter physics, leading to many important developments. Entanglement allows to separate parts of a system to be much more correlated than what is classically predicted, and it represents a key ingredient in the operations of a quantum computer.

Consider a system initialized in a pure state $|\psi\rangle$, defined in a one-dimensional Hilbert space H. If we divide our system into two subregions A and B we can write the Hilbert space as the tensor product $H = H_A \otimes H_B$. The pure state $|\psi\rangle$ can be decomposed as

$$|\psi\rangle = \sum_{i=1}^{N_A} \sum_{j=1}^{N_B} a_{ij} \, |i\rangle_A \otimes |j\rangle_B \,, \tag{2.49}$$

where $|i\rangle_A$ ($|j\rangle_B$) are basis states for the subsystem A (B) and N_A, N_B are the sizes of the partitions. We can perform a singular value decomposition on the matrix of coefficients a_{ij} in order to obtain the state in its Schmidt form[120]

$$|\psi\rangle = \sum_{\alpha=1}^{N_{min}} \Lambda_\alpha \, |\alpha\rangle_A \, |\alpha\rangle_B \,, \tag{2.50}$$

where the state $|\alpha\rangle_{A,B}$ form an orthonormal set for $H_{A,B}$ and $N_{min} = \min(N_A, N_B)$. The Schmidt values $\Lambda_\alpha \geq 0$ for a normalized state satisfy $\sum_\alpha \Lambda_\alpha = 1$, and are the main indicator of the level of entanglement between the two subregions. A state with no entanglement can be written as a simple product state in the Schmidt basis and thus only one Schmidt value is different from zero, while for an entangled state, more than one Λ_α contributes[121]. Considering the reduced density matrix of one subsystem, say A, the relation between entanglement and the Schmidt decomposition can be made more clear:

$$Hat\rho_A = \mathrm{Tr}_B \, |\psi\rangle \langle\psi| = \sum_\alpha \Lambda_\alpha^2 \, |\alpha\rangle_A \langle\alpha|_A \,. \tag{2.51}$$

The von Neumann entropy we defined in (1.45) is the *entanglement entropy* of the reduced density matrix, and it can be written as

$$S^A = -\sum_{\alpha=1}^{N_{min}} \Lambda_\alpha^2 \log \Lambda_\alpha^2. \tag{2.52}$$

From the above expression we can note that the entropy varies from 0, for a minimally entangled product state, to $\log N_{min}$ for a maximally entanglement state in which all Schmidt values are equal. For example, if we are dealing with a chain of spin-1/2 of length L, the maximal entanglement entropy for a bipartition of the chain is

$$S \propto L \log 2, \tag{2.53}$$

since $N_{min} = 2^{L/2}$. The result is that the maximal entropy of entanglement scales with the volume of the subregion, accordingly to the macroscopic thermodynamic entropy. Hence, in thermalizing systems which obey the ETH, since local observables computed in individual eigenstates agree with their ensemble averages, the entanglement entropy of any subregion A scales with the famous "volume-law" for generic highly excited states. In the language of quantum information theory, this means that the information is "scrambled" in such states and an effective representation of them requires many expansion coefficients of the wave function in terms of local basis states. It was formally proven by Hastings[122] that ground states of local, gapped Hamiltonians show a different scaling, called "area-law", and the entanglement entropy scales as the length of the boundary between the subregions. For a one dimensional system, this law implies that S scales as a constant independent of L.

Notably, in[101] it has been noted that MBL systems (and also Anderson localized systems) show an area-law scaling even for highly excited states. By now, several numerical studies confirmed in detail the behaviour of the entanglement entropy, showing the area law for excited states and deviations from it due to rare regions and states[29,123]. This area-law is one of the key features that denote the violation of the ETH in localized systems.

Figure 2.6 shows very clearly the difference between a disordered Heisenberg spin chain (2.26) at low disorder strength and at higher randomness. For weak disorder, the entropy per site S^E/L increase constantly, confirming the expected volume law for non-localized systems. At higher disorder strengths, deep in the MBL phase, the entanglement entropy

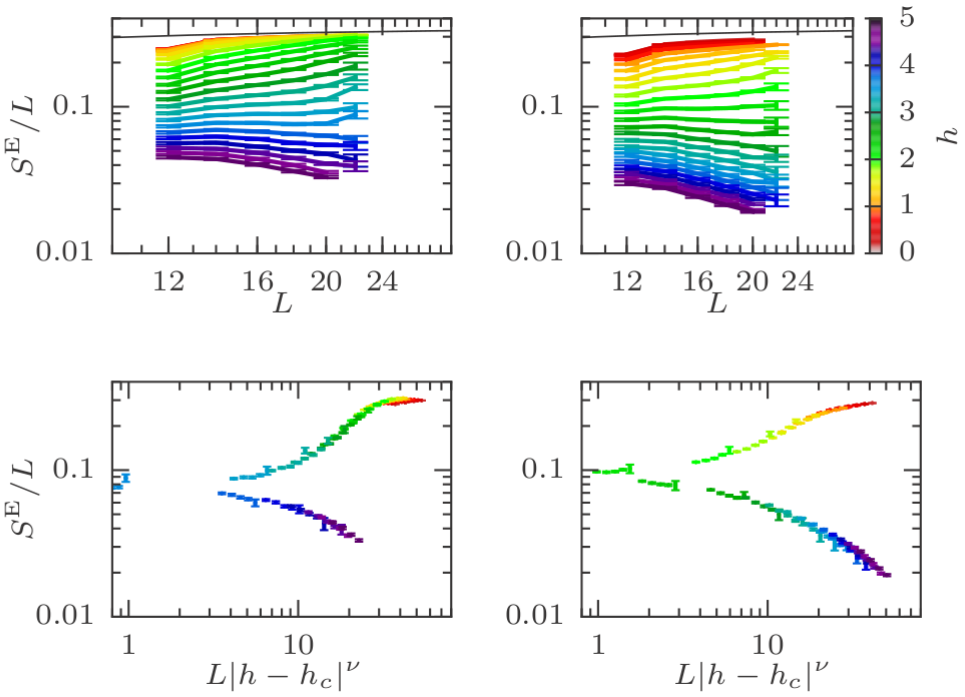

Figure 2.6: Entanglement entropy per site S^E/L as a function of system size L for various disorder strength values h for the Hamiltonian (2.26). The left panels are taken from the middle of the spectrum while the right ones from the upper sector. The volume law scaling leading to a constant S^E/L for weak disorder is opposed to the area law at larger disorder, detected by the decrease of S^E/L. From[29].

decreases with the system size L, distinctly showing an area-law scaling. Assuming a volume law scaling at the transition[124], it is possible to perform a scaling analysis of S_E/L using the ansatz $g[L^{1/\nu}(h-h_c)]$, estimating the critical disorder h_c and the critical exponent ν (for details on the fitting procedure, see Supp. Mat. of[29]).
Another example is provided by figure 2.7, which shows the standard deviation of entanglement over the disorder ensemble as a function of disorder strength δJ for different system sizes L and D independent disorder realizations[123]. The Hamiltonian which the data refer to is the transverse field quantum Ising chain with disordered couplings and a next-nearest neighbor Ising term,

$$H = -\sum_{i+1}^{L-1} J_i \sigma_i^z \sigma_{i+1}^z + J_2 \sum_{i=1}^{L-2} \sigma_i^z \sigma_{i+2}^z + h \sum_i^L \sigma_i^x, \quad J_i = J + \delta J_i, \tag{2.54}$$

where $J_i = J + \delta J_i$ are random and independent, with J_i chosen from a uniform distribu-

tion $[-\delta J_i, \delta J_i]$. At a fixed nonzero interaction strength J_2, an MBL transition is found at a certain critical value δJ_C, which depends on the energy density. In the left inset of figure 2.7 the plots show the mean of the distribution of entanglement entropies $\langle S \rangle$ in the exact eigenstates at the middle of the spectrum, for various system sizes L (different colors). At weak disorder $\langle S \rangle$ follows a volume-law approaching the value (2.53), signaled by the dashed lines. With increasing disorder the average entropy falls off towards the saturation value $S^E = \log 2$ deep in the localized phase. The standard deviation goes to zero both in the ergodic phase and in the localized phase, while it has a diverging peak at the critical disorder strength, i.e. at the transition. This can be understood considering that at disorder values close to the transition, the exact value of the entanglement entropy depends on the singular disorder realization. The set of states obtained for a specific configuration contains, near the transition, a large number of thermal states and a large number of localized states, and this leads to a large standard deviation of the entanglement.

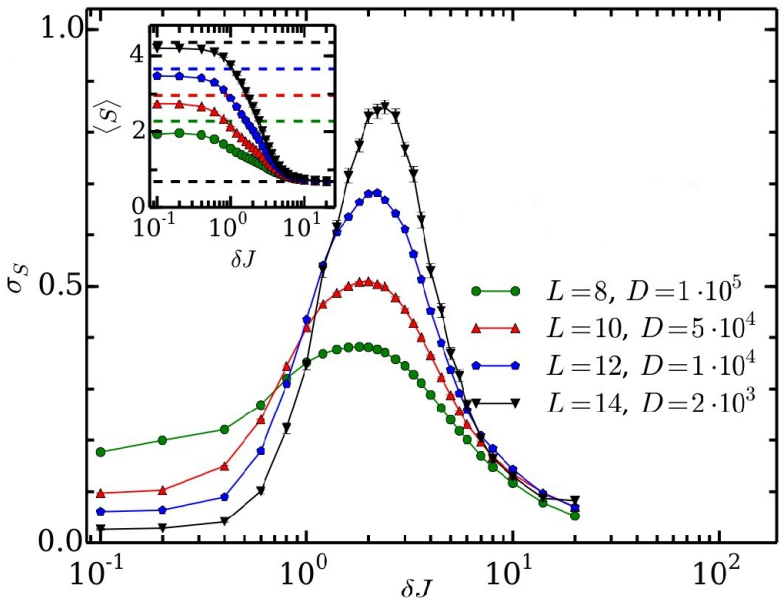

Figure 2.7: Standard deviation of entanglement entropy as a function of disorder strength δJ, for the Hamiltonian (2.54). The data are shown for different system sizes L and disorder realizations D at a fixed energy density in the middle of the spectrum. The left inset shows the mean entanglement entropy and the transition leading to a full localized phase, in which for all system sizes $\langle S \rangle$ approaches a constant value. Adapted from [123].

Now, the question may be: "How can the MBL phase be distinguished by its single-particle counterpart?". Indeed, the scaling of the entanglement entropy in both phases follows an area-law, and thus it is not a sufficient indicator. The difference lies in the dynamics of the entanglement, i.e. in the growth of S in time, starting from an initial product state. In ergodic systems, the entanglement spreads ballistically, with an energy-density dependent speed akin to the Lieb-Robinson velocity[80]. An intuitive explanation is that two separated regions A and B are entangled if the entanglement spreads sequentially through the subsystems lying inbetween. In Anderson localized systems, on the contrary, the absence of interactions and the localization of the $l-bits$ do not permit any spreading, leading to no growth of entanglement even at long times. Strikingly, the behaviour of entanglement dynamics in MBL systems is truly different from all we said so far. In[117,125] it was found that the entanglement follows a *logarithmic* growth in time in MBL phase. This peculiar property can be explained by exploiting again the l-bits framework, where two l-bits separated by a distance l can only get entangled through their direct interaction. The effective interaction between them is given by (2.37), and it decays exponentially with l. Hence, after a time t such that $J_0 t \sim 1$, all l-bits inside a sphere of radius $l \sim \xi \ln(J_0 t)$ become entangled.

In figure 2.8 is reported the entanglement growth in the random Heisenberg chain (2.26) for various values of the interaction strength. The difference between the single-particle case anche the MBL one can be seen very clearly: in the Anderson case (blue plot) $S(t)$ grows until the transition takes place, and then saturates without any further increase, while switching on the interaction term J_z leads to a logarithmic growth of entanglement after the critical point. The time at which the logarithmic growth starts is $J_z t \sim 1$, and all curves for different interacting strengths roughly collapse on a single curve when plotted against $J_z t$ (see inset).

This logarithmic growth is expected to continue indefinitely for an infinite system, while in finite systems $S(t)$ saturates to a value S_∞ that depends on the initial conditions only[117,126]. The saturation value shows an extensive scaling with the system size L (figure 2.9), but smaller than the one predicted for the thermal phase.

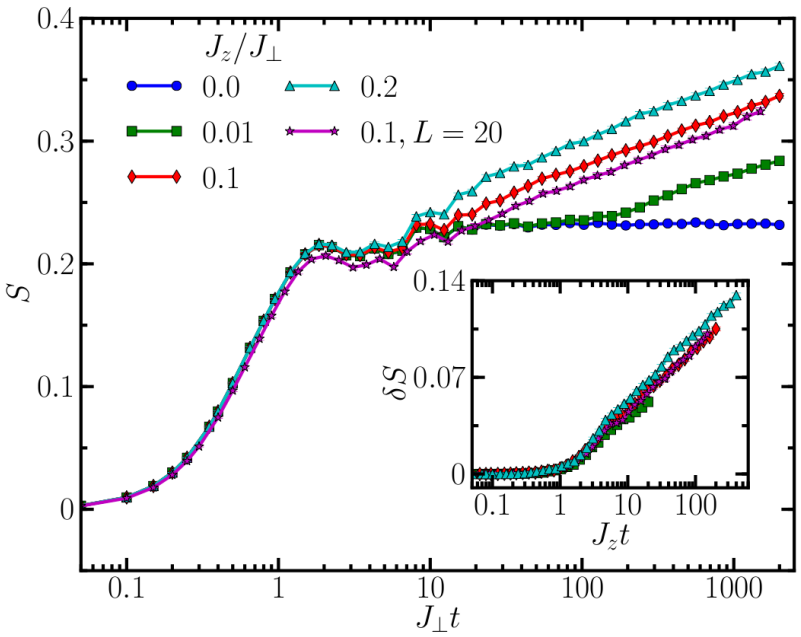

Figure 2.8: Entanglement growth after a quench starting from a factorized eigenstate of Hamiltonian (2.26), for different interaction strengths J_z. The inset shows the same data but with a rescaled time axis and subtracted $J_z = 0$ values[125].

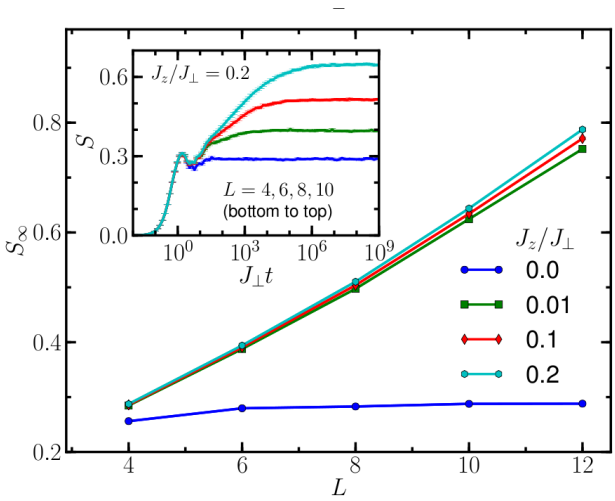

Figure 2.9: Saturation values of the entanglement entropy as a function of L for different J_z. The inset shows the approach to saturation for various system sizes.[125]

2.4 EXPERIMENTAL REALIZATIONS

We conclude this chapter with some references to interesting experimental setups which has proven to be very promising in MBL investigations.

As we stressed from the very beginning of the discussion about MBL, this phenomenon is expected to manifest itself in isolated quantum systems, decoupled from any external reservoir. As a result, experimental investigations on MBL systems have proven to be really challenging. Actually, even for Anderson insulators direct measurements of electronic wavefunctions localization has been elusive, although indirect probes were found thanks to the deep implications that localization causes in other properties [127,128], e.g. transport. The experimental revolution that we mentioned in the introduction of this chapter have resulted in the realization of isolated many-body systems with high tuning possibilities in terms of interactions and disorder strength. Experiments in ultracold atomic systems [129–132] represents an ideal setup in which investigate the elusive localization, and recent observations have demonstrated that a signature of the initial state persists in MBL systems for arbitrarily long times. To a good approximation these

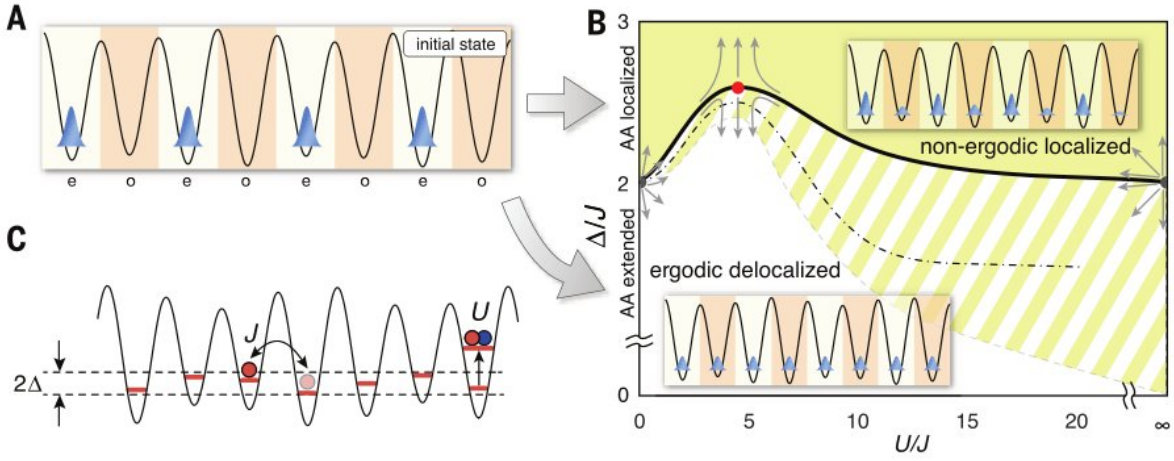

Figure 2.10: Diagram of the many-body system initial state and experimental procedure [129]. (A)The system is prepared in an initial state consisting in a particular CDW, in which all atoms occupy even sites. (B) Schematic phase diagram. In the ergodic phase, the system is expected to relax and equilibrate under its own dynamics, leading to the same number of atoms in even or odd sites. In the localized phase, the initial CDW persists for long times. (C) Representation of the three terms in Aubry-André Hamiltonian (2.55).

systems can be considered isolated[4], and the interaction strength can be tuned via a procedure called Feshbach resonance. In [129], the onsite disorder has been realized by

[4]Even if there is heating in this kind of setups, its effects are believed to be relevant on time scales much longer than those used during measurements [130].

superimposing lasers with incommensurate frequencies, creating a quasiperiodic potential which is also known to show MBL[133–135]. The system can be described by the 1D fermionic Aubry-André model with interactions,

$$HatH = -J\sum_{i,\sigma}(c^{\dagger}_{i,\sigma}c_{i+1,\sigma} + h.c. + \Delta\sum_{i,\sigma}\cos(2\pi\beta i + \phi)c^{\dagger}_{i,\sigma}c_{i,\sigma} + U\sum_{i} n_{i,\uparrow}n_{i,\downarrow}, \tag{2.55}$$

where $\sigma \in \{\uparrow,\downarrow\}$. The second sum represents the quasiperiodic disorderd term, i.e. the shift of the onsite potential due to an additional incommensurate lattice, where β is the ratio of lattice periodicities, Δ is the disorder strength and ϕ is a phase offset. As usual, U represents the onsite interaction energy, and $n_{i,\sigma} = c^{\dagger}_{i,\sigma}c_{i,\sigma}$ is the number operator. The most remarkable fact about this model is that for almost all irrational β all single-particle states are localized at the same critical disorder strength $\Delta/J + 2$[133]. By now, the main experimental observable in MBL measurements has been the *imbalance* I between the respective numbers of atoms on even N_e or odd N_o sites,

$$I = \frac{N_e - N_o}{N_e + N_o}. \tag{2.56}$$

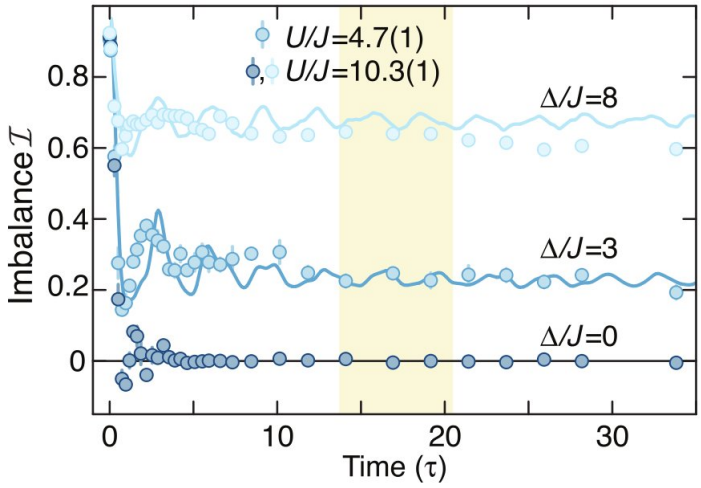

Figure 2.11: Evolution of imbalance I between atoms on even and odd sites for different disorder and interactions strength[129].

Preparing the system in an initial artificial charge density wave (CDW) order, I gives a measurement of the relaxation of this CDW in time (see figure 2.10). The results of the tracking of the time evolution of I are shown in 2.11, in which it can be seen that in the ergodic phase, for small disorder, the initial CDW ($I = 0.9$) quickly relaxes to zero, while

in the MBL phase the imbalance attains a finite stationary value. Since the imbalance decay to zero is a signature of the relaxation of the system towards thermal equilibrium, the behaviour of I for strong disorder is a significant hallmark of non-ergodic dynamics, and the persistence of the initial CDW pushes forward tantalizing ideas about how to exploit memory effects in MBL systems.

Another recent experimental study on a cold-atoms setup has remarkably shown signatures of localization in two dimensions[130], an open problem since the days of Anderson's original work. Here, the authors report observations of MBL for bosons in a two-dimensional optical lattice. Traces of MBL has been found also in trapped ion systems[136].

3

THE KITAEV MODEL

In this chapter we review the toy model proposed by Kitaev[41], a useful tool for the study of certain fermionic systems which have an energy gap in the bulk spectrum and show Majorana zero edge modes at the boundaries. The original Kitaev one dimensional model, with short range pairing between particles, has been studied within the framework of topologically ordered phases in one dimension. A two or more degenerate ground state, or more generally low energy states, is a key feature of a topological ordered phase, which appears without the breaking of any order parameter. We present a generalization of the Kitaev chain with long range interactions, whose strength decays as a power law.

3.1 KITAEV CHAIN

We consider a one-dimensional i.e., a *quantum wire*, superconductive system, without focusing on the particular superconductivity mechanism: we assume, for simplicity, that only a single spin component appears in the Hamiltonian. This effectively makes sense only in a *p*-wave, or *triplet*, superconductor, in which the induced pairing involves fermions with the same spin direction.
The model Hamiltonian, for a chain of $N \gg 1$ sites, is[41]

$$H = \sum_{j=1}^{N-1} \left[-t \left(c_j^\dagger c_{j+1} + c_{j+1}^\dagger c_j \right) + \Delta \left(c_{j+1}^\dagger c_j^\dagger + c_j c_{j+1} \right) \right] - \sum_{j=1}^{N} \mu \left(c_j^\dagger c_j - \frac{1}{2} \right), \tag{3.1}$$

where j labels the sites, μ is the chemical potential, t is the hopping amplitude and Δ is the superconducting pairing amplitude, which we assume to be real.[1] Each fermionic

[1] In general Δ would be a complex quantity, $|\Delta| e^{i\phi}$, with ϕ being the phase of the pairing potential.

state is described by a pair of annihilation and creation operators $c_j, c_j^\dagger$, respectively, which obey the usual anticommutation relation $\{c_i, c_j\} = \{c_i^\dagger, c_j^\dagger\} = 0$ and $\{c_i, c_j^\dagger\} = \delta_{i,j}$. We can note the breaking of time-reversal symmetry in (3.1), since we are considering the same value for all the spin projections: this means that the fermions in the system can be handled like spinless particles, and we can suppress the spin index[137].
We now want to rewrite the Hamiltonian (3.1) in terms of new operators called *Majorana operators*, formally defined as

$$a_{2j-1} = c_j^\dagger + c_j, \qquad a_{2j} = i(c_j^\dagger - c_j), \qquad j = 1, ..., N, \tag{3.2}$$

which are hermitian, satisfying the relation

$$a_i^\dagger = a_i, \qquad i = 1, ..., 2N. \tag{3.3}$$

From the anticommutation relations of the former fermionic operators we can obtain the anticommutation relations for Majorana operators:

$$\{a_{2j-1}, a_{2l-1}\} = 2\delta_{j,l} \tag{3.4a}$$

$$\{a_{2j}, a_{2l}\} = 2\delta_{j,l} \tag{3.4b}$$

$$\{a_{2j}, a_{2l-1}\} = 0. \tag{3.4c}$$

It is worth remarking the particular nature of the particles created (or annihilated) by the operators (3.2). In particle physics, Majorana fermions (MFs) are particles which are their own anti-particles[138], predicted by Ettore Majorana in his seminal work in 1937[139]. Even if the existence of such elementary particles is still an open question and occupies a central place in several frontiers of modern physics, MFs are likely to exist as quasi-particle excitations in certain condensed matter systems, like the one we are considering. This condensed matter version of MFs has attracted a solid theoretical interest, mainly because of their peculiar statistics: they are indeed *non-abelyan anyons*,

Anyway, with open boundary conditions, our assumption is not so severe, as we can set the phase ϕ equal to zero, or hide the phase dependence into a slightly different definition of Majorana operators:

$$a_{2j-1} = e^{-i\frac{\phi}{2}} c_j^\dagger + e^{i\frac{\phi}{2}} c_j, \qquad a_{2j} = ie^{-i\frac{\phi}{2}} c_j^\dagger - ie^{i\frac{\phi}{2}} c_j, \qquad j = 1, ..., N.$$

and their exchanges have to be managed carefully, as in general they do not commute. Moreover, any fermionic state can be obtained by the superposition of two MFs. This operation essentially corresponds to the splitting of a fermion into a real and an imaginary part. Following the definition (3.2), we get

$$c_j = \frac{1}{2}(a_{2j-1} + ia_{2j}), \qquad c_j^\dagger = \frac{1}{2}(a_{2j-1} - ia_{2j}). \tag{3.5}$$

A notable consequence is that Majorana operators only contain half a degree of freedom, and does not obey to the usual Pauli exclusion principle for normal fermions, but instead

$$a_j^2 = (a_j^\dagger)^2 = a_j^\dagger a_j = a_j a_j^\dagger = 1. \tag{3.6}$$

It is therefore meaningless to speak of the occupancy number of a Majorana mode in the usual form $n_i^{MF} = a_j^\dagger a_j$, since, exploiting the hermiticity of the operators, we have

$$n_i^{MF} \equiv 1, \tag{3.7}$$

and thus a Majorana mode can always be thought to be half filled and half empty. We can now rewrite (3.1) in terms of MFs, obtaining the Hamiltonian in the form

$$H = \frac{i}{2}\sum_{j=1}^{N-1}[(\Delta - t)a_{2j-1}a_{2j+2} + (\Delta + t)a_{2j}a_{2j+1}] - \frac{i}{2}\sum_{j=1}^{N}\mu a_{2j-1}a_{2j} \tag{3.8}$$

where we used the anticommutation relations (3.4).

3.1.1 PARTICULAR CASES

We consider two interesting special cases:

(a) $\Delta = t = 0, \mu < 0$: the Hamiltonian (3.8) turns out to be

$$H = -\mu\frac{i}{2}\sum_j a_{2j-1}a_{2j} = -\mu\sum_{j=1}^{N}(c_j^\dagger c_j). \tag{3.9}$$

In this trivial case we obtain a pairing between operators acting on the same site, thus forming a ground state with fermionic occupancy number $n_j = 0$.

(b) $\Delta = t > 0, \mu = 0$: this is the case where the Majorana modes physics is most easily understood, as we have

$$H = it\sum_{j=1}^{N-1} a_{2j}a_{2j+1}. \tag{3.10}$$

The curious thing here is that the pairing appears between Majorana operators from *different sites*. We can recast again our Hamiltonian through the definition of a new set of fermion operators:

$$\tilde{c}_j = \frac{1}{2}(a_{2j} + ia_{2j+1}), \qquad \tilde{c}_j^\dagger = \frac{1}{2}(a_{2j} - ia_{2j+1}), \tag{3.11}$$

which obey to the fermionic anticommutation rules. The Hamiltonian then becomes

$$\begin{aligned} H &= it\sum_{j=1}^{N-1} a_{2j}a_{2j+1} = -t\sum_{j=1}^{N-1}(\tilde{c}_j^\dagger + \tilde{c}_j)(\tilde{c}_j^\dagger - \tilde{c}_j) \\ &= -t\sum_{j=1}^{N-1}(1 - 2\tilde{c}_j^\dagger\tilde{c}_j) = 2t\sum_{j=1}^{N-1}\left(\tilde{c}_j^\dagger\tilde{c}_j - \frac{1}{2}\right). \end{aligned} \tag{3.12}$$

So far, it might seem that the Majorana operators are simply a merely formal and mathematical way to represent the chain Hamiltonian in some alternative fashion, where the physical excited states are obtained through the superposition of nearest neighboring MFs. On the contrary, something really meaningful about the physics of the system is contained inside the Hamiltonian (3.10): there are two Majorana operators, namely a_1 and a_{2N}, which no longer appear in any term of the Hamiltonian. We can describe these two operators, located ad the edges of the chain, by a single fermionic state, corresponding to a pair of operators defined as

$$\tilde{c}_M = \frac{1}{2}(a_1 + ia_{2N}), \qquad \tilde{c}_M^\dagger = \frac{1}{2}(a_1 - ia_{2N}). \tag{3.13}$$

This state, since a_1 and a_{2N} are localized on opposite ends of the wire, represents a highly non-local state, which absence from the Hamiltonian means that the energy required for its occupation is zero. We turn now our focus on the ground state of the system: a state $|\psi\rangle$, in order to be a ground state, must satisfy the condition

$$\tilde{c}_j |\psi\rangle = 0, \quad j = 1, ..., N-1. \tag{3.14}$$

In our case of interest, there are two orthogonal states $|\psi_0\rangle, |\psi_1\rangle$ which satisfies this property, related by (3.13):

$$|\psi_0\rangle = \frac{1}{2}(a_1 + ia_{2N})|\psi_1\rangle = \tilde{c}_M |\psi_1\rangle \tag{3.15a}$$

$$|\psi_1\rangle = \frac{1}{2}(a_1 - ia_{2N})|\psi_0\rangle = \tilde{c}_M^\dagger |\psi_0\rangle . \tag{3.15b}$$

Orthogonality of the states can be proven using (3.4):

$$\begin{aligned}\langle\psi_0|\psi_1\rangle &= \frac{1}{4}\langle\psi_1|\,(a_1 - ia_{2N})(a_1 - ia_{2N})\,|\psi_0\rangle \\ &= \frac{1}{4}\langle\psi_1|\,a_1^2 - ia_1a_{2N} - ia_{2N}a_1 - a_{2N}^2\,|\psi_0\rangle \\ &= \langle\psi_1|\,a_1a_{2N} - a_1a_{2N}\,|\psi_0\rangle = 0.\end{aligned} \tag{3.16}$$

As we mentioned earlier, defining an occupancy number of a Majorana state through the usual fermionic number operator is not truly significative. However, the fermionic states actually contain a certain number of particles, and they are eigenstates of the parity operator

$$HatP = \prod_{j=1}^{N-1}(-ia_{2j-1}a_{2j}) = \prod_{j=0}^{N-1}(1 - 2\tilde{c}_j^\dagger\tilde{c}_j). \tag{3.17}$$

The possible eigenvalues are ± 1, depending on whether the eigenstate is occupied by an even or odd number of particles. It is easy to see that the ground states ψ_0 and ψ_1 have opposite parity. We note that,

$$\begin{aligned}\{HatP, \tilde{c}_j^\dagger\} = HatP\tilde{c}_j^\dagger + \tilde{c}_j^\dagger HatP &= \prod_{j=0}^{N-1}(\tilde{c}_j^\dagger - 2\tilde{c_j}^\dagger\tilde{c}_j\tilde{c}_j^\dagger) + \prod_{j=0}^{N-1}(\tilde{c}_j^\dagger - 2\tilde{c_j}^\dagger\tilde{c}_j^\dagger\tilde{c}_j) \\ &= \prod_{j=0}^{N-1}(\tilde{c}_j^\dagger - 2\tilde{c_j}^\dagger\tilde{c}_j\tilde{c}_j^\dagger) - \prod_{j=0}^{N-1}(\tilde{c}_j^\dagger - 2\tilde{c_j}^\dagger\tilde{c}_j\tilde{c}_j^\dagger) = 0,\end{aligned} \tag{3.18}$$

and thus

$$HatP\,|\psi_1\rangle = HatP\tilde{c}_M^\dagger\,|\psi_0\rangle = -\tilde{c}_M^\dagger HatP\,|\psi_0\rangle = -\tilde{c}_M^\dagger(\pm\,|\psi_0\rangle) = \mp\,|\psi_1\rangle \tag{3.19}$$

from which the opposite parity of the ground states is demonstrated.

The two cases (a) and (b) represent two different topological phases, or univerality classes, of the system, as (a) presents a trivial ground state with no zero energy Majorana modes, while in (b), since the Hamiltonian (3.10) allows for an odd number of quasiparticles at zero energy cost, the ground state is two-fold degenerate, corrisponding to having an even or an odd total number of fermions in the system. [2] We will now see what happens

[2] A subtle observation is that the bulk properties of the two phases are exactly the same, as we can transform one phase to the other by a simple permutation of the operators $a_j \mapsto a_{j+1}$, which is a usual local operation in lattice models study. Anyway, we are essentially interested in the behaviour of the boundaries of the chain, and that remains clearly different since a map like the one just mentioned is not well defined at the boundaries of our system: only (b) has unpaired Majorana fermions at the ends of the wire.

when considering the general case with arbitrary values of Δ, t, μ, and we will derive the necessary conditions for the existence of Majorana zero energy modes at the end of the wire.

3.1.2 GENERAL CASE

First, we will analyze the spectrum of the original Hamiltonian (3.1), which we recall here:

$$H = \sum_{j=1}^{N-1} \left[-t \left(c_j^\dagger c_{j+1} + c_{j+1}^\dagger c_j \right) + \Delta \left(c_{j+1}^\dagger c_j^\dagger + c_j c_{j+1} \right) \right] - \sum_{j=1}^{N} \mu \left(c_j^\dagger c_j - \frac{1}{2} \right).$$

We'll assume now periodic boundary conditions, that correspond to the transformation of the wire into a closed ring, where interactions between sites 1 and N are allowed.[3] Subsequentially, our system acquires a translational invariance property, which we can exploit by switching to the momentum space through a discrete Fourier transform:

$$b_k = \frac{1}{\sqrt{N}} \sum_{j \in BZ} c_j \, \mathrm{e}^{-ikj}, \qquad b_k^\dagger = \frac{1}{\sqrt{N}} \sum_{j \in BZ} c_j^\dagger \, \mathrm{e}^{ikj} \tag{3.20}$$

where the k run through the first *Brillouin zone* and b_k ($b_k^\dagger$) annihilates (creates) a fermion with momentum k. According to our boundary conditions, the possible k are quantized as $k_n = \frac{2\pi}{N} n$, with $-N/2 \leq n \leq N/2$. The Hamiltonian then becomes[4]

$$H = \sum_{k \in BZ} \epsilon_k b_k^\dagger b_k - \sum_{k \in BZ} \left(\tilde{\Delta}_k b_k b_{-k} + h.c. \right) + \frac{\mu N}{2}, \tag{3.21}$$

where $\epsilon_k = -(\mu + 2t\cos(k))$ represent the energy levels with respect to the Fermi energy, and $\tilde{\Delta}_k = -i\Delta \sin(k)$ is the modified p-wave pairing amplitude. We can now introduce the Nambu spinor $\mathbf{b}_k^\dagger \equiv (b_k, b_{-k}^\dagger)$, trough which we can express (3.21) in its *Bogoliubov-de Gennes* form: [5]

$$H = \frac{1}{2} \sum_{k \in BZ} \mathbf{b}_k^\dagger H_{BdG} \mathbf{b}_k, \tag{3.22}$$

[3] We are basically saying that $c_{N+1} = c_1$.

[4] Reminding that

$$\sum_{j=1}^{N} e^{i(k'-k)j} = N\delta_{k,k'}.$$

[5] We are now neglecting the constant term $\frac{\mu N}{2}$

with

$$H_{BdG} = \begin{pmatrix} \epsilon_k & \tilde{\Delta}_k^* \\ \tilde{\Delta}_k & -\epsilon_k \end{pmatrix} = \begin{pmatrix} -(\mu + 2t\cos(k)) & i\Delta\sin(k) \\ -i\Delta\sin(k) & (\mu + 2t\cos(k)) \end{pmatrix} \tag{3.23}$$

Now, we can diagonalize the Hamiltonian through a Bogoliubov transformation:

$$\mathbf{b}_k = U^\dagger \boldsymbol{\eta}_k, \qquad \boldsymbol{\eta}_k = \begin{pmatrix} \eta_k \\ \eta_{-k}^\dagger \end{pmatrix}, \tag{3.24}$$

where the matrix U is

$$U = \begin{pmatrix} \cos(\theta_k) & i\sin(\theta_k) \\ i\sin(\theta_k) & \cos(\theta_k) \end{pmatrix}, \tag{3.25}$$

and θ_k is given by

$$\tan(2\theta_k) = -\frac{\sin(k)}{2t\cos(k) + \mu}. \tag{3.26}$$

The Hamiltonian, in the new Bogoliubov basis, is

$$H^B = \sum_{k \in BZ} E(k) \left(\eta_k^\dagger \eta_k - \frac{1}{2} \right), \tag{3.27}$$

where the $E(k)$ are obtained as the eigenvalues of the matrix $H'_{BdG} = U H_{BdG} U^\dagger$, and are

$$E(k) = \pm\sqrt{(2t\cos(k) + \mu)^2 + (2\Delta\sin(k)^2)}. \tag{3.28}$$

Returning now to our original dicussion about the existence of Majorana zero energy modes at the ends of the chain, we can argue that, for $L \to \infty$, the dispersion relation (3.28) holds even for open boundary conditions, as the bulk properties are the same both for a ring and for a chain. Thus, we can analyze the bulk spectrum to find zero energy modes in a gapped region in the limit $L \to \infty$. If these states exist, they are of the form [41]

$$b' = \sum_j (\alpha'_+ x_+^j + \alpha'_- x_-^j) a_{2j-1}, \tag{3.29a}$$

$$b'' = \sum_j (\alpha''_+ x_+^{-j} + \alpha''_- x_-^{-j}) a_{2j}, \tag{3.29b}$$

where the coefficients $\alpha'_+, \alpha'_-, \alpha''_+, \alpha''_-$ depend on the choice of the boundary conditions and $x_\pm$ is

$$x_\pm = \frac{-\mu \pm \sqrt{\mu^2 - 4t^2 + 4\Delta^2}}{2(t + \Delta)}. \tag{3.30}$$

With hard wall boundary conditions at $j = 0$ and $j = N + 1$ the coefficients are given by the following set of equations:

$$\alpha'_- + \alpha'_+ = 0 \tag{3.31a}$$

$$\alpha''_- + \alpha''_+ = 0 \tag{3.31b}$$

$$\alpha -' x_-^{-(N+1)} + \alpha'_+ x_+^{-(N+1)} = 0 \tag{3.31c}$$

$$\alpha -'' x_-^{-(N+1)} + \alpha''_+ x_+^{-(N+1)} = 0. \tag{3.31d}$$

Now, we are going to conjecture two expected existence domains of the two phases (a) and (b), analyzing two distinct cases:[41]

i) $|\mu| > 2|t|$: in this case, with respect to (3.31), we have

$$|x_+| = \left| \frac{1 + \sqrt{1 - \left(\frac{2t}{\mu}\right)^2 + \left(\frac{2\Delta}{\mu}\right)^2}}{\frac{2t}{|\mu|} + \frac{2\Delta}{|\mu|}} \right| > \left| \frac{1 + \frac{2\Delta}{|\mu|}}{\frac{2t}{|\mu|} + \frac{2t}{|\mu|}} \right| > \left| \frac{1 + \frac{2\Delta}{|\mu|}}{1 + \frac{2\Delta}{|\mu|}} \right| = 1 \tag{3.32}$$

$$|x_+ x_-| = \left| \frac{\mu^2 - \mu^2 + 4t^2 - 4\Delta^2}{4(t + \Delta)^2} \right| = \left| \frac{t - \Delta}{t + \Delta} \right| < 1. \tag{3.33}$$

These two equations combines with $|x_-| < 1$, but for $|\mu| > 0$ we would have $|x_+| < 1$ and $|x_-| > 1$. Thus, it is not possible to find a non trivial solution for both α'_- and α'_+ (or α''_-, α''_+) that satispfy the boundary conditions. Then, we can conlude that the supposed zero modes (3.29) do not exist in this domain.

ii) $|\mu| < 2t, \Delta \neq 0$: now we find that $|x_-|, |x_+| < 1$. This means that it is possible to have a zero-energy edge state of the form (3.29) that satisfies the boundary conditions with both α'_- and α'_+ (or α''_-, α''_+) non zero. The state b' is localized near $j = 0$, while b'' near $j = N$. If we have $|\mu| < -2t, |\Delta \neq 0$, simply b' and b'' switch their places. In conclusion, this is the existence domain of the phase (b).

As a final remark, we note that the above discussion is strictly exact only in the $L \to \infty$ limit. On the contrary, if the wire dimension is finite, as in reality, there is a small coupling between the two edge states. Kitaev modelled this interaction through an effective Hamiltonian, namely

$$H_{\text{eff}} = \frac{i}{2} \gamma b' b'', \qquad \gamma \propto e^{-\chi L}, \tag{3.34}$$

where L is the length of the chain and $\chi = \min(|\log |x_-||, |\log |x_+||)$. Furthermore, this Hamiltonian is still robust enough even with the inclusion of small electron-electron interactions.[41]

3.2 KITAEV CHAIN WITH LONG-RANGE INTERACTIONS

In this section we introduce and review the properties of a recently proposed [48] Hamiltonian that describes a generalization of the original Kitaev model (3.1) with long-range p-wave pairing, that decays with distance l as $l^{-\alpha}$. The model Hamiltonian is

$$H_{LRK} = \sum_{j=1}^{L} \left[-\mu \left(c_j^\dagger c_j - \frac{1}{2} \right) - t \left(c_j^\dagger c_{j+1} + c_{j+1}^\dagger c_j \right) + \Delta \sum_{l=1}^{L-1} d_l^{-\alpha} \left(c_{j+l}^\dagger c_j^\dagger + c_j c_{j+l} \right) \right], \tag{3.35}$$

where d_l^α is the function that gives the decaying interacting strenght between sites. If we again consider a closed ring, we define $d_l = l$ for $l < L/2$ and $d_l = (L - l)$ for $l > L/2$, and in both cases the decaying factor is given by the exponent α. The main feature of (3.35) is that even with long-range p-wave pairing, it remains still quadratic in the fermionic operators $c_j^\dagger, c_j$, meaning that the model can still be solved exactly. Another crucial aspect of (3.35) is that if one consider the limit $\alpha \to \infty$ i.e., reducing the problem to the study of (3.1), our model can be transformed, via a Jordan-Wigner map, into the XY-Ising model with pure nearest-neighbor interactions, that is a widely studied model able to describe effectively the quantum phase transition between a paramagnetic and an ordered phase [140] [141]. Anyway, for any finite value of α, the Hamiltonian (3.35) is no longer mappable into a spin model through a J-W transformation, and the phase diagrams of the two models can be different [48].

3.2.1 EXCITATION SPECTRUM

Following the exact same procedure of Sect.3.1.2, we consider a translationally invariant closed ring with anti-periodic boundary conditions ($c_i = -c_{i+L}$), in order to avoid the erasing of terms like $c_j c_{j+l}$ and $c_{j+l} c_{j+l+L}$ during the sum operation. Again, we are able to perform a discrete Fourier transform of the fermionic operators and switch to the lattice momenta space, but this time, due to the anti-periodic boundary conditions, our crystalline momenta will be quantized as $k_n = \frac{2\pi}{L}\left(n + \frac{1}{2}\right)$. The Hamiltonian assumes the form

$$H = -\sum_{k \in BZ} (\mu + 2t\cos(k)) b_k^\dagger b_k + i\Delta \sum_{k \in BZ} \sum_{l=1}^{L-1} \frac{\sin(kl)}{d_l^\alpha} (b_k b_{-k} - b_{-k}^\dagger b_k^\dagger) + \frac{\mu L}{2}. \tag{3.36}$$

We can define as $f_\alpha(k)$ the series

$$f_\alpha(k) = \sum_{l=1}^{L-1} \frac{\sin(kl)}{d_l^\alpha}, \tag{3.37}$$

with $d_l = \min[l, L-l]$. In the thermodynamic limit $L \to \infty$, we have

$$f_\alpha^\infty(k) = -i \sum_{l=1}^{\infty} \frac{\mathrm{e}^{ikl} + \mathrm{e}^{-ikl}}{d_l^\alpha} = -i[\mathrm{Li}_\alpha(\mathrm{e}^{ik}) - \mathrm{Li}_\alpha(\mathrm{e}^{-ik})], \tag{3.38}$$

where $\mathrm{Li}_\alpha(z)$ is the *polylogarithm*[142] of a complex variable z of order α:

$$\mathrm{Li}_\alpha(z) = \sum_{l=1}^{\infty} \frac{z^l}{l^\alpha} \tag{3.39}$$

So, neglecting the constant term $\frac{\mu L}{2}$, our long-range Kitaev Hamiltonian is

$$H_{LRK} = -\sum_{k \in BZ} (\mu + 2t\cos(k)) b_k^\dagger b_k + i\Delta \sum_{k \in BZ} f_\alpha(k)(b_k b_{-k} - b_{-k}^\dagger b_k^\dagger). \tag{3.40}$$

Following the steps described in Sect. 3.1.2, we diagonalize (3.40) via a Bogoliubov transformation:

$$\begin{pmatrix} b_k \\ b_{-k}^\dagger \end{pmatrix} = U^\dagger \begin{pmatrix} \eta_k \\ \eta_{-k}^\dagger \end{pmatrix} \tag{3.41}$$

where U is the same as (3.25), but θ_k is given by

$$\tan(2\theta_k) = -\frac{\Delta f_\alpha(k)}{2t\cos(k) + \mu}. \tag{3.42}$$

We can rewrite the Hamiltonian in the Bogoliubov basis and obtain the excitation spectrum:

$$H_{LRK}^B = \sum_{k \in BZ} \lambda_\alpha(k) \left(\eta_k^\dagger \eta_k - \frac{1}{2} \right), \tag{3.43}$$

$$\lambda_\alpha(k) = \sqrt{(2t\cos(k) + \mu)^2 + (\Delta f_\alpha(k))^2}. \tag{3.44}$$

We can also obtain the structure of the ground state, that has a BCS-like form:

$$|GS\rangle = \prod_k (\cos\theta_k - i\sin\theta_k b_k^\dagger b_{-k}^\dagger) |0\rangle, \tag{3.45}$$

where $|0\rangle$ is the vacuum state of fermion operators b_k.

3.3 CRITICALITY

In the thermodynamic limit $L \to \infty$, it is possible to evaluate the critical lines of our model. The momenta belong to the continuous interval $k \in [0, 2\pi]$, and the dispersion relation is given by (3.44), with $f_\alpha(k) = -i[\mathrm{Li}_\alpha(\mathrm{e}^{ik}) - \mathrm{Li}(\mathrm{e}^{-ik}]$. Studying the behaviour of $f_\alpha(k)$ we can determine the critical lines. For $\alpha > 1$, the series (3.39) is absolutely convergent, while for $\alpha < 1$ the series absolutely converges only for $z \neq 1$ ($k \neq 0$) and diverges as

$$\mathrm{Li}_\alpha(\mathrm{e}^{ik}) \sim \Gamma(1-\alpha)\frac{i^\alpha}{k^{1-\alpha}}, \quad \text{for } k \to 0. \tag{3.46}$$

Considering the particular cases $\alpha = 0, 1$ one gets the following expression for $\mathrm{Li}_\alpha(z)$,

$$\mathrm{Li}_1(z) = -\ln(1-z), \quad \mathrm{Li}_0(z) = \frac{z}{1-z}, \tag{3.47}$$

and substituting in (3.38) one obtains

$$f_1^\infty(k) = \pi - k, \quad f_0^\infty(k) = \cot\left(\frac{k}{2}\right). \tag{3.48}$$

The zeroes of $f_\alpha^\infty(k)$ are obtained by substituting $k = \pi$ for all $\alpha > 0$ into (3.38). In fact, in this case one has $f_\alpha^\infty(\pi) = 0$ as $\mathrm{Li}_\alpha(-1)$ reduces to the Dirichlet eta function, which is finite for all $\alpha > 0$. For $k = 0$ we have to be more careful, since we have $f_\alpha^\infty(0) = 0$ only when $\alpha > 1$ (see figure 3.1).

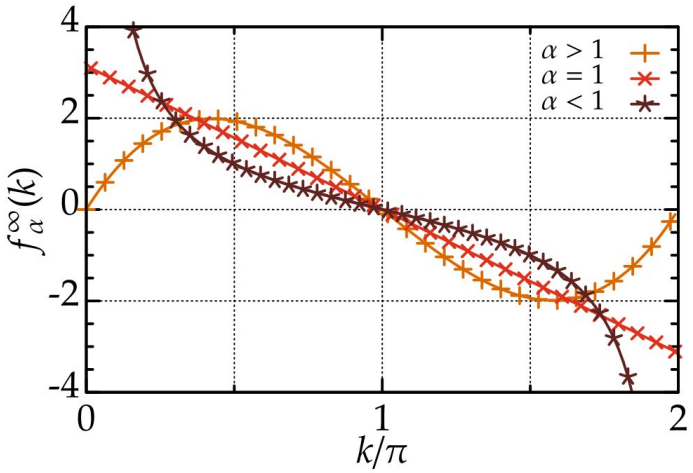

Figure 3.1: Behaviour of f_α^∞ for $\alpha > 1$, $\alpha = 1$, $\alpha < 1$.

Thus, for $\alpha > 1$ there are two critical values of k for which $f_\alpha^\infty(k_c) = 0$, $k_c = 0, \pi$, and both lines $\mu = 2\omega$ and $\mu = -2\omega$ are critical. On the other hand, when $\alpha \leq 1$ $f_\alpha^\infty(k_c) = 0$ only for $k_c = \pi$, implying that only $\mu = 2\omega$ represents a critical line, while $\mu = 2\omega$ is gapped because $f_\alpha^\infty(k) \to \infty$ for $k \to 0$. Hence, tuning α and ω in the limit $\alpha \to 0$, we are able to connect continuously the paramagnetic and ferromagnetic phases for $|\mu| > 2\omega$ and $|\mu| < 2\omega$ without closing the gap. Moreover, the presence of any finite α breaks the symmetry of the phase diagram of the short-range model across the line $\mu = 0$, since in (3.35) the transformation $a_i \to (-1)^i a_I^\dagger$ no longer connects $\mu > 0$ to $\mu < 0$.

3.3.1 ASYMPTOTIC BEHAVIOUR OF CORRELATION FUNCTIONS

Exploiting the integrability of the long range Hamiltonian (3.35), we can analyze the asymptotic nature of its correlation functions, computed on the ground state (3.45). Since the Hamiltonian is quadratic, we can use Wick's theorem to compute high orders correlators starting from the two point correlator $C_1(R) = \langle c_R^\dagger c_0 \rangle$ and the anomalous one $F_1(R) = \langle c_R^\dagger c_0^\dagger \rangle$, e.g.

$$C_2(R) = \langle n_R n_0 \rangle = \langle n_R \rangle \langle n_0 \rangle - \langle c_R^\dagger c_0^\dagger \rangle \langle c_R c_0 \rangle + \langle c_R^\dagger c_0 \rangle \langle a_R a_0^\dagger \rangle. \tag{3.49}$$

If we consider a finite chain in the limit $L \to \infty$ (with $R > 0$) the correlation functions $C_1(R)$ and $F_1(R)$ take the form[48]

$$C_1(R) = \langle c_R^\dagger c_0 \rangle = -\frac{1}{\pi} \Re \int_0^\pi dk \, \mathrm{e}^{ikR} \mathcal{C}_\alpha(k), \qquad \mathcal{C}_\alpha(k) = \frac{\cos(k) + \mu}{2\lambda_\alpha(k)} \tag{3.50}$$

$$F_1(R) = \langle c_R^\dagger c_0^\dagger \rangle = \frac{1}{\pi} \Im \int_0^\pi dk \, \mathrm{e}^{ikR} \mathcal{F}_\alpha(k), \qquad \mathcal{F}_\alpha(k) = \frac{\Delta f_\alpha(k)}{2\lambda_\alpha(k)}. \tag{3.51}$$

We are able to evaluate the asymptotic behaviour of the integrals in (3.50) and (3.51) since they are a particular case of *Fourier type integrals* of the form

$$I(R) = \int_a^b f(k) \, \mathrm{e}^{iRg(k)}, \tag{3.52}$$

with $g(k) = k$, and thus the following holds[143]:

Lemma. *Consider the integral*

$$I(R) = \int_a^b f(k) \, \mathrm{e}^{iRk}, \tag{3.53}$$

where $[a, b]$ is a real finite interval. Assume that $f(k)$ has $N + 1$ continuous derivatives and that $f^{(N+2)}(k)$ is piecewise continuous on $[a, b]$. Then, an asymptotic expansion can

be obtain in the limit $R \to \infty$:

$$I(R) \sim \sum_{n=0}^{N} \frac{(-1)^n}{(iR)^{(n+1)}} \left[f^{(n)}(b)\, \mathrm{e}^{iRb} - f^{(n)}(a)\, \mathrm{e}^{iRa} \right]. \tag{3.54}$$

Exploiting the above lemma, we will show the asymptotic form of (3.50) and (3.51) in three different cases: $\alpha = 0$, $\alpha = 1$ and $\alpha > 1$. As we will see, the most notable result of this calculation is the peculiar behaviour of the correlation functions, which show a surprising algebraic decay for $\alpha \leq 1$ at all length scales, and a hybrid exponential-algebraic decay for $\alpha > 1$. Usually, in a gapped system one assumes an exponential decay of correlations[144], but this surprising behaviour is consistent with the exponential-algebraic Lieb-Robinson bounds on the propagation of information in systems with power-law interactions.[145,146] Furthermore, this result on Lieb-Robinson bounds extended to quantum many-body systems with long-range interactions decaying by power-law has been proven recently in a more mathematically rigorous manner, showing that the group velocity of information propagation grows by power-law in time.[147]

$\boldsymbol{\alpha = 0}$

We have $f_0(k) = \cot(k/2)$, and thus

$$\lambda_0(k) = \sqrt{(\cos(k) + \mu)^2 + \Delta^2 \cot^2\left(\frac{k}{2}\right)}. \tag{3.55}$$

From (3.54), (3.50) and (3.51) we get the long range behaviours of the two-point correlator[48]:

$$C_1(R) = \frac{\mu + 1}{4\pi\Delta} \frac{1}{R^2} + \mathcal{O}(R^{-4}), \tag{3.56}$$

and the anomalous correlator:

$$F_1(R) = -\frac{1}{2\pi} \frac{1}{R} + \mathcal{O}(R^{-3}). \tag{3.57}$$

In the critical case $\mu = 1$, since $\mathcal{C}_0'(k) = (\cos(k) + \mu)/(4\Delta)$, we have $\mathcal{C}_0'(0) = -\mathcal{C}_0'(\pi) = 1/(2\Delta)$, which leads to

$$C_1(R) = \frac{\cos(\pi R) - 1}{2\pi\Delta R^2} + \mathcal{O}(R^{-4}). \tag{3.58}$$

We can study the anomalous correlator, for which we have $\mathcal{F}_0(0) = \mathcal{F}_0(\pi) = 1/2$, in a similar way, obtaining

$$F_1(R) = -\frac{\cos(\pi R)}{2\pi R} + \mathcal{O}(R^{-3}). \tag{3.59}$$

At this point, we can combine the previous results in order to get the density-density correlation functions $C_2(R)$, and exploiting (3.49) we have

$$C_2(R) = \langle n_R n_0 \rangle = \frac{1 - \cos(\pi R)}{2\pi R} + \mathcal{O}(R^{-4}), \tag{3.60}$$

which recalls a known result from the Luttinger model.[148]

$\boldsymbol{\alpha = 1}$

In this case we have

$$\lambda_1(k) = \sqrt{(\cos(k) + \mu)^2 + \Delta^2(\pi - k)^2}, \tag{3.61}$$

and thus

$$\mathcal{C}_1'(0) = \frac{\pi(1+\mu)\Delta^2}{2[\Delta^2\pi^2 + (1+\mu)^2]^{\frac{3}{2}}}, \qquad \mathcal{C}_1'(\pi) = 0. \tag{3.62}$$

Therefore, (3.50) shows a power-law behaviour:

$$C_1(R) = \frac{(1+\mu)\Delta^2}{[\Delta^2\pi^2 + (1+\mu)^2]^{\frac{3}{2}} R^2} = \mathcal{O}(R^{-4}). \tag{3.63}$$

For the anomalous correlator (3.51) we have

$$\mathcal{F}_1(0) = \frac{\Delta\pi}{2\sqrt{(\mu+1)^2 + \Delta^2\pi^2}}, \qquad \mathcal{F}_1(\pi) = 0, \tag{3.64}$$

so that

$$F_1(R) = -\frac{\Delta}{2\sqrt{(\mu+1)^2 + \Delta^2\pi^2} R} + \mathcal{O}(R^{-3}). \tag{3.65}$$

$\boldsymbol{\alpha > 1}$

Starting from (3.50), we can express the correlator as[48]

$$\begin{aligned} C_1(R) = \langle c_R^\dagger c_0 \rangle &= -\frac{1}{\pi} \Re \int_0^\pi dk\, \mathrm{e}^{ikR}\, \mathcal{C}_\alpha(k) \\ &= \frac{1}{\pi} \sum_n \cos\left((n=1)\frac{\pi}{2}\right) \frac{\mathcal{C}_\alpha^{(n)}(\pi)\cos(\pi R) - \mathcal{C}_\alpha^{(n)}(0)}{R^{n+1}}. \end{aligned} \tag{3.66}$$

In order to get a nonzero contribution from the above sum, we must fulfill the two following conditions:

- $\cos\left((n=1)\frac{\pi}{2}\right) \neq 0$, meaning that n must be odd;

- At least one between $\mathcal{C}_\alpha^{(n)}(\pi)$ and $\mathcal{C}_\alpha^{(n)}(0)$ must be nonzero.

Considering $\alpha > 1$, with α an odd integer, we have $\mathcal{C}^{(n)} \neq 0$ if $n \geq \alpha$, and we get the following long-range decay of $C_1(R)$:

$$C_1(R) = \frac{1}{\pi} \cos\left(\frac{\pi}{2}(\alpha+1)\right) \frac{\mathcal{C}^{(\alpha)}(0)}{R^{\alpha+1}} + \mathcal{O}(R^{-(\alpha+2)}). \tag{3.67}$$

Similarly, the anomalous correlator $F_1(R)$ is

$$F_1(R) = -\frac{\Delta}{\pi} \sin\left(\frac{\pi}{2}\alpha\right) \frac{\mathcal{F}^{(\alpha)}(0)}{R^{\alpha}} + \mathcal{O}(R^{-(\alpha+1)}). \tag{3.68}$$

3.3.2 ENTANGLEMENT SCALING

As we saw in the previous chapter about localized systems properties, one of the most exploited indicators in numerical studies over the last ten years has been the scaling of the entanglement entropy with system size. We consider a chain of length L, and a partition into two subregions A and B containing l and $L-l$ sites. Through the ground state (3.45) we can build the total density matrix as the projector

$$\rho = |GS\rangle \langle GS| , \tag{3.69}$$

and tracing out all the degrees of freedom of B we can obtain the reduced density matrix of the subsystem A,

$$\rho_A(l) = \mathrm{Tr}_B\, \rho. \tag{3.70}$$

Now, the von Neumann entanglement entropy S^A of the reduced density matrix ρ_A is given by (1.45), which we rewrite for convenience,

$$S_{VNEE}(l) = -\,\mathrm{Tr}\{\rho_A \log \rho_A\}. \tag{3.71}$$

We already said in 2.3.3 that for the ground states of local gapped Hamiltonians one does not find an extensive scaling of the entanglement with the system size, while one generally obtains an area-law, which reduces to the saturation of the entropy to a constant in one dimensional systems[122]. Furthermore, results from conformal field theory have also shown that the scaling changes at criticality, reflecting the universal behaviour of the system[149,150]. Summarizing these two different behaviours, we can say that away from criticality, since a gapped system has a finite correlation length[151] ξ_{corr}, the entropy saturates to a constant and obeys an area law,

$$S_{VNNE}(l) = \frac{c}{3} \log \xi_{corr}, \tag{3.72}$$

where c is the central charge of the underlying conformal field theory. Conversely, at criticality $S_{VNEE}(l)$ diverges logarithmically with the size l,

$$S^{c}_{VNEE}(l) = \frac{c}{3} \log \left[\frac{L}{\pi} \sin \left(\frac{\pi l}{L} \right) \right] + a, \tag{3.73}$$

where a is a nonuniversal term. In[48], exploiting the Peschel method described in the

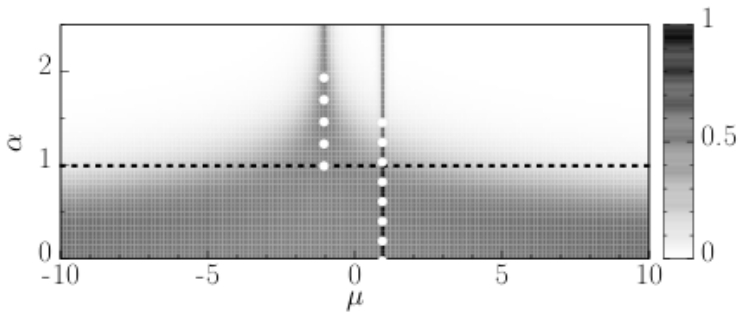

Figure 3.2: Phase diagram showing c_{eff} (greyscale) as a function of α and μ. Two violations of the area-law for the entanglement entropy scaling are visible around the critical lines $|\mu| = 1$. The horizontal dashed line separates two regions: correlation functions show an algebric decay for $\alpha < 1$ and a hybrid exponential-algebraic decay for $\alpha > 1$.[48]

appendix A, the von Neumann entropy for the Hamiltonian (3.35) is computed for different system sizes L and for different values of μ. The results for half of the chain, i.e. $S(L/2)$, show that for all α and μ the entropy is well approximated by (3.73) with an effective central charge c_{eff},

$$S(l) = \frac{c_{eff}}{3} \log \left[\frac{L}{\pi} \sin \left(\frac{\pi l}{L} \right) \right] + a. \tag{3.74}$$

In figure 3.2 c_{eff} is plotted fitting $S(L/2)$ for various values of α and μ. We can note that for $\alpha > 1$ c_{eff} is almost zero for any value of μ except for the critical lines $|\mu| = 1$ ($\Delta = 2\omega = 1$ are fixed), where logarithmic deviations become important. In particular, in the vicinity of $\mu = -1$ the violation of the area law is quite clear for $\alpha < 2$. For $\alpha < 1$ the effective central charge c_{eff} is different from zero in the whole gapped region $|\mu| \neq 1$, implying a violation of the area-law, an unexpected result that goes against (3.72). This peculiar behaviour of c_{eff} has to be ascribed to the very strong long-range pairing, which manifests its consequences in non-local quantities such as $S(L/2)$ and correlation functions.

The most remarkable observation here is that the violations of the area law in presence of a gap could be naively recognized as a failure of S to catch the real physics of the problem. Conversely, from a different point of view, we can say that S itself is able to capture a deep change in the nature of the ground state. For small α, long-range pairing becomes dominant, and its presence cannot be inferred simply from the spectrum structure.

3.3.3 ENTANGLEMENT DYNAMICS FOLLOWING A GLOBAL QUENCH

We can test our model criticality on the line $|\mu| = 2\omega$ by studying the time evolution of the entanglement entropy after a global quench. A quench is the abrupt change of one or more parameters of a system initially prepared in a state $|\psi\rangle$ (for example, it can be the ground state of a pre-quench Hamiltonian H_0), which is alloed to evolve for $t > 0$ with a different Hamiltonian H_1 [6]. For a system with short-range interactions, we can briefly review the entanglement dynamics in what is called the semiclassical approximation, following the work by Calabrese and Cardy[39]. This approximation is valid when the post-quench Hamiltonian H_1 can be written in terms of free particles: as the time evolution starts, pairs of quasi-particles with opposite momenta k and $-k$ are created in the system, which are free-moving entangled pairs governed by a steady group velocity v_g. The group velocity has an upper bound given by the Lieb-Robinson bound[152], which also defines an effective light-cone outside of which the correlations decay exponentially fast. Quasiparticles arriving in B from A entangle the two subregions, and since v_g is constant, the entropy between A and B grows linearly in time. In[153] was obtained a universal behaviour of $S(t)$ for a quench in a conformal field theory,

$$S(t) = \begin{cases} \frac{\pi c t}{6}, & \text{for } t < \frac{l}{2} \\ \frac{\pi c l}{12}, & \text{for } t > \frac{l}{2} \end{cases} , \tag{3.75}$$

which means that $S(t)$ grows linearly until it saturates at $t = l/2$.
The entanglement dynamics for long-range models has been studied in several other works, and some more particular behaviours have been identified[154–157].
For the long-range Kitaev model, we initially prepare the system in an initial state $|\psi_0\rangle$, which is choose as the ground state (3.45), with $\mu \gg 1$. Then we let the system evolve

[6] We already introduced the quenching procedure in the phenomenological discussion about the behaviour of local observables in MBL systems (see 2.3.2).

under the action of the Hamiltonian H_1, which is (3.35), switching to $\mu = 1$,

$$|\psi(t)\rangle = \mathrm{e}^{-iH_1 t}\,|\psi_0\rangle\,. \tag{3.76}$$

We can recast the Hamiltonian H_1 in a new Bogoliubov basis using the Bogoliubov angle $\theta^1_{q_n}$ given by (3.42),

$$H_1 = \sum_{n=1}^{L-1} \lambda^1_\alpha(q_n)\left(\eta^{1\dagger}_{k_n}\eta^1_{q_n} - \frac{1}{2}\right), \tag{3.77}$$

with

$$\lambda^1_\alpha(q_n) = \sqrt{(\cos(q_n)+1)^2 + f^2_\alpha(q_n)}. \tag{3.78}$$

Following appendix A, after the separation of the chain in two halves A and B, in order to compute the von Neumann entropy

$$S_{L/2}(t) = -\,\mathrm{Tr}\{\rho_A(t)\log\rho_A(t)\}, \tag{3.79}$$

we calculate the time correlation matrices $C_{ij}(t) = \langle c^\dagger_i(t)c_j(t)\rangle$ and $F_{ij}(t) = \langle c^\dagger_i(t)c^\dagger_j(t)\rangle$, where

$$c_j(t) = \mathrm{e}^{iH_1 t}\,c_j\,\mathrm{e}^{-iH_1 t}\,. \tag{3.80}$$

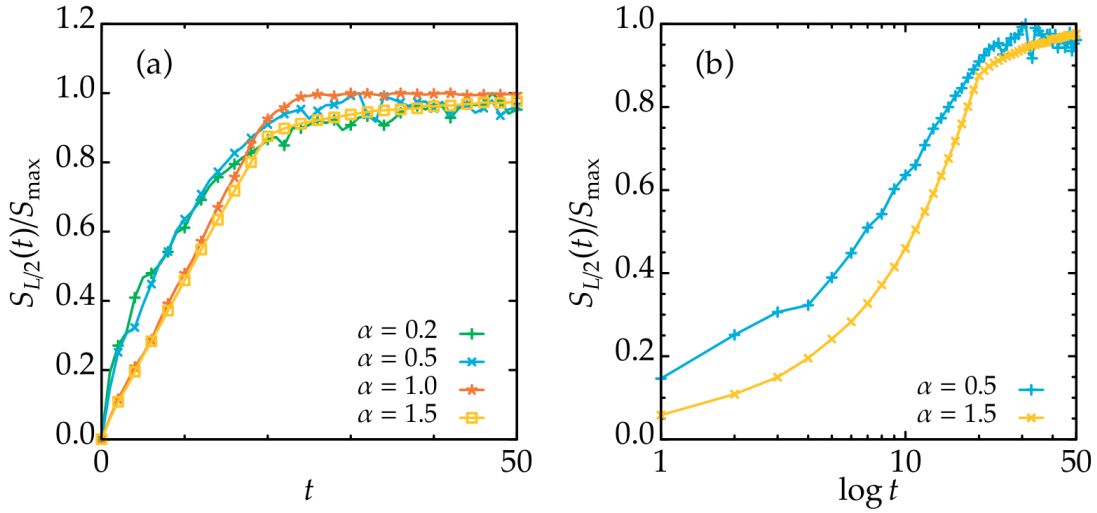

Figure 3.3: Time evolution of $S(L/2)$ after a global quench for a block of $l = 100$ sites embedded in infinite long system. For $\alpha > 1$ S(L/2) displays a linear growth in time, while for $\alpha < 1$ S(L/2) grows logarithmically.[48]

Computing the expectation values over the initial state $|\psi_0\rangle$, we obtain

$$C_{ij}(t) = \frac{2}{L}\sum_{n}^{L/2-1} \cos(q_n(i-j))[\sin^2(2\theta^1_{q_n} - \theta^0_{q_n})\sin^2(\lambda^1_\alpha(q_n)t) + \sin^2\theta^0_{q_n}\cos^2(\lambda^1_\alpha(q_n)t)], \tag{3.81}$$

and

$$\begin{aligned} F_{ij} = \frac{1}{L}\sum_{n}^{L/2-1} [&\sin(q_n(i-j))\sin 2\theta^1_{q_n}\cos(2\theta^0_{q_n} - 2\theta^1_{q_n} \\ &+ \sin(q_n(i-j))\sin(2\theta^0_{q_n} - 2\theta^1_{q_n})\cos^2\theta^1_{q_n}\, \mathrm{e}^{2it\lambda^1_\alpha(q_n)} \\ &- \sin(q_n(i-j))\sin(2\theta^0_{q_n} - 2\theta^1_{q_n})\sin^2\theta^1_{q_n}\, \mathrm{e}^{-2it\lambda^1_\alpha(q_n)}]. \end{aligned} \tag{3.82}$$

Considering $L \to \infty$ the sums in (3.81) and (3.82) are replaced by integrals, and we can erase the typical oscillations of $S(t)$ for finite-size systems. The plots in figure 3.3 show the evolution behaviour of $S(L/2)$ for different values of α and for a pre-quench value $\mu_0 = 1000$. When $\alpha > 1$ we obtain a linear growth, accordingly to (3.75), while for $\alpha \lesssim 1$ the entropy shows a logarithmic scaling in time.

4

DISORDERED KITAEV CHAIN WITH LONG-RANGE PAIRING

In this chapter we will describe our original work and ideas, grounded in the broad framework we discussed in the previous chapters. Exploiting some of the indicators discussed in chap. 2, we detected signatures of the transition between an ergodic phase, in which the states of our model are traditionally extended, and a localized non ergodic phase. We considered a modified version of the Kitaev Hamiltonian (3.35) with randomness induced on the pairing term Δ and open boundary conditions, expressed as

$$\begin{aligned} H_{LRK}^{dis} = \sum_{j=1}^{L} -\mu \left(c_j^\dagger c_j - \frac{1}{2} \right) - t \left(c_j^\dagger c_{j+1} + c_{j+1}^\dagger c_j \right) \\ + \Delta \sum_{j,l=1}^{L-1} \frac{\Delta_j + 1}{d_l^\alpha} \left(c_{j+l}^\dagger c_j^\dagger + c_j c_{j+l} \right), \end{aligned} \tag{4.1}$$

where Δ_j is randomly distributed within $[-W, W]$. Our single-particle Hamiltonian can be described by a $L \times L$ square matrix, which we can easily diagonalize via numerical methods, gaining immediate access to the whole energy spectrum and to the eigenstates of the system. In all our numerical simulations we kept $\mu = 0.5$, in order to explore the gapped phase, and $t = \Delta = 1$ sets the energy unit of our model. Although we restricted ourselves to this particular choice of the main model parameters, it would undoubtedly be interesting to expand our studies to different ranges of values and also with different boundary conditions.

4.1 NUMERICAL EVIDENCE OF EIGENSTATE LOCALIZATION

As a first characterization of the different phases of our system, we exploited a standard observable in localization studies of non-interacting systems, i.e. the Inverse Participation Ratio of the energy eigenstates. Since strong fluctuations of eigenfunctions represent one of the hallmarks of metal-insulator transitions, one can characterizes these fluctuations by a set of so called inverse participation ratios (IPR) [158]

$$IPR_{q,n} = \frac{\sum_i |\Psi_n(r_i)|^{2q}}{(\sum_i |\Psi_n(r_i)|^2)^q}, \tag{4.2}$$

where $\Psi_n(r_i)$ is a single-particle wave function labeled by n on the site i. Usually, the IPR is defined with $q = 2$ and it constitutes a useful measure of eigenfunction localization, since it is inversely proportional to the volume section of a system in which the eigenfunctions effectively spread[1]. For a finite d-dimensional system of size L, we have two different behaviours of extended and localized states in terms of $I_{2,\zeta}$:

$$\lim_{L\to\infty} IPR_n \propto \begin{cases} 1/L^d & \text{for extended states} \\ \text{const.} & \text{for localized states} \end{cases}, \tag{4.3}$$

for states far away from the Anderson transition, while a *multifractal* scaling appears near the transition [110,159,160],

$$\lim_{L\to\infty} IPR_n = L^{-d'} F[(W - W_c)L^{1/\nu}], \tag{4.4}$$

where d' is an effective dimension which can be different from the spatial dimensionality d because of the multifractality of the eigenfunctions, F is a universal function of W_c, which is the critical value of the parameter which drives the system towards the transition, and ν, the critical exponent of the correlation length ξ (see (2.11). Moreover, (4.3) provides another useful insight on the phenomenology of localization phenomena: the inverse of IPR, which we can call with a justified lack of fantasy Participation Ratio (PR), gives for the extended states

$$PR = \lim_{L\to\infty} (IPR_n)^{-1} = L^d, \tag{4.5}$$

and thus gives an intuitive estimate of the number of sites on which the eigenstates have support. As one can imagine, in the extended regime the wavefunctions spread over all

[1]From now on, we neglect the index q, meaning $IPR_{2,n} \equiv IPR_n$.

sites, while in the localized phase the eigenstate has support only on a finite number of sites.

In order to enlighten the interplay between the disorder and the long-range nature of our model, we evaluated the IPR for different values of the disorder strength W and the long-range decaying parameter α.

The contour plot in figure 4.1 shows the IPR as a function of the disorder strength W and the long-range decaying parameter α, providing an interesting outcome, although at a qualitative level: the localized regime is attainable by the tuning of W and α, and it does not depend on the disorder alone as in short-range models.

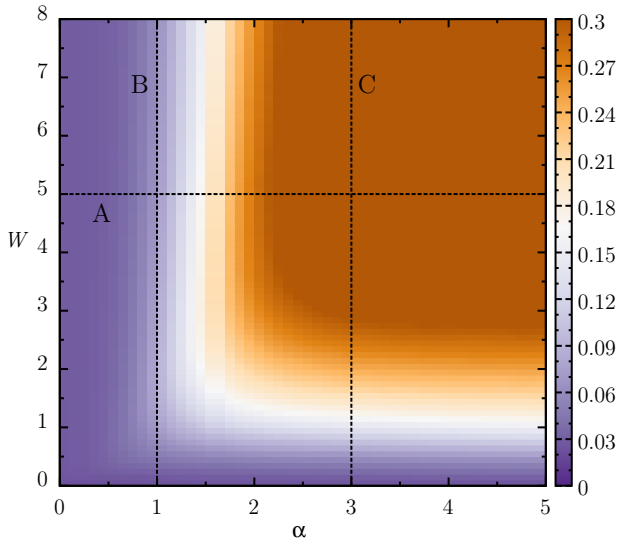

Figure 4.1: Colour plot of the IPR of the whole spectrum of the Hamiltonian (4.1) as a function of the disorder strength W and the decaying factor α for a system size $L = 100$, averaged over 400 disorder realizations. The lines A, B, C represent the cuts which we used to obtain the plots in figures 4.5 (a) and (b), 4.3.

The first numerical analysis was performed on a chain of size $L = 100$ (the scaling with the size L will be showed later), averaging over all the IPRs obtained for each single eigenstates in the whole spectrum. We also averaged over 400 different disorder realizations[2] in order to achieve adequate statistical certainty. This procedure leaves us

[2]The numer of disorder configurations was proven to be sufficient for our purposes for each L and W we employed in our simulations.

with a quantity defined as:

$$IPR\,(\alpha, W) = \frac{1}{L}\sum_{n} \langle IPR_n(\alpha, W)\rangle_{dis}\,, \tag{4.6}$$

where $\left\langle \cdots \right\rangle_{dis}$ stands for the averaging over many different disorder configurations. The behaviour of the IPR of the whole spectrum as a function of the two main parameters provides information about the transition of the system from the extended phase to the localized phase, and we can note some fundamental features: first of all, the IPR vanishes for any value of W if $0 \leq \alpha \lesssim 1$, i.e. in the strong long-range limit. This means that the eigenfunctions fail to localize due to the spreading of the correlations between each site, and the effects of the disorder cannot emerge. At the same time, there is no localization even in weak disorder regime $0 \leq W \leq 1$, where $IPR \sim 0$ for any α. The localized phase seems to appear when $W \geq 1$ and $\alpha \geq 1.5$, and the IPR reaches its steady maximum value deep in the localized phase for $W \gtrsim 3$ and $\alpha \gtrsim 2$.
In order to gain some more detailed insight we proceeded plotting the IPR as a function of α ($W = 5$) and W ($\alpha = 3$) for different chain sizes $L = 100, 200, 300, 400, 500$, averaging over the whole spectrum for 400 different disorder configurations.
The dotted lines at $W = 5$ and $\alpha = 1, 3$ indicate the cuts along which we studied the transition between the extended and localized phases in more detail, evaluating the IPR in two different ways, fixing α or W and calculating the IPR as a function of the only parameter left free to vary.
We can see that the IPR vanishes more evidently in the ergodic phase for $L \to \infty$ in both cases, while it maintain a constant value for (a) $\alpha \gtrsim 3$ and for (b) $W \gtrsim 3$, where the eigenfunctions are localized. At the point $W = 5$, $\alpha = 3$ the IPR has a value of $\simeq 0.349$, meaning that the number of sites over which the eigenfunctions can spread is $PR \simeq 3$. It can be easily noticed that the transition in (a) appears sharper than (b), in which it appears quite smooth. This difference made us investigate further, examining IPR_n for every single-particle eigenstate, i.e. without averaging over the whole spectrum like in (4.6). In order to compare results obtained from several different disorder configurations, we rescaled the energy values to the window $[0, 1]$ as

$$E = \frac{\epsilon - \epsilon_{min}}{\epsilon_{max} - \epsilon_{min}}, \tag{4.7}$$

where ϵ_{min} and ϵ_{max} are the eigenvalues of the ground state and the highest excited state,

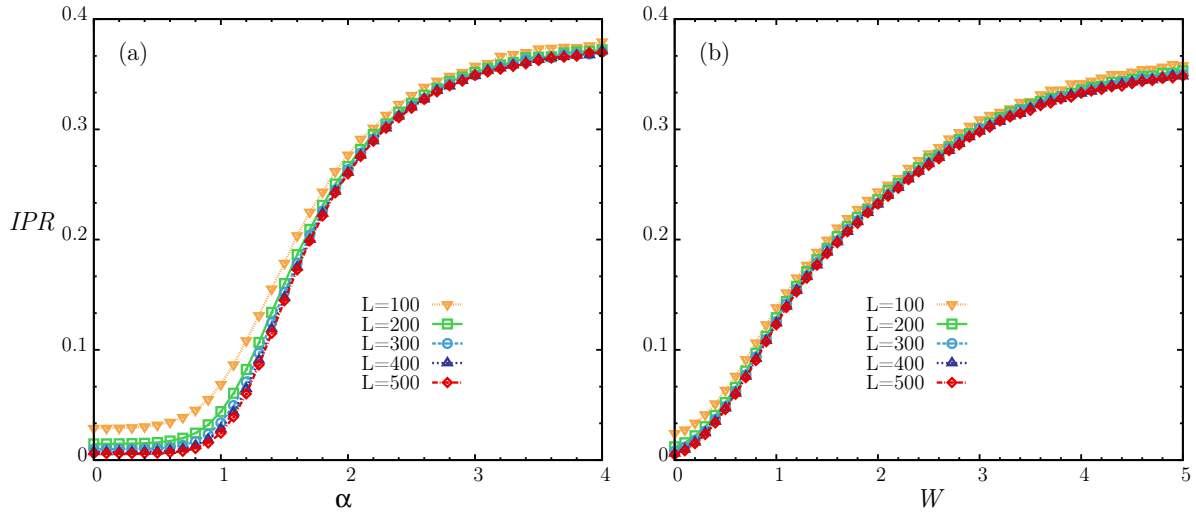

Figure 4.2: Plots of the IPR as a function of the long-range parameter α (a) and the disorder strength W (b), averaged over the whole energy spectrum for different system sizes and several disorder realizations. In panel (a) the IPR curve was obtained for a fixed value of the disorder $W = 5$, while in (b) we kept $\alpha = 3$.

respectively.

Figure 4.3 shows some numerical outcomes we obtained from these simulations. As we can note in the left panel of 4.3, the IPR highlights the lack of localization and the survival of ergodicity even for high disorder strengths for values of α sufficiently small, confirming our first observation for the IPR averaged over the whole spectrum. As a matter of fact, for $\alpha \to 0$, in the strong long-range limit, no signature of localization appears whatever W is.

For $\alpha > 1$ the IPR increases as W grows, showing evidences of localization of the eigenfunctions and a peculiar mobility edge in the phase diagram, as it can be seen in the central panel of 4.3, where localization first appears at the edges of the spectrum. In the intermediate-strong disorder limit $W = 5$, the third panel on the right shows localization of all the eigenstates only for $\alpha \gtrsim 1.5$. The difference between the central and the right panel underlies what we noticed about the sharpness of the transition in figure 4.2 (a): for α constant, the IPR shows a mobility edge as a function of the disorder, and in the intermediate regime $1 \leq W \leq 4$ the system is in a mixed phase in which a certain fraction of the states is still extended and the remaining fraction is localized, producing the smoother and slower transition which is visible in 4.2 (b). On

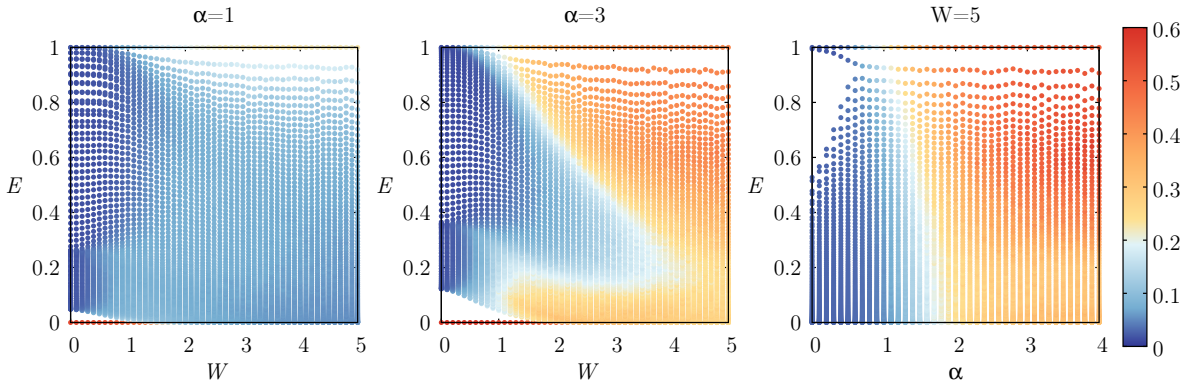

Figure 4.3: IPR as a function of the energy, rescaled to the window $[0, 1]$, for different values of the disorder strength W and α. In the left and central panels α is fixed and the IPR is calculated state by state at growing values of W. Conversely, the right panel shows the IPR as a function of energy and α, in a medium-high disorder regime $W = 5$. The data were obtained for a chain of $L = 200$ sites over 400 different disorder configurations.

the contrary, the phase diagram obtained from the IPR as a function of α does not show a mobility edge for W fixed.

Furthermore, we note that, as we increase the disorder strength, the low-energy gap of our model is closed, while some new gaps are visible in the high-excited region of the spectrum. It is worth noting the particular IPR of the ground state, in which the SP wavefunctions appear localized, probably due to the survival of the Majorana edge states described for the short-range Kitaev Hamiltonian in sect.3.1.1.

4.2 ENERGY LEVEL STATISTICS

In the first chapter (sect. 1.1.2), starting from basic concepts underlying random matrix theory and chaos, we discussed which properties and behaviours can be considered defining indicators of the actual chaoticity (and thus ergodicity) of quantum systems. As we explained, the manifestation of Wigner-Dyson surmise (1.8) in the distribution of the energy level spacing is now believed to be one of this ergodicity-revealing hallmarks. More specifically, the transition between the GOE distribution and the Poisson distribution, typical of non ergodic systems (see sect.1.1.4), has been massively employed in the study of localization in disordered systems, both in single-particle investigations [161–166] and in interacting many-body systems [29,101,104,167,168].

In sect.(2.3.1) we reviewed some of these works, whose basic ideas were exploited and applied to the study of the long-range Kitaev model (3.35). After a numerical diagonalization and a sorting of the eigenvalues in ascending order, we calculated the energy difference between two adjacent eigenstates $\delta_n = \epsilon_n - \epsilon_{n+1}$ for the entire spectrum. Although δ_n is by far the most common observable in spectral statistics analysis, universality of RMT means that random matrix ensembles like GOE and GUE[3] are able to describe the energy level in a *statistical* way, which requires local energy windows with mean level density set to unity. Nonetheless, different models show significative differences in their level density, and in order to compare spectral observables or correlation functions like the nearest-neighbor spacing distribution one needs an operation called *unfolding*[57], which consists in a switch of the initial variables, i.e. the actual eigenvalues ϵ_n, to new ones $\hat{\epsilon}_n = \mathcal{N}(\epsilon_n)$, where $\mathcal{N}(\epsilon)$ is the mean number of levels less than ϵ, obtained either by averaging over many realizations in the case of disordered systems, or by local smoothing over an energy window large compared to the level spacing but small compared to variations of $\mathcal{N}(\epsilon)$. This procedure leads to an unfolded spectrum which has automatically a mean level spacing equal to one, and its statistical properties can thus be directly compared with those of RMT. When treating systems which have a known functional form of $\mathcal{N}(\epsilon)$, the unfolding can be easily implemented, but in many-body problems where $\mathcal{N}(\epsilon)$ increases as a stretched exponential function of energy[169] and it is difficult to have access to a large number of disorder realizations because of the increase of the Hilbert space dimension with the number of particles, one has to define some new quantity able to characterize the correlations between adjacent gaps in the spectrum.

As we quickly discussed in sect.2.3.1, Oganesyan and Huse[104] proposed a new observable defined as the ratio

$$r_n = \frac{\min \delta_n, \delta_{n+1}}{\max \delta_n, \delta_{n+1}}, \tag{4.8}$$

which implies that $0 \leq r_n \leq 1$.

[3]We recall that while for quantum systems which classical counterpart is integrable the Berry-Tabor conjecture[66] states that their level statistics follows a Poisson law, Bohigas, Giannoni and Schmit conjectured[64] that the case of quantum Hamiltonians with chaotic classical dynamics must fall into one of the ensembles of RMT. These ensembles correspond to Hermitian random matrices whose entries are independently distributed respectively real (GOE) or complex (GUE) random variables. More complex random entries, like quaternionic variables (GSE), are far beyond the aim of this discussion.

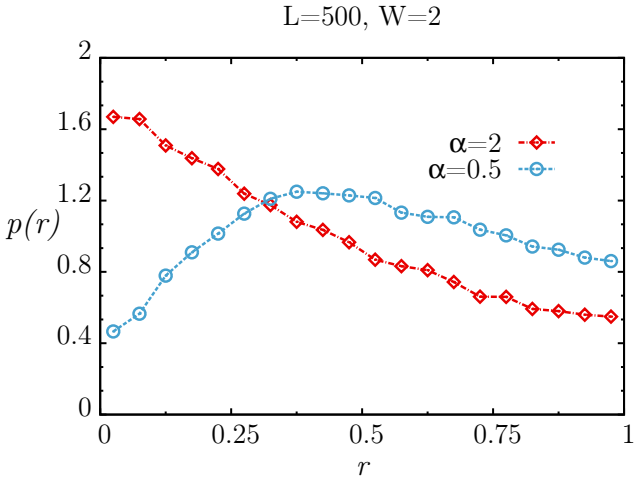

Figure 4.4: Distribution of the adjacent spacing ratio r for a chain of $L = 500$ sites for 200 different disorder configurations. The two curves are obtained keeping the disorder strength $W = 2$ constant for two different values of α.

In the localized regime[4] the distribution $p(r)$ is Poissonian, and its mean value $\langle r_n \rangle_{loc}$ is

$$p(r)_{loc} = \frac{2}{(1+r)^2}, \qquad \langle r_n \rangle_{loc} = 2\ln 2 - 1 \simeq 0.386. \tag{4.9}$$

On the other hand, in the ergodic phase a "Wigner-like" surmise has been derived by Atas[170] for GOE random matrices:

$$p(r)_{GOE} = \frac{27}{8}\frac{r + r^2}{(1 + r + r^2)^{5/2}}, \tag{4.10}$$

for which the mean value $\langle r_n \rangle_{GOE}$ can be numerically evaluated using large GOE random matrices[5]:

$$\langle r_n \rangle_{GOE} = 0.5295(1). \tag{4.11}$$

We analyzed the $\langle r \rangle$ statistics in open chains of $L = 100, 200, 300, 400, 500$ sites with 400 different randomness configurations, and the outcomes are shown in figure 4.5. In analogy with the IPR numerical simulations, we considered two different cases: (a) shows the mean adjacent gap ratio at $W = 5$ fixed as a function of the long-range factor α, while in (b) we plotted $\langle r \rangle$ at $\alpha = 3$ as a function of the disorder strength. We note

[4] Or, more generally, for integrable and non ergodic systems.

[5] In [104], GOE data were obtained from 1000 random matrices of size 3432, which is the number of states in a half-filled chain of L = 14.

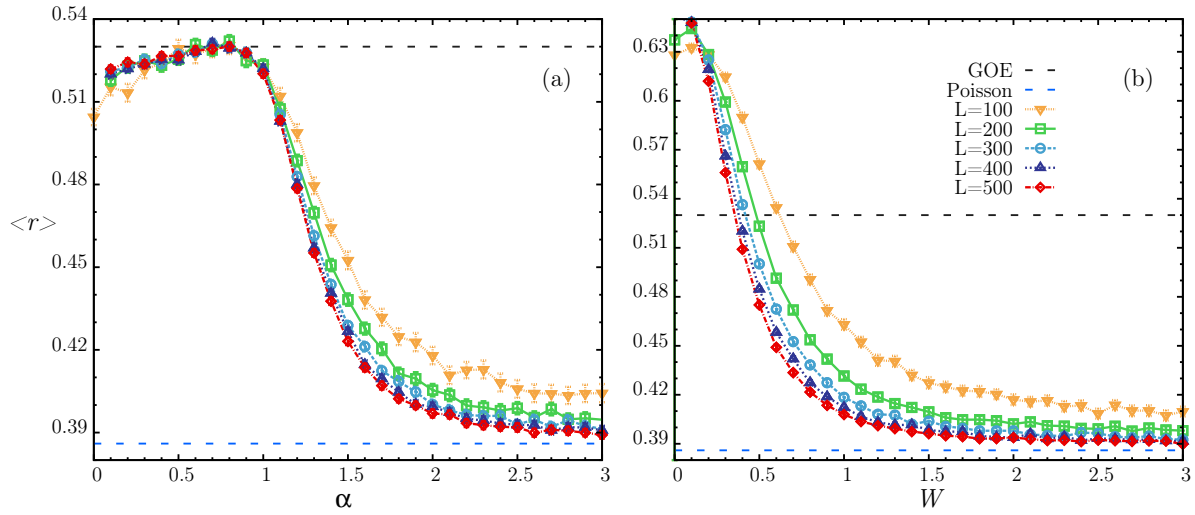

Figure 4.5: (a) Scaling of the mean adjacent gap ratio as a function of α at $W = 5$ for different chain lengths $L = 100, 200, 300, 400, 500$ (see legend in (b)). The black dotted line represents the expected $\langle r \rangle_{GOE}$ value in the extended phase while the blue dotted line the expected Poisson value of the localized phase. (b) Mean gap ratio $\langle r \rangle$ as a function of disorder W at $\alpha = 3$.

that in (a) the GOE and Poisson predictions are in good agreement with the data we obtained in the regimes $0 \leq \alpha \leq 1$ and $\alpha \geq 2$. Between these two limits the mean gap ratio decreases from $\langle r \rangle_{GOE}$ (black dotted line) to $\langle r \rangle_{loc}$ (blue dotted line), implying a transition between the diffusive and the localized phase. As expected, longer chains show a more pronounced Poisson behaviour in the localized regime, approaching $\langle r \rangle_{loc}$ more precisely.

In panel (b), $\langle r \rangle$ shows an unexpected behaviour in the window $0 \leq W \leq 1$ for $\alpha = 3$, in which the mean value of the adjacent gap ratio does not agree with the GOE prediction, with a quick decrease from a maximum value of $\langle r \rangle \simeq 0.66$ at $W = 0$ (the slight inital increase for $L = 100, 200$ curves are probably due to finite-size effects) to the predicted Poisson value for $W \geq 1$. This hints the existence of a third regime in which the level spacing distribution does not follow neither Poisson or Wigner-Dyson statistics. In figure 4.6 we can see in a more evident way the emergence of this unexpected phase for $0 \leq W \leq 1$ and $\alpha > 1$. The contour plot was obtained for a chain of $L = 100$ sites plotting $\langle r \rangle$ as a function of both W and α following the same procedure of previous simulations, i.e. averaging over 400 different disorder realizations. The overall look of

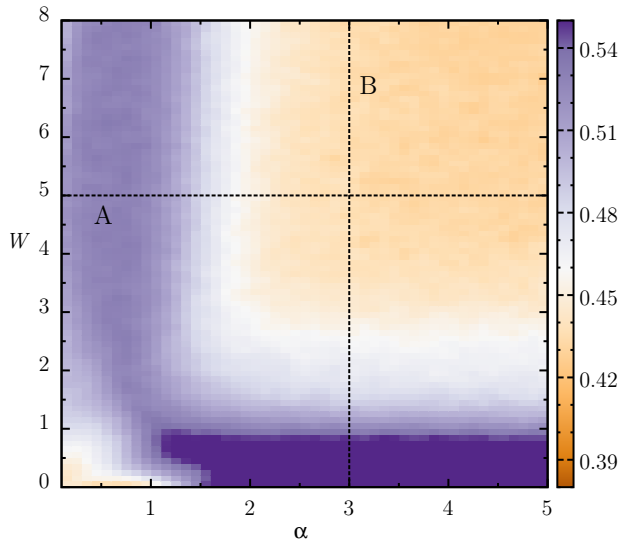

Figure 4.6: Contour plot showing the mean level spacing $\langle r \rangle$ as a function of W and α for a system of $L = 100$ sites and 400 disorder realizations. The lines A and B are the cuts along which we obtained the data plotted in figure 4.5.

figure 4.6 reminds of 4.1, but provides more information on the model nature, revealing the existence of a third regime for $0 \leq W \leq 1$ which the IPR analysis was not able to catch. However, combining the information obtained from both the IPR and $\langle r \rangle$ data, we can deduce that the eigenstates in this phase are extended because of the vanishing of IPR, and the system may thus show diffusive dynamics although the level statistics does not agree with RMT predictions for ergodic systems.

Moreover, we note that also in the region $0 \leq W, \alpha \leq 1$ the system shows a particular behaviour, which is not due to finite-size effects, as it can be inferred by figure 4.7, in which we plotted $\langle r \rangle$ for different syztem sizes for $\alpha = W \in [0, 1]$. In this region the mean level spacing ratio increases from $\langle r \rangle \simeq 0.44$ at $\alpha = W = 0.1$ and approaches the GOE predicted value at $\alpha = W \simeq 0.88$, before beginning to step down, signaling the beginning of the transition to the localized phase.

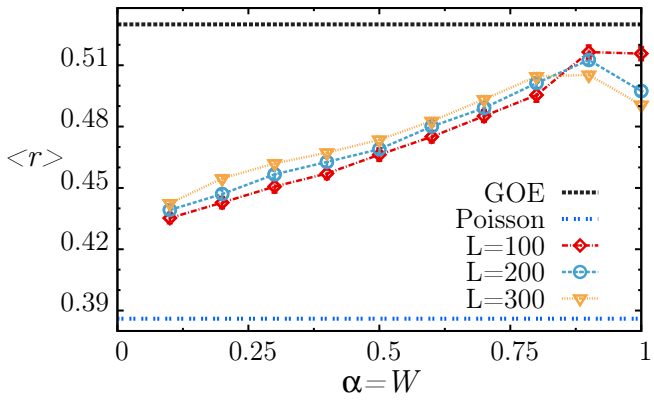

Figure 4.7: Plot of the mean spacing ratio $\langle r \rangle$ as a function of $\alpha = W \in [0, 1]$ for different chain sizes $L = 100, 200, 300$ for 400 disorder realizations.

4.3 ENTANGLEMENT SCALING

As we discussed abundantly in the previous chapters, entanglement has become a major object of research in recent times, mainly because of its capability to retrieve the scaling behaviour in proximity of critical points[171,172]. In particular, the most studied measure of entanglement is the entanglement entropy, which we defined in sect.2.3.3 and discussed its scaling with the system size as a defining property of localized systems. We now expand some concepts on the entanglement entropy of gapped quantum Hamiltonians, in order to get a useful decription which we can exploit to get a better understanding of our numerical results.

4.3.1 ENTANGLEMENT ENTROPY IN EXCITED STATES

In sect.3.3.2 we already told that for the ground states of local gapped Hamiltonians near critical points the entanglement entropy does not show an extensive scaling with the system size, and conformal field theory follows the scaling (3.73), which becomes in the thermodynamic limit

$$S(l) = \frac{c}{3} \log \left[\frac{L}{\pi} \sin \left(\frac{\pi l}{L} \right) \right] + a \simeq \frac{c}{3} \log l + a, \qquad L \to \infty, \tag{4.12}$$

where c is the central charge of the underlying conformal field theory, a is non universal constant and l is the size of a partition of a chain of length L. Much less attention has been devoted to the study of entanglement entropy in excited states, which can exhibit

deep changes in the behaviour of $S(l)$ [173–176]. The study of entanglement in excited states can be more handly making use of two technical tools. The first is the Peschel method described in appendix A, which permits to reduce the dependence of the complexity of the problem on the size of the system from 2^L to L, studying the two-point correlation matrix instead of the reduced density matrix of the subsystem. The second argument can be applied when the correlation matrix is of Toeplitz form, as in our case. Then we can estimate the behaviour of the entanglement entropy exploiting the Fischer-Hartwig conjecture [177]. We consider states that can be expressed as Slater determinants

$$|\Psi_K\rangle = \prod_{k\in K} b_k^\dagger |0\rangle \,, \tag{4.13}$$

where $|0\rangle$ is the vacuum state in Fock space and

$$b_k^\dagger = \sum_{i=1}^{L} \phi_k^*(i) a_n^\dagger, \quad k = 1 - L/2, \cdots, L/2 \tag{4.14}$$

is a basis for the creation and annihilation operators such that $b_k, b_k^\dagger$ satisfy canonical anticommutation relations. $K \subset \{1-L/2, \cdots, L/2\}$ is the subset of excited modes in $|\Psi_K\rangle$. If we divide a fermionic chain described by a free, translational invariant Hamiltonian in two subsets $A = \{1, \cdots, l\}$ and $B = \{l+1, \cdots, L\}$, we can factorize the Hilbert space of the system as $\mathcal{H} = \mathcal{H}_A \otimes \mathcal{H}_B$, and our aim is to study the entanglement between the two subsystems. The computational time needed to compute the entanglement entropy from the reduced density matrix $\rho_A = \mathrm{Tr}(|\Psi_K\rangle \langle\Psi_K|)$ grows, in principle, exponentially with the size of the subsystem, but the algorithm developed by Peschel allows to reduce the exponential growth to a potential one. Recalling here the main results of this procedure (see Appendix A for details), we are able to write the entanglement entropy as

$$S_A(l) = \sum_{k=1}^{l} [-\gamma_k \log \gamma_k - (1-\gamma_k)\log(1-\gamma_k)], \tag{4.15}$$

where γ_k are the eigenvalues of the correlation matrix $C = \mathrm{Tr}\{\rho_A c_i^\dagger c_j\}$ for simple quadratic Hamiltonians of type (A.1). In order to analitically compute the entropy of the subsystem, the correlation matrix must have a Toeplitz form, i.e.

$$C_{ij} = C_{i+1,j+1} = \xi_{i-j}, \tag{4.16}$$

which is a consequence of the translational invariance of the system. This holds under the following conditions: if the operators $b_k, b_k^\dagger$ fullfill canonical anticommutation relations,

the matrix built with the coefficients $\phi_k(i)$ is unitary, and they form an orthonormal basis. We can thus get the inverse relation

$$a_i = \sum_{k=1-L/2}^{L/2} \phi_k^*(i) b_k, \tag{4.17}$$

and calculate the correlation matrix C_{ij} for the state (4.13) as

$$C_{ij} = \langle a_i^\dagger a_j \rangle = \sum_{k \in K} \phi_k(i) \phi_k^*(j). \tag{4.18}$$

If we require Cij to be a Toeplitz matrix, we must have

$$\phi_k(i)\phi_k^*(j) = \xi_k(i-j), \tag{4.19}$$

which means that $\phi_k(i)\phi_k^*(j)$ must be invariant under translations in i. A natural choice of a set of functions which satisfy the condition (4.19) and constitutes an orthonormal basis are the coefficients of the discrete Fourier transform

$$\phi_k(i) = \frac{1}{\sqrt{L}} \mathrm{e}^{2\pi \mathrm{i} k(i-j)} / L. \tag{4.20}$$

The correlation matrix then assumes the form

$$C_{ij} = \frac{1}{L} \sum_{k \in K} \mathrm{e}^{2\pi \mathrm{i} k(i-j)/L}, \tag{4.21}$$

and we can define the matrix $V = 2C - \mathbb{I}$, which will be useful in the following, as

$$V_{ij} = \frac{1}{L} \left(\sum_{k \in \mathcal{K}} \mathrm{e}^{2\pi \mathrm{i} k(i-j)/L} - \sum_{k \notin \mathcal{K}} \mathrm{e}^{2\pi \mathrm{i} k(i-j)/L} \right). \tag{4.22}$$

Denoting as $v_k = 2\gamma_k - 1$ the eigenvalues of $V(A) = 2C(A) - \mathbb{I}_l$, where $C(A)$ is the correlation matrix of the subsystem A which contains l sites, we can write the entanglement entropy as

$$S(A) = -\sum_{k=1}^{l} \left[\frac{1-v_k}{2} \log\left(\frac{1-v_k}{2}\right) + \frac{1+v_k}{2} \log\left(\frac{1+v_k}{2}\right) \right] \tag{4.23}$$

Now, transforming the sum in the previous equation into a complex integral on a contour that encloses the eigenvalues of $V(A)$ we are able to obtain a functional form of $S(l)$ which is useful to our purposes. We introduce the function

$$f(x,y) = -\frac{x-y}{2} \log\left(\frac{x-y}{2}\right) - \frac{x+y}{2} \log\left(\frac{x+y}{2}\right), \tag{4.24}$$

and applying the Cauchy's theorem we can recast the entropy as the complex integral

$$S(A) = \lim_{\varepsilon \to 0^+} \frac{1}{4\pi\,\mathrm{i}} \oint_{\mathcal{C}} f(1+\varepsilon, \lambda) \frac{d \log D_l(\lambda)}{d\lambda} d\lambda, \tag{4.25}$$

where $D_l(\lambda)$ is the determinant of $\lambda \mathbb{I}_l - V(A)$,

$$D_l(\lambda) = \prod_{k=1}^{l} (\lambda - v_k). \tag{4.26}$$

In the thermodynamic limit we can approximate the set of excited modes K with an occupation density, describing the state (4.13) through a periodic function $g(\theta) \in [-1, 1]$ defined by

$$\frac{1}{2\pi} \int_{-\pi}^{\pi} F(\theta) g(\theta) d\theta = \lim_{L \to \infty} \frac{1}{L} \left[\sum_{k \in K} F\left(\frac{2\pi k}{N}\right) - \sum_{k \notin K} F\left(\frac{2\pi k}{N}\right) \right], \tag{4.27}$$

where F can be any continuous function. We can then replace the sum in (4.22) with an integral, obtaining

$$V_{ij} = \frac{1}{2\pi} \int_{-\pi}^{\pi} g(\theta) e^{\mathrm{i}(i-j)\theta} d\theta. \tag{4.28}$$

We are interested in occupation densities which are piecewise constant functions: denoting the set of discontinuity points $\{\theta_1, \cdots, \theta_R\}$ they are described as

$$g(\theta) = t_r, \quad \theta_{r-1} \leq \theta < \theta_R. \tag{4.29}$$

Now we use the Fischer-Hartwig factorization[178,179] to express $\tilde{g}(\theta) = \lambda - g(\theta)$ in the form

$$\tilde{g}(\theta) = h(\theta) \prod_{r=1}^{R} \tau_r(\theta - \theta_r), \tag{4.30}$$

where

$$h(\theta) = \prod_{r=1}^{R} (\lambda - t_{r-1})^{\frac{\theta_r - \theta_{r-1}}{2\pi}}, \tag{4.31}$$

$$\tau_r(\theta) = e^{-i\beta_r(\pi - \theta)}, \quad \theta \in [0, 2\pi), \tag{4.32}$$

and the function β_r is given by

$$\beta_r = -\frac{1}{2\pi\,\mathrm{i}} \log\left(\frac{\lambda - t_{r-1}}{\lambda - t_r}\right). \tag{4.33}$$

At this point, we can exploit the Fischer-Hartwig conjecture, which states that in the limit $l \to \infty$ the determinant $D_l(\lambda)$ reads

$$D_l \approx (F[h])^l \left(\prod_{r=1}^{R} l^{-\beta_r^2} \right) E[\{\beta_r\}, \{\theta_r\}], \tag{4.34}$$

where

$$F[h] = \exp\left[\frac{1}{2\pi} \int_0^{2\pi} \log(h(\theta)) d\theta \right] \tag{4.35}$$

$$E[\{\beta_r\}, \{\theta_r\}] = \prod_{r=1}^{R} G(1+\beta_r) G(1-\beta_r) \prod_{1 \le r \ne r' \le R} (1 - \mathrm{e}^{i(\theta_r - \theta_{r'})})^{\beta_r \beta_{r'}}, \tag{4.36}$$

with $G(z)$ the Barnes G-function[6]. We can now compute the logarithmic derivative of $D_l(\lambda)$,

$$\frac{d \log D_l(\lambda)}{d\lambda} = \frac{d \log F[h]}{d\lambda} l - \sum_{r=1}^{R} \frac{d\beta_r^2}{d\lambda} \log l + \frac{d \log E}{d\lambda} + \dots, \tag{4.37}$$

where the dots stand for vanishing terms in the limit $L \to \infty$, and inserting it in (4.25) we finally get the following form for the entropy of the block A containing l sites:

$$S_i(l) = a_i + b_i l + c_i \log(l), \tag{4.38}$$

for the single i-th state, which tells us that the entropy in excited states is given by three different contributions, a linear term which comes from the ground state[181], a logarithmic term and an additive constant[7].

4.3.2 NUMERICAL RESULTS

We performed a numerical evaluation of the entanglement entropy $S(l)$ in the whole spectrum of the long-range Kitaev model (4.1), fitting the obtained data with the form (4.39) and obtaining some insights on the scaling of the entropy with the subsystem size. The entropy (4.38) is actually referred to a single state, and performing an average operation on the entire spectrum we obtained

[6] The Barnes G-function (or Double Gamma function) is defined as[180]

$$G(z+1) = (2\pi)^{z/2} \, \mathrm{e}^{-\frac{1}{2}[z(z+1)+\gamma z^2]} \prod_{n=1}^{\infty} \left[\left(1 + \frac{z}{n}\right)^n \mathrm{e}^{-z + \frac{z^2}{2n}} \right],$$

where γ is the Euler-Mascheroni constant.

[7] A detailed derivation of the coefficients a, b and c can be found in[182].

$$S(l) = \frac{1}{l}\sum_{i=1}^{l} S_i(l) = a + bl + c\log l. \tag{4.39}$$

Starting from the diagonalized Hamiltonian, We constructed many-particle states of the form

$$H = \sum_k \eta_k^\dagger \eta_k \Lambda_k, \tag{4.40}$$

$$\eta_k^\dagger |GS\rangle = 0 \qquad \forall \;\; k, \tag{4.41}$$

$$|\psi_i\rangle = \prod_k (\eta_k^\dagger)^{n_{k,i}} |GS\rangle \quad \text{with} \quad n_{k,i} = \{0,1\}. \tag{4.42}$$

In figure 4.8 we show the results of the simulations conducted at constant disorder strength $W = 5$ for different values of α and system size L. In panel (a) we kept $L = 200$ fixed, while plotting the entanglement entropy of a subset of sites as a function of its size l for $\alpha = 0, 0.5, 1, 1.5, 3$. For $\alpha \leq 1$ we can note that the entropy scales in a hybrid way with both linear and logarithmic contributions, although the linear term is dominant in the large L limit. In the intermediate regime $1 \leq \alpha \leq 2$ the linear term vanishes (panel (b)), while the logarithmic coefficient c remains finite. Thus, for $\alpha \in [1, 2]$ the system is in a mixed phase we individuated also in the level statistics analysis. Finally, for $\alpha \geq 2$ the logarithmic coefficient vanishes, leaving only the contribution of the constant term a. This means that the entanglement entropy follows an area-law scaling for $\alpha \geq 2$, implying that the system is in a localized phase.

We performed the same analysis for fixed $\alpha = 3$, studying the scaling of the entanglement entropy with the subsystem size l for various disorder strength $W = 0, 0.5, 1, 1.5, 3$ (figure 4.9). The entanglement shows even in this case the transition from the extended regime, in which the entropy follows the scaling (4.39), to the localized phase, where the entanglement scales only as a constant following an area-law. The localized regime appears for $W \geq 2$, where both b and c goes to 0, while the extended phase is obtained for $\alpha \leq 0.5$. As in the previous case, the intermediate regime $0.5 \leq \alpha \leq 2$ shows only the logarithmic contribution. The numerical results and estimates provided by the entanglement study are consistent with the results obtained previously through the IPR and spectral analysis.

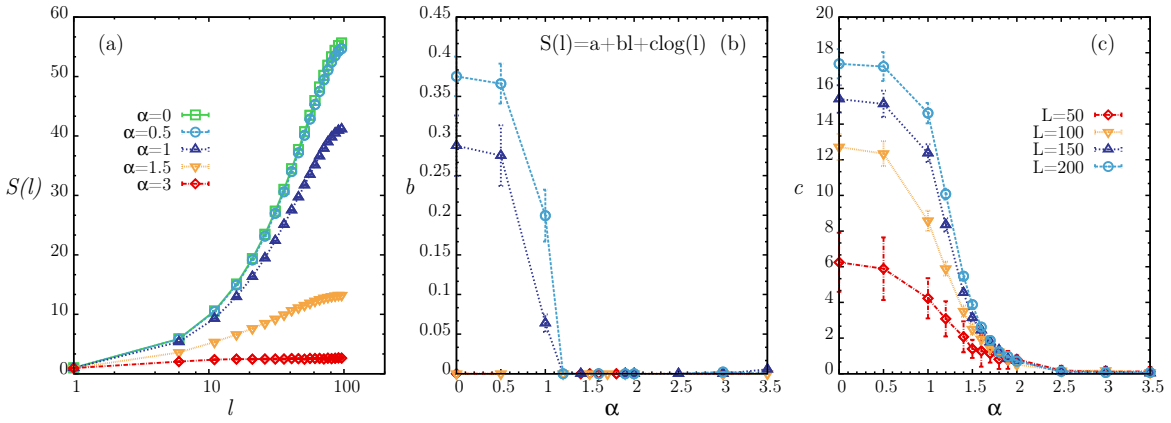

Figure 4.8: (a) Entanglement entropy as a function of the size l of the subsystem (logarithmic scale), for a total chain length of $L = 200$. The data were collected at $W = 5$ for different values of α, averaging over many disorder configurations. (b) shows the scaling of the coefficient b of the linear term in (4.39) for different system sizes as a function of α, while in (c) we plotted the coefficient of the logarithmic term which contributes to the entanglement entropy $S(l)$. The shaded region indicates the zone in which we estimated the transition to occur.

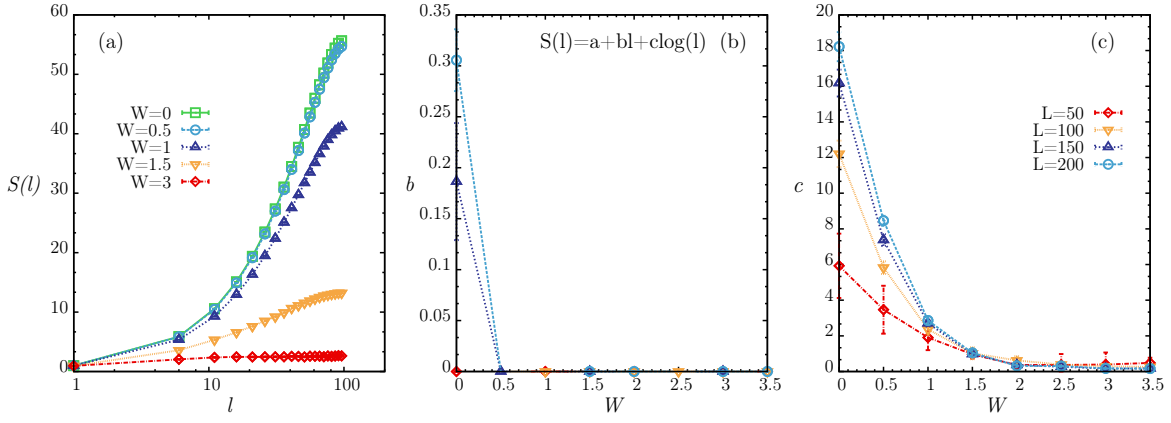

Figure 4.9: (a) Scaling of the entanglement entropy of a subsystem of l sites embedded in a chain of total length $L = 200$. as a function of l. The simulation was performed at $\alpha = 3$ with the same procedure described for plots in figure 4.8, and the panels (b) and (c) show the behaviour of the coefficients of linear and logarithmic contributions to $S(l)$.

5

CONCLUSIVE REMARKS AND PERSPECTIVES

This work was devoted to the study and understanding of several aspects of thermalization and localization in disordered fermionic chains in one dimension. We started from the very beginning, discussing some fundamental problems hidden in the construction of quantum statistical mechanics itself, like the extension to the quantum realm of essential concepts such as *ergodicity* and *thermalization*. Starting from classical chaos and Random Matrix Theory, we tried to give a quite comprehensive description of what constitutes the modern understanding of quantum chaos and thermalization mechanisms, with focus on the Eigenstate Thermalization Hypothesis. We then described a particular class of system which fails to thermalize and do not satisfy the ETH: *localized* systems and their generalization to many-body physics, i.e. *Many-Body Localized* systems. The recent renaissance of interest towards localization phenomena in disordered quantum systems, related to modern advances in experimental physics and to the availability of powerful computational methods, along with the fascinating results and open questions generated by several contributions in the last decade, represents the true driving force behind our efforts into this work. Motivated by a recent work [48], which we reviewed in chapter 3, we focused on the study of a modified version of the long-range Kitaev chain, with a disorder term induced on the superconducting gap Δ. Our aim was to examine the behaviour of this disordered free model through some of the most exploited tools in recent literature on the subject, i.e. spectral analysis and entanglement scaling study, and to point out the interplay between the long-range parameter and the disorder, in

order to obtain some new insights on the nature of the localization-delocalization transition. We were able to perform a numerical diagonalization of the Hamiltonian (4.1) and to gain access to its whole spectrum, obtaining signatures of eigenfunction localization through the study of the Inverse Participation Ratio (IPR), a quantity which vanishes in the extended phase and maintains a finite value in the localized one, implying a limited spreading of the wavefunctions upon a small fraction of sites in the latter. Our results on the IPR, averaged over the whole spectrum, highlighted the existence of a localized regime attainable by the tuning of the long-range parameter α and the disorder strength W, which becomes evident for $\alpha \geq 2$ and $W \geq 3$, where the spectrum appears fully localized. Fixing three main cuts of interest ($\alpha = 3, \alpha = 1$ and $W = 5$), we investigated the IPR scaling for different system sizes L averaged over many disorder realizations, noting that the IPR in the ergodic phase vanishes more clearly at greater L values. We then performed a more detailed analysis of the localization transition considering the IPR_n for every single state as a function of the energy, the disorder strength (for constant α) and the long-range parameter α (for constant disorder W). Our outcomes confirmed that in the limit of $\alpha \to 0$, i.e. when the range of interactions are maximally spread, all eigenstates appear extended, and there is no localization even for high disorder strengths. For $\alpha \geq 1$ localization begins to appear at the edges of the spectrum, and increasing the disorder strength the phase diagram shows a mobility edge, which is not visible plotting the IPR_n as a function of energy and α for $W = 5$, since every eigenstate appears localized for $\alpha \geq 1.5$. At this point we went on with a spectral analysis, studying the level statistics of our model, which permits to identify the transition between ergodic and localized phases through the crossing from a GOE distribution to a Poissonian. We calculated the mean adjacent gap ratio $\langle r \rangle$ and evaluated its behaviour for different system sizes and different values of W and α. We identified a localized regime for $\alpha \geq 2$ at $W = 5$ fixed, while for $\alpha \leq 1$ the system seems to be in an extended phase. In the region $1 \leq \alpha \leq 2$ there is an intermediate phase in which we could not detect the exact critical point at which the transition occurs. Keeping the range of interactions fixed at $\alpha = 3$, we repeated the same study with $W \in [0, 3]$, noting two main features: while for $W \leq 1$ the mean gap ratio $\langle r \rangle$ approaches the expected value for a Poisson distribution (in the large L limit), implying the manifestation of localization, we recognized the emergence of an unexpected regime for $0 \leq W \leq 1$, in which the system is not localized but does not show good agreement with the theoretical predictions for ergodic

systems. This surprising behaviour seems to survive even in the short-range limit of our model, and it would thus require further investigation. At last, we concluded our study with an analysis of the entanglement, computing the bipartite entanglement entropy as a function of the subsystem size l. Our results confirmed the area-law scaling of the entropy with l in the localized phase for the entire spectrum, i.e. even for excited states. In the extended phase, our model behaves in a hybrid fashion, showing both linear and logarithmic corrections to the entropy with respect to the size l.

Far from being exhaustive, our work outlined some interesting localization properties of a fermionic long-range model with a superconducting pairing term, which to our knowledge has not been treated in the literature so far[1]. It would be interesting to investigate some more aspects of this kind of models, especially related to dynamical features. In particular, the study of the entanglement evolution via quenching procedures represents an intriguing future perspective, since it would provide some key insights on the nature of the localization itself, which could help distinguishing between traditional Anderson localization and Many-Body localization phenomena. Other efforts may be directed to a response analysis of our fermionic chain under the action of some external forces and fields, in order to detect some memory effects due to localization which can be extremely fascinating, even in the perspective of possible experimental realizations.

[1] During the completion of this thesis, we became aware of a very recent work [183] discussing disordered Kitaev chains with long-range pairing, which, however, presents several differences with respect to our study.

BIBLIOGRAPHY

[1] J.W. Gibbs. *Elementary Principles in Statistical Mechanics: Developed with Especial Reference to the Rational Foundations of Thermodynamics*. C. Scribner's sons, 1902.

[2] Jos Uffink. Compendium of the foundations of classical statistical physics, March 2006. Chapter for "Handbook for Philsophy of Physics", J. Butterfield and J. Earman (eds) to appear.

[3] J. v. Neumann. Beweis des ergodensatzes und desh-theorems in der neuen mechanik. *Zeitschrift für Physik*, 57(1):30–70, 1929.

[4] L.D. Landau and E.M. Lifshitz. *Statistical Physics*. Number v. 5. Elsevier Science, 2013.

[5] G. Morandi, F. Napoli, and E. Ercolessi. *Statistical Mechanics: An Intermediate Course*. Statistical Physics. World Scientific, 2001.

[6] Yakov G. Sinai. Dynamical systems with elastic reflections. *Russian Mathematical Surveys*, pages 137+, October 2007.

[7] Tamás Tasnádi. The behavior of nearby trajectories in magnetic billiards. *Journal of Mathematical Physics*, 37(11):5577–5598, 1996.

[8] Nándor Simányi. Proof of the ergodic hypothesis for typical hard ball systems. *Annales Henri Poincaré*, 5(2), 2004.

[9] J. Fermi, E. Pasta and S. Ulam. Studies of nonlinear problems. 1955.

[10] E. V. Kozik and B. V. Svistunov. Theory of decay of superfluid turbulence in the low-temperature limit. *Journal of Low Temperature Physics*, 156(3):215–267, 2009.

[11] J. P. Bouchaud. Weak ergodicity breaking and aging in disordered systems. *J. Phys. I France*, 2(9):1705–1713, 1992.

[12] J. M. Deutsch. Quantum statistical mechanics in a closed system. *Phys. Rev. A*, 43:2046–2049, Feb 1991.

[13] Mark Srednicki. Chaos and quantum thermalization. *Phys. Rev. E*, 50:888–901, Aug 1994.

[14] Marcos Rigol, Vanja Dunjko, and Maxim Olshanii. Thermalization and its mechanism for generic isolated quantum systems. *Nature*, 452(7189):854–858, Apr 2008.

[15] P. W. Anderson. Absence of diffusion in certain random lattices. *Phys. Rev.*, 109:1492–1505, Mar 1958.

[16] D.M. Basko, I.L. Aleiner, and B.L. Altshuler. Metal–insulator transition in a weakly interacting many-electron system with localized single-particle states. *Annals of Physics*, 321(5):1126 – 1205, 2006.

[17] I. V. Gornyi, A. D. Mirlin, and D. G. Polyakov. Interacting electrons in disordered wires: Anderson localization and low-t transport. *Phys. Rev. Lett.*, 95:206603, Nov 2005.

[18] M. Aidelsburger, M. Atala, S. Nascimbène, S. Trotzky, Y.-A. Chen, and I. Bloch. Experimental realization of strong effective magnetic fields in an optical lattice. *Phys. Rev. Lett.*, 107:255301, Dec 2011.

[19] A. K. Tuchman, C. Orzel, A. Polkovnikov, and M. A. Kasevich. Nonequilibrium coherence dynamics of a soft boson lattice. *Phys. Rev. A*, 74:051601, Nov 2006.

[20] Immanuel Bloch. Quantum gases in optical lattices. *Physics World*, 17(4):25, 2004.

[21] D. Porras and J. I. Cirac. Effective quantum spin systems with trapped ions. *Phys. Rev. Lett.*, 92:207901, May 2004.

[22] A. Friedenauer, H. Schmitz, J. T. Glueckert, D. Porras, and T. Schaetz. Simulating a quantum magnet with trapped ions. *Nat Phys*, 4(10):757–761, Oct 2008.

[23] P. Schindler, M. Muller, D. Nigg, J. T. Barreiro, E. A. Martinez, M. Hennrich, T. Monz, S. Diehl, P. Zoller, and R. Blatt. Quantum simulation of dynamical maps with trapped ions. *Nat Phys*, 9(6):361–367, Jun 2013. Article.

[24] Joseph W. Britton, Brian C. Sawyer, Adam C. Keith, C. C Joseph Wang, James K. Freericks, Hermann Uys, Michael J. Biercuk, and John J. Bollinger. Engineered two-dimensional ising interactions in a trapped-ion quantum simulator with hundreds of spins. *Nature*, 484(7395):489–492, Apr 2012.

[25] R. Blatt and C. F. Roos. Quantum simulations with trapped ions. *Nat Phys*, 8(4):277–284, Apr 2012.

[26] U. Schollwöck. The density-matrix renormalization group. *Rev. Mod. Phys.*, 77:259–315, Apr 2005.

[27] Román Orús. A practical introduction to tensor networks: Matrix product states and projected entangled pair states. *Annals of Physics*, 349:117 – 158, 2014.

[28] Marcos Rigol. Breakdown of thermalization in finite one-dimensional systems. *Phys. Rev. Lett.*, 103:100403, Sep 2009.

[29] David J. Luitz, Nicolas Laflorencie, and Fabien Alet. Many-body localization edge in the random-field heisenberg chain. *Phys. Rev. B*, 91:081103, Feb 2015.

[30] W. M. C. Foulkes, L. Mitas, R. J. Needs, and G. Rajagopal. Quantum monte carlo simulations of solids. *Rev. Mod. Phys.*, 73:33–83, Jan 2001.

[31] Hideo Aoki, Naoto Tsuji, Martin Eckstein, Marcus Kollar, Takashi Oka, and Philipp Werner. Nonequilibrium dynamical mean-field theory and its applications. *Rev. Mod. Phys.*, 86:779–837, Jun 2014.

[32] W. Kohn. Nobel lecture: Electronic structure of matter—wave functions and density functionals. *Rev. Mod. Phys.*, 71:1253–1266, Oct 1999.

[33] Silvano Garnerone. Pure state thermodynamics with matrix product states. *Phys. Rev. B*, 88:165140, Oct 2013.

[34] Silvano Garnerone and Thiago R. de Oliveira. Generalized quantum microcanonical ensemble from random matrix product states. *Phys. Rev. B*, 87:214426, Jun 2013.

[35] S. Bravyi, M. B. Hastings, and F. Verstraete. Lieb-robinson bounds and the generation of correlations and topological quantum order. *Phys. Rev. Lett.*, 97:050401, Jul 2006.

[36] B. Nachtergaele and R. Sims. Lieb-Robinson Bounds in Quantum Many-Body Physics. *ArXiv e-prints*, April 2010.

[37] Bruno Nachtergaele and Robert Sims. Lieb-robinson bounds and the exponential clustering theorem. *Communications in Mathematical Physics*, 265(1):119–130, 2006.

[38] Jens Eisert and Tobias J. Osborne. General entanglement scaling laws from time evolution. *Phys. Rev. Lett.*, 97:150404, Oct 2006.

[39] Pasquale Calabrese and John Cardy. Entanglement and correlation functions following a local quench: a conformal field theory approach. *Journal of Statistical Mechanics: Theory and Experiment*, 2007(10):P10004, 2007.

[40] Karel Van Acoleyen, Michaël Mariën, and Frank Verstraete. Entanglement rates and area laws. *Phys. Rev. Lett.*, 111:170501, Oct 2013.

[41] A Yu Kitaev. Unpaired majorana fermions in quantum wires. *Physics-Uspekhi*, 44(10S):131, 2001.

[42] Chetan Nayak, Steven H. Simon, Ady Stern, Michael Freedman, and Sankar Das Sarma. Non-abelian anyons and topological quantum computation. *Rev. Mod. Phys.*, 80:1083–1159, Sep 2008.

[43] A. D. K. Finck, D. J. Van Harlingen, P. K. Mohseni, K. Jung, and X. Li. Anomalous modulation of a zero-bias peak in a hybrid nanowire-superconductor device. *Phys. Rev. Lett.*, 110:126406, Mar 2013.

[44] V. Mourik, K. Zuo, S. M. Frolov, S. R. Plissard, E. P. A. M. Bakkers, and L. P. Kouwenhoven. Signatures of majorana fermions in hybrid superconductor-semiconductor nanowire devices. 336(6084):1003–1007, 2012.

[45] Leonid P. Rokhinson, Xinyu Liu, and Jacek K. Furdyna. The fractional a.c. josephson effect in a semiconductor-superconductor nanowire as a signature of majorana particles. *Nat Phys*, 8(11):795–799, Nov 2012.

[46] Anindya Das, Yuval Ronen, Yonatan Most, Yuval Oreg, Moty Heiblum, and Hadas Shtrikman. Zero-bias peaks and splitting in an al-inas nanowire topological superconductor as a signature of majorana fermions. *Nat Phys*, 8(12):887–895, Dec 2012.

[47] Sankar Das Sarma, Michael Freedman, and Chetan Nayak. Majorana zero modes and topological quantum computation. *Npj Quantum Information*, 1:15001 EP –, Oct 2015. Review Article.

[48] Davide Vodola, Luca Lepori, Elisa Ercolessi, Alexey V. Gorshkov, and Guido Pupillo. Kitaev chains with long-range pairing. *Phys. Rev. Lett.*, 113:156402, Oct 2014.

[49] Falko Pientka, Leonid I. Glazman, and Felix von Oppen. Topological superconducting phase in helical shiba chains. *Phys. Rev. B*, 88:155420, Oct 2013.

[50] Philipp Hauke and Markus Heyl. Many-body localization and quantum ergodicity in disordered long-range ising models. *Phys. Rev. B*, 92:134204, Oct 2015.

[51] Moure, N., Haas, S., and Kettemann, S. Many-body localization transition in random quantum spin chains with long-range interactions. *EPL*, 111(2):27003, 2015.

[52] Bo Li. Many-body localization in a long range {XXZ} model with random-field. *Physica B: Condensed Matter*, 502:82 – 87, 2016.

[53] Haoyuan Li, Jia Wang, Xia-Ji Liu, and Hui Hu. Many-body localization in ising models with random long-range interactions. *Phys. Rev. A*, 94:063625, Dec 2016.

[54] Alexander L. Burin. Localization in a random xy model with long-range interactions: Intermediate case between single-particle and many-body problems. *Phys. Rev. B*, 92:104428, Sep 2015.

[55] K. Vogtmann, A. Weinstein, and V.I. Arnol'd. *Mathematical Methods of Classical Mechanics*. Graduate Texts in Mathematics. Springer New York, 1997.

[56] A N Kolmogorov. On conservation of conditionally periodic motions for a small change in Hamilton's function. *Dokl. Akad. Nauk SSSR*, 98:527–530, 1954.

[57] Madan Lal Mehta, editor. volume 142 of *Pure and Applied Mathematics*. Elsevier, 2004.

[58] A. Müller–Groeling T. Guhr and H.A. Weidenmüller. Random-matrix theories in quantum physics: common concepts. *Physics Reports*, 299(4–6):189 – 425, 1998.

[59] Martin C. Gutzwiller. Periodic orbits and classical quantization conditions. *Journal of Mathematical Physics*, 12(3):343–358, 1971.

[60] E. P. Wigner. Characteristic vectors of bordered matrices with infinite dimensions. *The Annals of Mathematics*, 62(3):548–564, 1955.

[61] Eugene P. Wigner. On the distribution of the roots of certain symmetric matrices. *Annals of Mathematics*, 67(2):325–327, 1958.

[62] Freeman J. Dyson. Statistical theory of the energy levels of complex systems. i. *Journal of Mathematical Physics*, 3(1):140–156, 1962.

[63] Y. Alhassid. The statistical theory of quantum dots. *Rev. Mod. Phys.*, 72:895–968, Oct 2000.

[64] O. Bohigas, M. J. Giannoni, and C. Schmit. Characterization of chaotic quantum spectra and universality of level fluctuation laws. *Phys. Rev. Lett.*, 52:1–4, Jan 1984.

[65] T. A. Brody, J. Flores, J. B. French, P. A. Mello, A. Pandey, and S. S. M. Wong. Random-matrix physics: spectrum and strength fluctuations. *Rev. Mod. Phys.*, 53:385–479, Jul 1981.

[66] M. V. Berry and M. Tabor. Level clustering in the regular spectrum. *Proceedings of the Royal Society of London A: Mathematical, Physical and Engineering Sciences*, 356(1686):375–394, 1977.

[67] M. V. Berry. Semi-classical mechanics in phase space: A study of wigner's function. *Philosophical Transactions of the Royal Society of London A: Mathematical, Physical and Engineering Sciences*, 287(1343):237–271, 1977.

[68] M. Hillery, R.F. O'Connell, M.O. Scully, and E.P. Wigner. Distribution functions in physics: Fundamentals. *Physics Reports*, 106(3):121 – 167, 1984.

[69] Anatoli Polkovnikov. Phase space representation of quantum dynamics. *Annals of Physics*, 325(8):1790 – 1852, 2010.

[70] O. Bohigas, R. U. Haq, and A. Pandey. *Fluctuation Properties of Nuclear Energy Levels and Widths : Comparison of Theory with Experiment*, pages 809–813. Springer Netherlands, Dordrecht, 1983.

[71] D. Wintgen and H. Friedrich. Classical and quantum-mechanical transition between regularity and irregularity in a hamiltonian system. *Phys. Rev. A*, 35:1464–1466, Feb 1987.

[72] Lea F. Santos and Marcos Rigol. Onset of quantum chaos in one-dimensional bosonic and fermionic systems and its relation to thermalization. *Phys. Rev. E*, 81:036206, Mar 2010.

[73] Lea F. Santos and Marcos Rigol. Localization and the effects of symmetries in the thermalization properties of one-dimensional quantum systems. *Phys. Rev. E*, 82:031130, Sep 2010.

[74] M. A. Cazalilla, R. Citro, T. Giamarchi, E. Orignac, and M. Rigol. One dimensional bosons: From condensed matter systems to ultracold gases. *Rev. Mod. Phys.*, 83:1405–1466, Dec 2011.

[75] Ranjan Modak and Subroto Mukerjee. Finite size scaling in crossover among different random matrix ensembles in microscopic lattice models. *New Journal of Physics*, 16(9):093016, 2014.

[76] Ranjan Modak, Subroto Mukerjee, and Sriram Ramaswamy. Universal power law in crossover from integrability to quantum chaos. *Phys. Rev. B*, 90:075152, Aug 2014.

[77] Many-body localization and thermalization in quantum statistical mechanics. *Annual Review of Condensed Matter Physics*, 6(1):15–38, 2015.

[78] Lea F. Santos, Anatoli Polkovnikov, and Marcos Rigol. Weak and strong typicality in quantum systems. *Phys. Rev. E*, 86:010102, Jul 2012.

[79] J. M. Deutsch, Haibin Li, and Auditya Sharma. Microscopic origin of thermodynamic entropy in isolated systems. *Phys. Rev. E*, 87:042135, Apr 2013.

[80] Hyungwon Kim and David A. Huse. Ballistic spreading of entanglement in a diffusive nonintegrable system. *Phys. Rev. Lett.*, 111:127205, Sep 2013.

[81] L.D. Landau and E.M. Lifshits. *Quantum Mechanics: Non-relativistic Theory*. Butterworth-Heinemann. Butterworth-Heinemann, 1977.

[82] S. Goldstein, J. L. Lebowitz, R. Tumulka, and N. Zanghì. Long-time behavior of macroscopic quantum systems. *The European Physical Journal H*, 35(2):173–200, 2010.

[83] Mark Srednicki. The approach to thermal equilibrium in quantized chaotic systems. *Journal of Physics A: Mathematical and General*, 32(7):1163, 1999.

[84] J T Edwards and D J Thouless. Numerical studies of localization in disordered systems. *Journal of Physics C: Solid State Physics*, 5(8):807, 1972.

[85] G. Feher, R. C. Fletcher, and E. A. Gere. Exchange effects in spin resonance of impurity atoms in silicon. *Phys. Rev.*, 100:1784–1786, Dec 1955.

[86] G. Feher and E. A. Gere. Electron spin resonance experiments on donors in silicon. ii. electron spin relaxation effects. *Phys. Rev.*, 114:1245–1256, Jun 1959.

[87] N F Mott. The basis of the electron theory of metals, with special reference to the transition metals. *Proceedings of the Physical Society. Section A*, 62(7):416, 1949.

[88] N. F. Mott. Electrons in disordered structures. *Advances in Physics*, 16:49–144, January 1967.

[89] E. Abrahams, P. W. Anderson, D. C. Licciardello, and T. V. Ramakrishnan. Scaling theory of localization: Absence of quantum diffusion in two dimensions. *Phys. Rev. Lett.*, 42:673–676, Mar 1979.

[90] D. J. Thouless. Maximum metallic resistance in thin wires. *Phys. Rev. Lett.*, 39:1167–1169, Oct 1977.

[91] D. J. Thouless. Electrons in disordered systems and the theory of localization. , 13:93–142, October 1974.

[92] Franz Wegner. The mobility edge problem: Continuous symmetry and a conjecture. *Zeitschrift für Physik B Condensed Matter*, 35(3):207–210, 1979.

[93] Larkin A. I. Efetov, K. B. and D.E. Kheml'nitskii. Interaction of diffusion modes in the theory of localization. *Sov. Phys. - JETP*, 52, 1980.

[94] K. Jüngling and R. Oppermann. Effects of spin interactions in disordered electronic systems: Loop expansions and exact relations among local gauge invariant models. *Zeitschrift für Physik B Condensed Matter*, 38(2), 1980.

[95] Ferdinand Evers and Alexander D. Mirlin. Anderson transitions. *Rev. Mod. Phys.*, 80:1355–1417, Oct 2008.

[96] Franz J. Wegner. Electrons in disordered systems. scaling near the mobility edge. *Zeitschrift für Physik B Condensed Matter*, 25(4):327–337, 1976.

[97] L. Fleishman and P. W. Anderson. Interactions and the anderson transition. *Phys. Rev. B*, 21:2366–2377, Mar 1980.

[98] Boris L. Altshuler, Yuval Gefen, Alex Kamenev, and Leonid S. Levitov. Quasiparticle lifetime in a finite system: A nonperturbative approach. *Phys. Rev. Lett.*, 78:2803–2806, Apr 1997.

[99] N. Mott. Conduction in glasses containing transition metal ions. *Journal of Non Crystalline Solids*, 1:1–17, December 1968.

[100] B.L. Altshuler and A.G. Aronov. 1 - electron–electron interaction in disordered conductors. In A.L. EFROS and M. POLLAK, editors, *Electron–Electron Interactions in Disordered Systems*, volume 10 of *Modern Problems in Condensed Matter Sciences*, pages 1 – 153. Elsevier, 1985.

[101] Arijeet Pal and David A. Huse. Many-body localization phase transition. *Phys. Rev. B*, 82:174411, Nov 2010.

[102] P. Jordan and E. Wigner. Über das paulische aquivalenzverbot. *Zeitschrift für Physik*, 47(9-10):631–651, 1928.

[103] Nandkishore R. Huse D. A. Many-body localization and thermalization in quantum statistical mechanics. *Annual Review of Condensed Matter Physics*, 6(1):15–38, 2015.

[104] Vadim Oganesyan and David A. Huse. Localization of interacting fermions at high temperature. *Phys. Rev. B*, 75:155111, Apr 2007.

[105] Trithep Devakul and Rajiv R. P. Singh. Early breakdown of area-law entanglement at the many-body delocalization transition. *Phys. Rev. Lett.*, 115:187201, Oct 2015.

[106] R Berkovits and B I Shklovskii. Statistics of energy spectra of a strongly disordered system of interacting electrons. *Journal of Physics: Condensed Matter*, 11(3):779, 1999.

[107] Y. Avishai, J. Richert, and R. Berkovits. Level statistics in a Heisenberg chain with random magnetic field. , 66(5):052416, August 2002.

[108] Emilio Cuevas, Mikhail Feigel'man, Lev Ioffe, and Marc Mezard. Level statistics of disordered spin-1/2 systems and materials with localized cooper pairs. *Nature Communications*, 3:1128 EP –, Oct 2012. Article.

[109] Nariyuki Minami. Local fluctuation of the spectrum of a multidimensional anderson tight binding model. *Comm. Math. Phys.*, 177(3):709–725, 1996.

[110] Alexander D. Mirlin. Statistics of energy levels and eigenfunctions in disordered systems. *Physics Reports*, 326(5–6):259 – 382, 2000.

[111] Amy C. Cassidy, Charles W. Clark, and Marcos Rigol. Generalized thermalization in an integrable lattice system. *Phys. Rev. Lett.*, 106:140405, Apr 2011.

[112] Jean-Sébastien Caux and Fabian H. L. Essler. Time evolution of local observables after quenching to an integrable model. *Phys. Rev. Lett.*, 110:257203, Jun 2013.

[113] Maksym Serbyn, Z. Papić, and Dmitry A. Abanin. Local conservation laws and the structure of the many-body localized states. *Phys. Rev. Lett.*, 111:127201, Sep 2013.

[114] David A. Huse, Rahul Nandkishore, and Vadim Oganesyan. Phenomenology of fully many-body-localized systems. *Phys. Rev. B*, 90:174202, Nov 2014.

[115] Cécile Monthus. Many-body localization: construction of the emergent local conserved operators via block real-space renormalization. *Journal of Statistical Mechanics: Theory and Experiment*, 2016(3):033101, 2016.

[116] Maksym Serbyn, Z. Papić, and D. A. Abanin. Quantum quenches in the many-body localized phase. *Phys. Rev. B*, 90:174302, Nov 2014.

[117] Maksym Serbyn, Z. Papić, and Dmitry A. Abanin. Universal slow growth of entanglement in interacting strongly disordered systems. *Phys. Rev. Lett.*, 110:260601, Jun 2013.

[118] M. Serbyn, M. Knap, S. Gopalakrishnan, Z. Papić, N. Y. Yao, C. R. Laumann, D. A. Abanin, M. D. Lukin, and E. A. Demler. Interferometric probes of many-body localization. *Phys. Rev. Lett.*, 113:147204, Oct 2014.

[119] Yasaman Bahri, Ronen Vosk, Ehud Altman, and Ashvin Vishwanath. Localization and topology protected quantum coherence at the edge of hot matter. *Nature Communications*, 6:7341 EP –, Jul 2015. Article.

[120] A. Pathak. *Elements of Quantum Computation and Quantum Communication.* CRC Press, 2013.

[121] M.A. Nielsen and I.L. Chuang. *Quantum Computation and Quantum Information.* Cambridge Series on Information and the Natural Sciences. Cambridge University Press, 2000.

[122] M B Hastings. An area law for one-dimensional quantum systems. *Journal of Statistical Mechanics: Theory and Experiment*, 2007(08):P08024, 2007.

[123] Jonas A. Kjäll, Jens H. Bardarson, and Frank Pollmann. Many-body localization in a disordered quantum ising chain. *Phys. Rev. Lett.*, 113:107204, Sep 2014.

[124] T. Grover. Certain General Constraints on the Many-Body Localization Transition. *ArXiv e-prints*, 2014.

[125] Jens H. Bardarson, Frank Pollmann, and Joel E. Moore. Unbounded growth of entanglement in models of many-body localization. *Phys. Rev. Lett.*, 109:017202, Jul 2012.

[126] Arun Nanduri, Hyungwon Kim, and David A. Huse. Entanglement spreading in a many-body localized system. *Phys. Rev. B*, 90:064201, Aug 2014.

[127] Juliette Billy, Vincent Josse, Zhanchun Zuo, Alain Bernard, Ben Hambrecht, Pierre Lugan, David Clement, Laurent Sanchez-Palencia, Philippe Bouyer, and Alain Aspect. Direct observation of anderson localization of matter waves in a controlled disorder. *Nature*, 453(7197):891–894, Jun 2008.

[128] Giacomo Roati, Chiara D/'Errico, Leonardo Fallani, Marco Fattori, Chiara Fort, Matteo Zaccanti, Giovanni Modugno, Michele Modugno, and Massimo Inguscio. Anderson localization of a non-interacting bose-einstein condensate. *Nature*, 453(7197):895–898, Jun 2008.

[129] Michael Schreiber, Sean S. Hodgman, Pranjal Bordia, Henrik P. Lüschen, Mark H. Fischer, Ronen Vosk, Ehud Altman, Ulrich Schneider, and Immanuel Bloch. Observation of many-body localization of interacting fermions in a quasirandom optical lattice. *Science*, 349(6250):842–845, 2015.

[130] Jae-yoon Choi, Sebastian Hild, Johannes Zeiher, Peter Schauß, Antonio Rubio-Abadal, Tarik Yefsah, Vedika Khemani, David A. Huse, Immanuel Bloch, and Christian Gross. Exploring the many-body localization transition in two dimensions. *Science*, 352(6293):1547–1552, 2016.

[131] S. S. Kondov, W. R. McGehee, W. Xu, and B. DeMarco. Disorder-induced localization in a strongly correlated atomic hubbard gas. *Phys. Rev. Lett.*, 114:083002, Feb 2015.

[132] Pranjal Bordia, Henrik P. Lüschen, Sean S. Hodgman, Michael Schreiber, Immanuel Bloch, and Ulrich Schneider. Coupling identical one-dimensional many-body localized systems. *Phys. Rev. Lett.*, 116:140401, Apr 2016.

[133] Serge Aubry and Gilles André. Analyticity breaking and anderson localization in incommensurate lattices. *Ann. Israel Phys. Soc*, 3(133):18, 1980.

[134] Shankar Iyer, Vadim Oganesyan, Gil Refael, and David A. Huse. Many-body localization in a quasiperiodic system. *Phys. Rev. B*, 87:134202, Apr 2013.

[135] Detecting a many-body mobility edge with quantum quenches. *SciPost Phys.*, 1:010, 2016.

[136] J. Smith, A. Lee, P. Richerme, B. Neyenhuis, P. W. Hess, P. Hauke, M. Heyl, D. A. Huse, and C. Monroe. Many-body localization in a quantum simulator with programmable random disorder. *Nat Phys*, 12(10):907–911, Oct 2016.

[137] M. Leijnse and K. Flensberg. Introduction to topological superconductivity and majorana fermions. *Semiconductor Science and Technology*, 27(12):124003, 2012.

[138] F. Wilczek. Majorana returns. *Nature Physics*, 5:614–618, September 2009.

[139] Ettore Majorana. Teoria simmetrica dell'elettrone e del positrone. *j-NUOVO-CIMENTO-8*, 14(4):171–184, April 1937.

[140] Eytan Barouch, Barry M. McCoy, and Max Dresden. Statistical mechanics of the XY model. i. *Phys. Rev. A*, 2:1075–1092, Sep 1970.

[141] Eytan Barouch and Barry M. McCoy. Statistical mechanics of the xy model. ii. spin-correlation functions. *Phys. Rev. A*, 3:786–804, Feb 1971.

[142] Milton Abramowitz and Irene A. Stegun. *Handbook of Mathematical Functions with Formulas, Graphs, and Mathematical Tables.* Dover, New York, ninth dover printing, tenth gpo printing edition, 1964.

[143] M.J. Ablowitz and A.S. Fokas. *Complex Variables: Introduction and Applications*. Cambridge Texts in Applied Mathematics. Cambridge University Press, 2003.

[144] Matthew B. Hastings and Tohru Koma. Spectral gap and exponential decay of correlations. *Communications in Mathematical Physics*, 265(3):781–804, 2006.

[145] Zhe-Xuan Gong, Michael Foss-Feig, Spyridon Michalakis, and Alexey V. Gorshkov. Persistence of locality in systems with power-law interactions. *Phys. Rev. Lett.*, 113:030602, Jul 2014.

[146] Michael Foss-Feig, Zhe-Xuan Gong, Charles W. Clark, and Alexey V. Gorshkov. Nearly linear light cones in long-range interacting quantum systems. *Phys. Rev. Lett.*, 114:157201, Apr 2015.

[147] Takuro Matsuta, Tohru Koma, and Shu Nakamura. Improving the lieb–robinson bound for long-range interactions. *Annales Henri Poincaré*, pages 1–10, 2016.

[148] T. Giamarchi. *Quantum Physics in One Dimension*. International Series of Monographs on Physics. Clarendon Press, 2003.

[149] Pasquale Calabrese and John Cardy. Entanglement entropy and quantum field theory. *Journal of Statistical Mechanics: Theory and Experiment*, 2004(06):P06002, 2004.

[150] Christoph Holzhey, Finn Larsen, and Frank Wilczek. Geometric and renormalized entropy in conformal field theory. *Nuclear Physics B*, 424(3):443 – 467, 1994.

[151] M. B. Hastings. Lieb-schultz-mattis in higher dimensions. *Phys. Rev. B*, 69:104431, Mar 2004.

[152] Elliott H. Lieb and Derek W. Robinson. The finite group velocity of quantum spin systems. *Communications in Mathematical Physics*, 28(3):251–257, 1972.

[153] Pasquale Calabrese and John Cardy. Evolution of entanglement entropy in one-dimensional systems. *Journal of Statistical Mechanics: Theory and Experiment*, 2005(04):P04010, 2005.

[154] J. Schachenmayer, B. P. Lanyon, C. F. Roos, and A. J. Daley. Entanglement growth in quench dynamics with variable range interactions. *Phys. Rev. X*, 3:031015, Sep 2013.

[155] M. Ghasemi Nezhadhaghighi and M. A. Rajabpour. Entanglement dynamics in short- and long-range harmonic oscillators. *Phys. Rev. B*, 90:205438, Nov 2014.

[156] P. Hauke and L. Tagliacozzo. Spread of correlations in long-range interacting quantum systems. *Phys. Rev. Lett.*, 111:207202, Nov 2013.

[157] Jens Eisert, Mauritz van den Worm, Salvatore R. Manmana, and Michael Kastner. Breakdown of quasilocality in long-range quantum lattice models. *Phys. Rev. Lett.*, 111:260401, Dec 2013.

[158] F. Evers and A. D. Mirlin. Fluctuations of the inverse participation ratio at the anderson transition. *Phys. Rev. Lett.*, 84:3690–3693, Apr 2000.

[159] A. Mildenberger, F. Evers, and A. D. Mirlin. Dimensionality dependence of the wave-function statistics at the anderson transition. *Phys. Rev. B*, 66:033109, Jul 2002.

[160] J. Brndiar and P. Markoš. Universality of the metal-insulator transition in three-dimensional disordered systems. *Phys. Rev. B*, 74:153103, Oct 2006.

[161] K. Binder. Critical properties from monte carlo coarse graining and renormalization. *Phys. Rev. Lett.*, 47:693–696, Aug 1981.

[162] B. Wischmann and E. Müller-Hartmann. Level statistics and localization: A study of the 1d anderson model. *Zeitschrift für Physik B Condensed Matter*, 79(1):91–99, 1990.

[163] B. I. Shklovskii, B. Shapiro, B. R. Sears, P. Lambrianides, and H. B. Shore. Statistics of spectra of disordered systems near the metal-insulator transition. *Phys. Rev. B*, 47:11487–11490, May 1993.

[164] Ph. Jacquod and D. L. Shepelyansky. Emergence of quantum chaos in finite interacting fermi systems. *Phys. Rev. Lett.*, 79:1837–1840, Sep 1997.

[165] H. Obuse and K. Yakubo. Critical level statistics and anomalously localized states at the anderson transition. *Phys. Rev. B*, 71:035102, Jan 2005.

[166] Xiaopeng Li, Sriram Ganeshan, J. H. Pixley, and S. Das Sarma. Many-body localization and quantum nonergodicity in a model with a single-particle mobility edge. *Phys. Rev. Lett.*, 115:186601, Oct 2015.

[167] Maksym Serbyn and Joel E. Moore. Spectral statistics across the many-body localization transition. *Phys. Rev. B*, 93:041424, Jan 2016.

[168] Elliott Baygan, S. P. Lim, and D. N. Sheng. Many-body localization and mobility edge in a disordered spin-$\frac{1}{2}$ heisenberg ladder. *Phys. Rev. B*, 92:195153, Nov 2015.

[169] H. A. Bethe. An attempt to calculate the number of energy levels of a heavy nucleus. *Phys. Rev.*, 50:332–341, Aug 1936.

[170] Y. Y. Atas, E. Bogomolny, O. Giraud, and G. Roux. Distribution of the ratio of consecutive level spacings in random matrix ensembles. *Phys. Rev. Lett.*, 110:084101, Feb 2013.

[171] Luigi Amico, Rosario Fazio, Andreas Osterloh, and Vlatko Vedral. Entanglement in many-body systems. *Rev. Mod. Phys.*, 80:517–576, May 2008.

[172] J. Eisert, M. Cramer, and M. B. Plenio. Colloquium: Area laws for the entanglement entropy. *Rev. Mod. Phys.*, 82:277–306, Feb 2010.

[173] F. C. Alcaraz and M. S. Sarandy. Finite-size corrections to entanglement in quantum critical systems. *Phys. Rev. A*, 78:032319, Sep 2008.

[174] Vincenzo Alba, Maurizio Fagotti, and Pasquale Calabrese. Entanglement entropy of excited states. *Journal of Statistical Mechanics: Theory and Experiment*, 2009(10):P10020, 2009.

[175] M. Dalmonte, E. Ercolessi, and L. Taddia. Critical properties and rényi entropies of the spin-$\frac{3}{2}$ xxz chain. *Phys. Rev. B*, 85:165112, Apr 2012.

[176] L. Taddia, J. C. Xavier, F. C. Alcaraz, and G. Sierra. Entanglement entropies in conformal systems with boundaries. *Phys. Rev. B*, 88:075112, Aug 2013.

[177] Estelle L. Basor and Kent E. Morrison. The fisher-hartwig conjecture and toeplitz eigenvalues. *Linear Algebra and its Applications*, 202:129 – 142, 1994.

[178] Michael E. Fisher and Robert E. Hartwig. *Toeplitz Determinants: Some Applications, Theorems, and Conjectures*, pages 333–353. John Wiley Sons, Inc., 2007.

[179] P. J. Forrester and N. E. Frankel. Applications and generalizations of fisher–hartwig asymptotics. *Journal of Mathematical Physics*, 45(5):2003–2028, 2004.

[180] E. W. Barnes. The theory of the double gamma function. *Philosophical Transactions of the Royal Society of London A: Mathematical, Physical and Engineering Sciences*, 196(274-286):265–387, 1901.

[181] B.-Q. Jin and V. E. Korepin. Quantum spin chain, toeplitz determinants and the fisher—hartwig conjecture. *Journal of Statistical Physics*, 116(1):79–95, 2004.

[182] F Ares, J G Esteve, F Falceto, and E Sánchez-Burillo. Excited state entanglement in homogeneous fermionic chains. *Journal of Physics A: Mathematical and Theoretical*, 47(24):245301, 2014.

[183] Xiaoming Cai. Disordered kitaev chains with long-range pairing. *Journal of Physics: Condensed Matter*, 29(11):115401, 2017.

[184] Ingo Peschel. Calculation of reduced density matrices from correlation functions. *Journal of Physics A: Mathematical and General*, 36(14):L205, 2003.

[185] Ming-Chiang Chung and Ingo Peschel. Density-matrix spectra for two-dimensional quantum systems. *Phys. Rev. B*, 62:4191–4193, Aug 2000.

[186] Ming-Chiang Chung and Ingo Peschel. Density-matrix spectra of solvable fermionic systems. *Phys. Rev. B*, 64:064412, Jul 2001.

[187] H. Bruus and K. Flensberg. *Many-Body Quantum Theory in Condensed Matter Physics: An Introduction*. Oxford Graduate Texts. OUP Oxford, 2004.

[188] Michel Gaudin. Une démonstration simplifiée du théorème de wick en mécanique statistique. *Nuclear Physics*, 15:89 – 91, 1960.

[189] T. Lieb, E. Schultz and D. Mattis. Two soluble models of an antiferromagnetic chain. *Annals Phys.*, 16:407–466, 1961.

Appendices

A

ENTANGLEMENT ENTROPY FROM CORRELATION MATRICES

We illustrate here a straight-forward procedure developed by Peschel[184], that allows the computation of entanglement entropies starting from the knowledge of the reduced density matrices and the correlation functions in solvable fermionic or bosonic models.

Given a certain chain or lattice model, we can partition the whole system and restrict to only a subset of *sites*, which properties can be described by operators named reduced density matrices (RDMs)[121]. [1] In[185] [186] it was found that such quantities have an exponential form of the tipe e^{-H_A}, with H_A again a solvable fermionic or bosonic Hamiltonian related to a subsystem. The method shown here explains how to recover the RDMs grounding all the considerations in the study of correlation functions. Once known the exact spectrum of the RDM, the entanglement entropy follows directly. In the following, we describe two cases of solvable hamiltonians, namely a quadratic Hamiltonian that could represents a simple system of fermions hopping between lattice sites, and a more general Hamiltonian, suitable for a generic free particles theory.

[1] It is interesting to note that RDMs refer to a subset of sites, and in contrast to some other operators and quantities they do not involve a subset of *particles*.

A.1 FERMIONIC QUADRATIC HAMILTONIAN

We consider a Hamiltonian of the following form:

$$\mathcal{H} = \sum_{i,j=1}^{L} c_i^\dagger H_{ij} c_j, \tag{A.1}$$

with $c_i^\dagger$, c_i the usual fermionic creation and annihilation operators and L the size of the system. Exploiting the Wick theorem, we know that for free particles systems, i.e. when the Hamiltonian is quadratic, higher order Green's functions involving more than one particle can be factorized into products of single-particle Green's functions.[187] Thus, considering a Slater-like eigenstate of the Hamiltonian (A.1), we can calculate all orders correlation functions starting from the two point correlator

$$C_{ij} = \langle c_i^\dagger c_j \rangle, \tag{A.2}$$

$$\langle c_i^\dagger c_j^\dagger c_k c_l \rangle = \langle c_i^\dagger c_l \rangle \langle c_j^\dagger c_k \rangle - \langle c_i^\dagger c_k \rangle \langle c_j^\dagger c_l \rangle = C_{il} C_{jk} - C_{ik} C_{jl} \tag{A.3}$$

Our aim here is to connect the correlation matrix C to the RDM of a subsystem of the whole lattice. If we restrict to a subset A of l sites, any value that operators assume in A can be computed using equivalently both the total density matrix ρ of the total system or the reduced density matrix ρ_A of the subsystem.[121] Therefore, the two-point function C_{ij} can be expressed also as

$$C_{ij} = \mathrm{Tr}_A\{\rho_A c_i^\dagger c_j\} = \mathrm{Tr}_A\{\rho c_i^\dagger c_j\}, \tag{A.4}$$

and the higher orders correlators must be factorized as in (A.2).

The above property actually holds if ρ (and ρ_A) is the exponential of a free-fermion operator[188], as we mentioned in the introduction of this appendix, and thus one can write

$$\rho_A = \frac{1}{Z_A} e^{-H_A}, \tag{A.5}$$

where H_A holds the same properties and the same form of the total $\mathcal{H}$, i.e.

$$H_A = \sum_{i,j=1}^{l} c_i^\dagger A_{ij} c_j, \tag{A.6}$$

Z_A is the reduced partition function of A and l is the size of the subsystem. H_A can be diagonalized introducing new fermionic operators $a^\dagger$, a defined as

$$c_i = \sum_{k=1}^{l} U_{ik} a_k, \tag{A.7}$$

where U is a unitary matrix, i.e. such that $UU^\dagger = U^\dagger U = \mathbb{I}$. If we choose U in order to diagonalize the matrix A, we obtain

$$H_A = \sum_{k,k'=1}^{l} a_k^\dagger \left(\sum_{i,j=1}^{l} U_{ik}^\dagger A_{ij} U_{jk'} \right) a_{k'} = \sum_{k=1}^{l} \epsilon_k a_k^\dagger a_k. \tag{A.8}$$

The above form of H_A implies the following factorized form of the RDM ρ_A, in which each term can be viewed as a single-particle RDM ρ_k:

$$\rho_A = \bigotimes_{k=1}^{l} \rho_k = \bigotimes_{k=1}^{l} \frac{e^{-\epsilon_k a_k^\dagger a_k}}{1+e^{-\epsilon_k}}, \qquad \rho_k = \begin{bmatrix} \frac{1}{1+e^{\epsilon_k}} & 0 \\ 0 & \frac{1}{1+e^{-\epsilon_k}} \end{bmatrix} \tag{A.9}$$

where we set the reduced partion function $Z_k = 1 + e^{-\epsilon_k}$ for each ρ_k in order to achieve the required normalization. Inserting (A.9) in (A.4) we find

$$C_{ij} = \mathrm{Tr}\{\rho_A c_i^\dagger c_j\} = \mathrm{Tr}\{\rho_A c_i^\dagger c_j\} = \sum_{n,m=1}^{l} U_{in}^\dagger U_{jm} \, \mathrm{Tr}_A \left\{ \bigotimes_{k=1}^{l} \frac{e^{-\epsilon_k a_k^\dagger a_k}}{1+e^{-\epsilon_k}} a_n^\dagger a_m \right\}, \tag{A.10}$$

and we note that the result of the trace calculation leaves us with

$$\mathrm{Tr}_A \left\{ \bigotimes_{k=1}^{l} \frac{e^{-\epsilon_k a_k^\dagger a_k}}{1+e^{-\epsilon_k}} a_n^\dagger a_m \right\} = \frac{\delta_{nm}}{1+e^{\epsilon_n}}, \tag{A.11}$$

and thus

$$C_{ij} = \sum_{n=1}^{l} U_{in}^\dagger \frac{1}{1+e^{\epsilon_n}} U_{jn}. \tag{A.12}$$

Finally, since we chose U to be unitary, we can obtain from (A.12) the eigenvalues $\gamma_k = (1+e^{\epsilon_k})^{-1}$ of the correlation matrix C and subsequentially point out the relation between the eigenvalues ϵ_k of the entanglement Hamiltonian H_A and γ_k:

$$\epsilon_k = \log \frac{1-\gamma_k}{\gamma_k}. \tag{A.13}$$

Therefore, we succeeded in our task of finding a direct procedure to obtain the RDM of the subsystem A from the correlation matrix: indeed, we can get ϵ_k from γ_k after diagonalizing C, and therefore we can calculate ρ_A with (A.9).

A.2 GENERIC FREE THEORY

We consider now a more general Hamiltonian

$$\mathcal{H} = \sum_{i,j=1}^{L} [c_i^\dagger H_{ij} c_j + \frac{1}{2}(c_i^\dagger K_{ij} c_j^\dagger + h.c.)], \tag{A.14}$$

where the hermiticity of $\mathcal{H}$ implies that H is hermitian and the anticommutation rules requires K to be antihermitian. Since we have now two matrices in the Hamiltonian, we are unable to gain all the desired informations from the study of C alone. In fact, we need to consider also the anomalous two-points correlator

$$F_{ij} = \langle c_i c_j \rangle, \tag{A.15}$$

which is obviously null in the case of a system described by (A.1). Including F, (A.3) must be modified, leading to

$$\langle c_i^\dagger c_j^\dagger c_k c_l \rangle = \langle c_i^\dagger c_l \rangle \langle c_j^\dagger c_k \rangle - \langle c_i^\dagger c_k \rangle \langle c_j^\dagger c_l \rangle + \langle c_i^\dagger c_j^\dagger \rangle \langle c_k c_l \rangle. \tag{A.16}$$

Following the same arguments of the previous section, the RDM of a subset A, obtained through a partition of the total system, takes the form

$$H_A = \sum_{i,j=1}^{l} [c_i^\dagger A_{ij} c_j + \frac{1}{2}(c_i^\dagger B_{ij} c_j^\dagger + h.c.)], \tag{A.17}$$

which represents a generalization of (A.6), with A hermitian and B antihermitian. Now we have to define some new operators a, $a^\dagger$ that diagonalize the entanglement hamiltonian, in order to recover the RDM factorization (A.9). The usual diagonalization procedure for this type of Hamiltonians has been settled by Lieb, Schultz and Mattis [189], and it involves a Bogoliubov transformation of the form

$$a_k = \sum_{i=1}^{l} (g_{ki} c_i + h_{ki} c_i^\dagger), \tag{A.18a}$$

$$a_k^\dagger = \sum_{i=1}^{l} (g_{ki} c_i^\dagger + h_{ki} c_i), \tag{A.18b}$$

where g and h are $l \times l$ real matrices. The transformation leads to the diagonal form of H_A

$$H_A = \sum_{k=1}^{l} \epsilon_k a_k^\dagger a_k. \tag{A.19}$$

Thus, it is possible to write

$$[a_k, H_A] - \epsilon_k a_k = 0, \tag{A.20}$$

and we can obtain a set of equations for the coefficients g_{ki} and h_{ki} substituting in (A.20) the explicit form of the operators (A.18):

$$\epsilon_k g_{ki} = \sum_{j=1}^{l} (g_{kj} A_{ji} - h_{kj} B_{ji}) \tag{A.21a}$$

$$\epsilon_k h_{ki} = \sum_{j=1}^{l} (g_{kj} B_{ji} - h_{kj} A_{ji}) \,. \tag{A.21b}$$

This couple of equations can be simplified by introducing the linear combinations $\phi_{ki} = g_{ki} + h_{ki}$ and $\psi_{ki} = g_{ki} - h_{ki}$, which leads to the new equations

$$\phi_k (A - B)(A + B) = \epsilon_k^2 \phi_k \tag{A.22a}$$

$$\psi_k (A + B)(A - B) = \epsilon_k^2 \psi_k. \tag{A.22b}$$

Since A and B are hermitian and antihermitian respectively, we can choose ϕ_k and ψ_k to be real and orthonormal:

$$\sum_{i=1}^{l} \phi_{ki} \phi_{k'i} = \sum_{i=1}^{l} \psi_{ki} \psi_{k'i} = \delta_{k,k'}. \tag{A.23}$$

The canonical transformation (A.18) can be recasted in a more useful form using directly ϕ_k and ψ_k:

$$a_k = \sum_{i=1}^{l} \left(\frac{\phi_{ki} + \psi_{ki}}{2} c_i + \frac{\phi_{ki} - \psi_{ki}}{2} c_i^\dagger \right), \tag{A.24}$$

which can be easily inverted to get

$$c_i = \sum_{k=1}^{l} \left(\frac{\phi_{ki} + \psi_{ki}}{2} a_k + \frac{\phi_{ki} - \psi_{ki}}{2} a_k^\dagger \right). \tag{A.25}$$

Computing the traces in the calculation of $C_{ij} = \mathrm{Tr}_A\{\rho_A c_i^\dagger c_j\}$ and $F_{ij} = \mathrm{Tr}_A\{\rho_A c_i c_j\}$ and exploiting the property (A.23), we get the expressions

$$C_{ij} = \frac{\delta_{ij}}{2} + \frac{1}{4} \sum_{k=1}^{l} (\phi_{ki} \psi_{kj} + \psi_{kj} \phi_{ki}) \tanh \frac{\epsilon_k}{2}, \tag{A.26}$$

$$F_{ij} = \frac{1}{4} \sum_{k=1}^{l} (\phi_{ki} \psi_{kj} - \psi_{kj} \phi_{ki}) \tanh . \frac{\epsilon_k}{2}, \tag{A.27}$$

Thus, in the general case we do not get a direct diagonalization of C and F, but we can note how the following combination of the two matrices is in diagonal form:

$$[(C - \frac{\mathbb{I}}{2} - F)(C - \frac{\mathbb{I}}{2} + F)]_{ij} = \frac{1}{4} \sum_{k=1}^{l} \psi_{ki} \tanh^2 \frac{\epsilon_k^2}{2} \psi_{kj}. \tag{A.28}$$

Thus, the relation of interest is between ϵ_k and the eigenvalues γ_k of $(C-\frac{\mathbb{I}}{2}-F)(C-\frac{\mathbb{I}}{2}+F)$, and it is given by

$$\epsilon_k = 2\,\mathrm{arctanh}(2\sqrt{\gamma_k}). \tag{A.29}$$

A.3 ENTANGLEMENT ENTROPY

Finally, we can now compute explicitly the *Von Neumann entanglement entropy* (VNEE) for the subset A of a bipartite system $S = A + B$, defined as[121]

$$S(A) = -\,\mathrm{Tr}_A\{\rho_A \log \rho_A\}. \tag{A.30}$$

A notable feature of VNNE is the fact that it depends only on the bipartition of the system and it is not an extensive quantity, and in particular we have

$$S(A) = A(B). \tag{A.31}$$

From (A.30), we can write the VNEE in the alternative form

$$S(A) = -\sum_k \lambda_k \log \lambda_k, \tag{A.32}$$

where the λ_k's are the eigenvalues of ρ_A and the sum runs over the whole spectrum of the RDM. Since ρ_A is factorized as in (A.9), we are able to express also the VNEE as a sum of single modes VNEE's:

$$S(A) = \sum_{k=1}^{l} \left[-\frac{1}{1+e^{\epsilon_k}} \log \frac{1}{1+e^{\epsilon_k}} - \left(1 - \frac{1}{1+e^{\epsilon_k}}\right) \log \left(1 - \frac{1}{1+e^{\epsilon_k}}\right) \right], \tag{A.33}$$

since $\frac{1}{1+\epsilon_k}$ and $\left(1 - \frac{1}{1+\epsilon_k}\right)$ are the eigenvalues of each ρ_k. Recalling the results seen in the last sections, if the system is decribed by an Hamiltonian of the type (A.1), we obtain $\gamma_k = \frac{1}{1+\epsilon_k}$, where γ_k are the eigenvalues of the correlation matrix C, and thus (A.33) becomes

$$S(A) = \sum_{k=1}^{l} [-\gamma_k \log \gamma_k - (1-\gamma_k)\log(1-\gamma_k)]. \tag{A.34}$$